# BIOPHYSICAL CHARACTERIZATION OF THE ENERGY AND TONB-DEPENDENCE OF THE FERRIC ENTEROBACTIN TRANSPORT PROTEIN FEPA

by

LORNE DONNELL JORDAN

B.S., Bowling Green State University, 2009

M.S., University of Oklahoma, 2012

AN ABSTRACT OF A DISSERTATION

submitted in partial fulfillment of the requirements for the degree

DOCTOR OF PHILOSOPHY

Department of Biochemistry and Molecular Biophysics
College of Arts and Sciences

KANSAS STATE UNIVERSITY
Manhattan, Kansas

2015

## Abstract

The goal of the research included in this dissertation is to provide a more complete model of the role of TonB, an energy transducing protein that resides in the inner membrane and is an essential component of the iron transport of *Escherichia coli* under iron-starved conditions. Using fluorescent hybrid proteins, the anisotropy of TonB in the cytoplasmic membrane (CM) of *Escherichia coli* was determined. With the aim of understanding the bioenergetics of outer membrane (OM) iron transport, the dependence of TonB motion on the electrochemical gradient and the effect of CM proteins ExbB and ExbD on this phenomenon was monitored and analyzed. The native *E. coli* siderophore, enterobactin chelates $Fe^{+3}$ in the environment and ferric enterobactin (FeEnt) enters the cell by energy- and TonB-dependent uptake through FepA, its OM transporter. The TonB-ExbBD complex in the CM is hypothesized to transfer energy to OM transporters such as FepA. We observed the polarization of GFP-TonB hybrid proteins and used metabolic inhibitors (CCCP, azide and dinitrophenol) and chromosomal deletions of *exbBD* to study these questions. The results showed higher anisotropy (R) values for GFP-TonB in energy-depleted cells, and lower R-values in bacteria lacking ExbBD. Metabolic inhibitors did not change the anisotropy of GFP-TonB in *ΔexbBD* cells. These findings suggest that TonB undergoes constant, energized motion in the bacterial CM, and that ExbBD mediates its coupling to the

electrochemical gradient. By spectroscopic analyses of extrinsic fluorophore labeled site-directed Cys residues in 7 surface loops of Escherichia coli FepA, binding and transport of ferric enterobactin (FeEnt) was characterized.

Changes in fluorescence emissions reflected conformational motion of loops that altered the environment of the fluorophore, and we observed these dynamics as quenching phenomena during FeEnt binding and transport in living cells or outer membrane vesicles. Cys residues in each of the 7 surface loops (L2, L3, L4, L5, L7 L8, and L11) behaved individually and characteristically with regard to both fluorophore maleimide reactivity and conformational motion. Fluorescence measurements of FeEnt transport, by either microscopic or spectroscopic methodologies, demonstrated that ligand uptake occurs uniformly throughout the cell envelope, and susceptibility of FeEnt uptake to the proton ionophore m-chlorophenyl hydrazone (CCCP) at concentrations as low as 5 uM. The latter result recapitulates the sensitivity of inner membrane major facilitator transporters to CCCP (Kaback, 1974), providing further evidence of the electrochemical gradient as a driving force for TonB-dependent metal transport.

# BIOPHYSICAL CHARACTERIZATION OF ENERGY AND TONB DEPENDENCE OF THE FERRIC ENTEROBACTIN TRANSPORT PROTEIN FEPA

by

LORNE DONNELL JORDAN

B.S., Bowling Green State University, 2009

M.S., University of Oklahoma, 2012

A DISSERTATION

submitted in partial fulfillment of the requirements for the degree

DOCTOR OF PHILOSOPHY

Department of Biochemistry and Molecular Biophysics
College of Arts and Sciences

KANSAS STATE UNIVERSITY
Manhattan, Kansas

2015

Approved by:

Major Professor
Phillip E. Klebba, PhD

## Abstract

The goal of the research included in this dissertation is to provide a more complete model of the role of TonB, an energy transducing protein that resides in the inner membrane and is an essential component of the iron transport of *Escherichia coli* under iron-starved conditions. Using fluorescent hybrid proteins, the anisotropy of TonB in the cytoplasmic membrane (CM) of *Escherichia coli* was determined. With the aim of understanding the bioenergetics of outer membrane (OM) iron transport, the dependence of TonB motion on the electrochemical gradient and the effect of CM proteins ExbB and ExbD on this phenomenon was monitored and analyzed. The native *E. coli* siderophore, enterobactin chelates $Fe^{+3}$ in the environment and ferric enterobactin (FeEnt) enters the cell by energy- and TonB-dependent uptake through FepA, its OM transporter. The TonB-ExbBD complex in the CM is hypothesized to transfer energy to OM transporters such as FepA. We observed the polarization of GFP-TonB hybrid proteins and used metabolic inhibitors (CCCP, azide and dinitrophenol) and chromosomal deletions of *exbBD* to study these questions. The results showed higher anisotropy (R) values for GFP-TonB in energy-depleted cells, and lower R-values in bacteria lacking ExbBD. Metabolic inhibitors did not change the anisotropy of GFP-TonB in *ΔexbBD* cells. These findings suggest that TonB undergoes constant, energized motion in the bacterial CM, and that ExbBD mediates its coupling to the

electrochemical gradient. By spectroscopic analyses of extrinsic fluorophore labeled site-directed Cys residues in 7 surface loops of Escherichia coli FepA, binding and transport of ferric enterobactin (FeEnt) was characterized.

Changes in fluorescence emissions reflected conformational motion of loops that altered the environment of the fluorophore, and we observed these dynamics as quenching phenomena during FeEnt binding and transport in living cells or outer membrane vesicles. Cys residues in each of the 7 surface loops (L2, L3, L4, L5, L7 L8, and L11) behaved individually and characteristically with regard to both fluorophore maleimide reactivity and conformational motion. Fluorescence measurements of FeEnt transport, by either microscopic or spectroscopic methodologies, demonstrated that ligand uptake occurs uniformly throughout the cell envelope, and susceptibility of FeEnt uptake to the proton ionophore m-chlorophenyl hydrazone (CCCP) at concentrations as low as 5 uM. The latter result recapitulates the sensitivity of inner membrane major facilitator transporters to CCCP (Kaback, 1974), providing further evidence of the electrochemical gradient as a driving force for TonB-dependent metal transport

## Table of Contents

## List of Figures and Tables

## ACKNOWLEDGEMENT

I started working in Dr. Phillip Klebba's laboratory in late 2009, without much of an idea about iron transport or Gram-negative bacteria. However, my doctoral work, included in this dissertation, has helped to define me as a biochemist and as a molecular biophysicist. I am grateful that the ferric enterobactin transport system in *E. coli* became a major part of my life over the past several years. As part of Dr. Klebba's laboratory group, I was given an opportunity to learn protein purification techniques, microscopy, spectroscopic techniques, and molecular biological techniques. I spent the first three years of my studies at the University of Oklahoma and the last three years at Kansas State University. At both institutions, I grew as an individual nearly as much as I have grown as a scientist. I must take this opportunity to thank Dr. Klebba for his mentorship and taking me under his wing these past few years. I must also thank Dr. Salete Newton, who offered advice and training throughout my studies. Thank you to Dr. Simin Pulat, who encouraged me and offered the opportunity to fulfill my dream of earning a PhD. Additionally, I would like to thank Dr. Wai Tak Yip for his time and for offering his expertise to train me in physical chemistry techniques. Thank you to Dr. Yongyao Zhuo for her collaboration and major contributions to my fusion protein studies. Finally, thank you to all my labmates, who became my family away from home.

## Dedication

At its core, science is defined by exploration; indeed, the impetus to pursue scientific research is entwined with a strong desire to gain understanding and to advance the goals of humanity, through an evolving nature. Immanuel Kant once wrote of two things that fill the minds of sentient beings. While the power of his words more than sufficiently inspire the soul, I often still ponder two other phenomena, which I consider of equal majesty. The natural force of kindness and the beautiful creativity within others have continually filled me with *"ever new and increasing admiration and awe."* In this moment forward, I have chosen to seize a great opportunity and to appropriate it as my vehicle in exploring *"the starry heavens above and the moral law within."* I am forever thankful for the gentle encouragement toward realizing my dreams, otherwise deferred. I hope to someday honor those who freely shone some of their light onto my path, by likewise offering a photon… or two, to those in need.

I dedicate this dissertation and the entire pursuit of my PhD to my loving family, to my supportive friends who encouraged success and inspired growth, and to my creator, through whom all things are possible.

− *Ad Majorem Dei Gloriam*

## Preface

The major goal of my doctoral research has been centered on improving our understanding of the TonB-dependent transport system dedicated to ferric enterobactin translocation into *Escherichia coli*. This system is of vital import to bacteria, since they, like most organisms, require iron to survive. Two proteins play a central role in this process, the ferric enterobactin receptor and transporter, known as FepA, and an energy transducing inner membrane protein, TonB.

This dissertation, as whole, is an overview of three aspects of the iron transport process. Included in Chapter 2, is a study that focuses on the importance of ferric enterobactin in colonizing a host's gut during infection. This study highlights the fierce competition that occurs between different species, and even between different strains of bacteria, for the nutrient resources of their host environment. In the third chapter, I present work from a study that revealed coordination among the extracellular loops of FepA. Since FepA must first bind its ligand in order to facilitate transport, we investigated the dynamics of ferric enterobactin binding and discovered an ordered interaction between the loops and the ligand.

The work discussed in Chapter 4 is the result of a merge between biochemistry and physical chemistry, which allowed us to probe the motion of TonB *in vivo*. Finally, in the concluding chapter, I review our laboratory's

current model for TonB-dependent transport. I present this dissertation with many thanks to my advisor and dear colleagues, without whom, this work could not have been accomplished.

# Chapter 1:Studies of Siderophore Transport

## 1.1 Introduction

Most of Earth's living organisms require iron to sustain basic metabolic processes that underlie homeostasis, growth, and reproduction. Moreover, cellular respiration for almost all of these organisms is made possible by iron-containing proteins of the electron transport chain. Iron is also used as a cofactor for essential enzymes, such as ribonucleotide reductase, which are common to both eukaryotic and prokaryotic organisms (Miethke and Marahiel, 2007). Although this indispensible nutrient is abundant in the environment, its bioavailability is low. The term bioavailability addresses the ease of acquisition and utilization of a given nutrient by living systems. When such a vital resource like iron becomes scarce, common dependence often results in competition.

Biologically relevant ferrous iron ($Fe^{2+}$) is readily oxidized by $O_2$ in the atmosphere or within animal tissues (Miethke and Marahiel, 2007), giving rise to resource scarcity. The resulting prevalent ferric form is also nearly water insoluble ($K_{sp} \sim 10^{-38}$). The most commonly occurring forms are ferric oxide hydrate complexes, which have a solubility of $1.4 \times 10^{-9}$ M at pH 7 and $10^{-3}$ at pH 5 (Liu et al., 2014; Miethke and Marahiel, 2007; Schaible and Kaufmann, 2004). The availability of biologically relevant forms of iron in the environment is around $10^{-18}$ M near pH 7.0, while most

bacteria, excluding lactobacilli, need at least $10^{-8}$ M iron to propagate (Carrano and Raymond, 1978; Miethke and Marahiel, 2007; Stintzi et al., 2000).

Shortages of bioavailable iron present a major challenge to organisms seeking homeostatic iron levels, single-cell and multi-cellular, alike (Fischbach et al., 2006; Nairz et al., 2010; Stintzi et al., 2000). For example, in bacteria, iron-depleted conditions result in an upregulation of siderophore-mediated iron-uptake systems. Animals generally obtain enough iron from their diets, however, low iron stores cause animals to absorb more when consuming iron-containing food sources.

### 1.2 Iron-related host defenses

Multicellular host organisms prevent accessibility of iron to potential pathogens by tight regulation (Hentze et al., 2010). Most microorganisms seeking iron homeostasis in otherwise iron-deficient environments secrete siderophores. The presence of these iron chelators, indicating the presence of an impending threat, activates plant immunity. Although plant immune defenses are arguably less complicated than those of most animals, plants respond to pathogens in many ways that allow the plant to divert resources and become more resilient to infection or the effects of infection. Most notably, cell wall rigidification, reduction of reactive oxygen

species (ROS) detoxification, and induction of defense hormone signaling can allow plants to cope with infectious organisms (Aznar et al., 2014).

Importantly, for humans and other mammals, iron plays a central role in binding oxygen to be carried by red blood cells. Iron resides within each of the heme groups (porphyrin rings) of hemoglobin, four total, which allows $O_2$ delivery from the lungs to distal tissues. Once oxygen reaches the various muscle tissues of the body, it is transferred to another heme-containing protein, myoglobin, which stores oxygen. Although iron is required for important chemistry within the body, it is potentially harmful in large concentrations (Bullen et al., 2005). Iron in animals is kept under tight regulation, due to otherwise toxic effects. These effects include denaturation of proteins, DNA strand breakage, and oxidative degradation of lipids through peroxidation (Schaible and Kaufmann, 2004). This toxicity naturally results from iron's interaction with oxygen, creating free radicals that cause damage to cells. Various reactive oxygen species (ROS) are created as a result of the electron transport chain reactions, oxidoreductases. In addition to sequestering iron from pathogens, storage proteins like ferritin are used to prevent formation of ROSs. Too much iron in growth media results in slowed growth rates for bacteria, indicating that elevated iron levels are also presented as a stress signal to bacteria (Stevanovic et al., 2013).

During bacterial infection, a battle between host and pathogen occurs for control of host iron stores (Nairz et al., 2010). In every battle there are weapons that aid in achieving the ultimate goal of resource dominance. For animal hosts the innate immune system provides several main defenses against invading bacteria. However, bacteria have many ways of subverting those host defenses. As part of this chapter, I will outline some of the proteins that have the biggest impact on the outcome of an infection.

The primary way animals reduce the availability of iron is by controlling the amount being absorbed and by limiting the labile pool of uncomplexed free-circulating iron (Dauros-Singorenko and Swift, 2014). Animal storage proteins help restrict access to their cellular iron supply. When humans consume iron, the body only absorbs about 1-2 mg daily (Nairz et al., 2010). This is due to the presence of iron regulatory proteins, which either “sense” the intracellular concentration of iron or the amount of oxidative-stress experienced by the cell (Miethke and Marahiel, 2007). A key protein involved in this process is hepcidin, a small protein that binds and signals the degradation of the mammalian iron exporter, ferroportin (Heming et al., 2011). Since ferroportin is the only means by which a cell may export iron, hepcidin effectively controls cellular iron release.

In addition to limiting the overall iron supply, the mammalian innate immune system possesses pattern-recognition receptors (PRRs) that

activate either proinflammatory signaling cascades or signal phagocytosis “perceived” pathogens (Johnson and Wessling-Resnick, 2012; Liu et al., 2014). Among these PRRs are toll-like receptors, which have heme recognition sites. TLRs are expressed on the majority of immune cells and recognize specific types of pathogen-associated threats to signal an appropriate immune response (Lambris et al., 2008; Madar et al., 2015; Okumura and Nizet, 2014).

Too much free heme in the blood or tissues can elicit an immune response; since, free heme is associated with cell damage caused by pathogens. The outcome of heme binding to TLRs is the promotion of reactive oxygen species (ROS), mediated by tumor necrosis factor-α in humans (Okumura and Nizet, 2014). Neutrophils subsequently gather in response to ROS generation and release lipocalin-2 and lactoferrin, which bind ferric-ion chelators released by bacteria (Nairz et al., 2010). In addition, iron storage and scavenging proteins are often upregulated during bacterial infection, consequently limiting their ability to multiply (Hentze et al., 2010; Troxell and Hassan, 2013; Zeng et al., 2015).

The major iron reservoir in mammals is red blood cells (RBCs). The hemoglobin (Hb) of red blood cells contains around 65% of the body’s iron supply. In addition to this large pool of iron, an abundance of iron is also found in the oligomeric storage protein, ferritin. Ferritin sequesters

approximately 30% of the host's iron supply, with each oligomer capable of binding up to 4,500 ferric ions (Miethke and Marahiel, 2007).

When iron is circulating in blood plasma, it is bound to transferrin. Once it reaches the target cell, iron is transferred to intracellular shuttle proteins. These proteins include a mammalian iron chelator, the mammalian siderophore 2,5-dihydroxybenzoic acid in association with lipocalin-2. The mammalian siderophore is directly comparable to the bacterial siderophore moiety 2,3-DHBA, which is iron-binding part of the siderophore secreted by *Escherichia coli* (Liu et al., 2014).

Bacteria seek to parasitize the various mammalian iron-containing proteins, due to an iron-stress response from low concentrations of available iron. The siderophores secreted as a result have an extremely high affinity for iron. For instance, the Gram-negative bacterium *Escherichia coli* (*E. coli*) secretes the siderophore enterobactin, with a $K_D$ of 0.2 nM (Newton et al., 1999). It is important to note, different bacterial species secrete specific siderophores. Nonetheless, most bacterial siderophores are better adapted for iron chelation and can out-compete mammalian proteins.

### 1.3 Bacterial Iron-acquisition

For bacteria, production of proteins related to iron uptake is a costly process, so transcription may be turned on or turned off depending on the

stress experienced by cells. Over time gene regulators have evolved with the exclusive function of controlling iron homeostasis. An excellent example of which is a transcriptional regulator known as the ferric uptake regulator (Fur) that controls the production of specialized iron uptake systems in bacteria (Fillat, 2014; Rabsch et al., 2007; Troxell and Hassan, 2013; Xiao et al., 2011). Investigation into the genome-wide iron availability response of wildtype *E. coli* MG1655 presented over 80 genes regulated by forms of the Fur repressor or repression factors acting on holo-Fur (Seo et al., 2014).

Under iron-replete conditions, iron passes freely into the cell through porins. However, in iron-deplete conditions they must harvest iron via siderophores, which sequester the metal from the immediate environment with high affinity (Fischbach et al., 2006). The Fur operon regulates both the transcription of siderophores and ligand-specific siderophore receptors/transporters that translocate iron-siderophores across the bacterial membrane barrier. In such a situation, microbes rely on Fur-regulated proteins for survival (Fillat, 2014)

The Fur transcriptional repressor acts as a molecular on/off switch. When iron is replete, $Fe^{2+}$ binds to the Fur repressor, creating holo-Fur which then associates with “Fur boxes”. These Fur boxes are located within promoters upstream of iron transport genes, including genes for the TonB-ExbBD complex, and are bound by Fur-$Fe^{2+}$. The sequence of Fur

binding sites is GATAAT and it appears in doubles on the gene sequence, since holo-Fur sits on the gene in units of four as two dimers (Escolar et al., 1998). Binding by holo-Fur blocks RNA polymerase from association with the promoters for the iron uptake genes (Althaus et al., 1999; Braun, 2003; Stojiljkovic et al., 1994). Under iron-deplete conditions, the Fur repressor-$Fe^{2+}$ cofactor for Fur is no longer available and apo-Fur dissociates from the Fur boxes. All of the promoters for the previously repressed iron-transport genes are accessible to polymerases and transcription occurs in this case (Noinaj et al., 2010).

### 1.4 Bacterial Cell Envelopes

It is important to note the key features of the *E.* coli cell envelope in order to fully understand the proteins involved in the translocation of siderophores for our model system. Firstly, the cell envelope presents a major difference between Gram-positive and Gram-negative bacteria. Its varying characteristics are a hallmark of the strengths and weaknesses of the two classes. In both cases, the cell envelope contains many proteins, which aid bacteria in acquiring various sugars, amino acids, vitamins, and metals (Silhavy et al., 2010).

Another commonality between Gram-negative and Gram-positive bacteria is the presence of an exoskeleton that provides rigidity and distinctive cell shape. This skeleton is a matrix of small peptides and

sugars. The repeating disaccharide constituent is N-acetyl glucosamine-N-acetyl muramic acid (Silhavy et al., 2010). Sphere-shaped cells, called spheroplasts, result in cells that lack this essential scaffolding. Aside from providing structural support, the peptidoglycan layer also acts as a defensive barrier.

All Gram-negative bacteria possess a trilaminar cell envelope comprised of an inner membrane (IM), outer membrane (OM), and a periplasmic space (PS). The OM provides an extra barrier to the environment and molecules harmful to the cell. It contains many beta barrel proteins that recognize, export, and/or import nutrients. A thin peptidoglycan layer lies just under the inner-leaflet of the OM and extends 4-6 nm. The peptidoglycan is attached via murein lipoprotein and peptidoglycan-associated lipoprotein (Pal), which also interacts with Tol system proteins (Bouveret et al., 1995). The periplasmic space is an aqueous compartment, which resides between the IM and OM. This space separates the OM from the IM and contains many different shuttle proteins. Lastly, electron transport chain proteins and proton motive force (PMF)-dependent proteins reside within the IM.

Proton motive force is derived from a combination of the pH gradient across the IM and the associated voltage potential, known together as an electrochemical proton gradient (Martin et al., 2015). Protons pumped across the IM from the cytoplasm to the periplasmic side, form a pH

gradient. The positive charge associated with protons also generates the voltage gradient. The generated proton motive force powers OM active transport (Bradbeer, 1993).

Gram-positive bacteria have a single cytoplasmic membrane and a thick network of peptidoglycan extends 30-100 nm from the extracellular surface (Silhavy et al., 2010). Since a single membrane separates these bacteria from the extracellular environment, they are more susceptible to antibiotics than their Gram-negative counterparts. Antibiotics acting on peptidoglycan can easily access their targets. Within the peptidoglycan, teichoic acids form polymer chains that increase the stability and resilience of the cell wall.

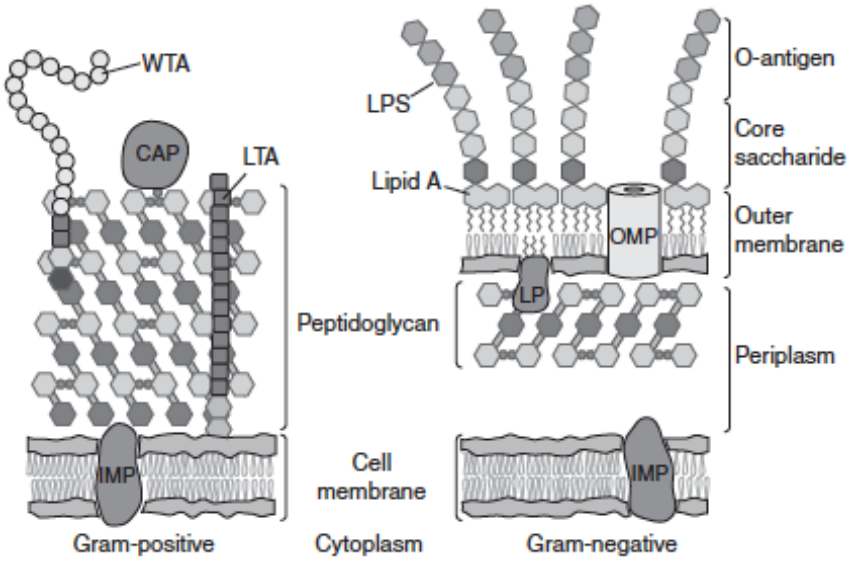


**Figure 1-1** Silhavy, T.J., Kahne, D., Walker, S., 2010. The bacterial cell envelope. Cold Spring Harb Perspect Biol 2, a000414. Copyright Cold Spring Harbor Laboratory Press 2010. Published with the permission of Cold Spring Harbor Laboratory Press.

Shown is a cartoon depicting the Gram-positive cell envelope (left) and the Gram-negative cell envelope (right). Covalently attached proteins (CAP), wall teichoic acid (WTA), and lipoteichoic acid (LTA) are common to Gram-positive bacteria. Lipoprotein (LP), outer membrane proteins (OMP), and other components of the outer membrane are common to Gram-negative bacteria.

### 1.5 General information on *E. coli*

Our model organism is *E. coli*, a Gram-negative bacterium, further characterized as a non-spore forming rod. Most strains generally reside in the intestinal tract of warm-blooded animals, as a part of the commensal bacterial community. These types of bacteria do not cause disease in their host. Despite the often-beneficial effects of commensal *E. coli*, there are nine distinct strains that cause severe discomfort, disease, and infection. In a substantial number of cases these strains may even result in host death. Notably, the non-commensal strains can encode upwards of 5,000 additional genes (Schmidt, 2010). Larger genomes provide an opportunity for greater protein diversity, and thereby, more tools to undermine host defenses. The major disease-causing strains include enteropathogenic, enteroinvasive, enterotoxigenic, and enterohemorrhagic *E. coli* (Clements and Cardenas, 1990; Faundez et al., 1988). There are at least five other subsets that occur less commonly; nonetheless, they present a major threat to humans. Among these strains, one of the most lethal pathovars causes neonatal meningitis and sepsis (Schmidt, 2010).

Enteropathogenic *E. coli* is transmitted through water, compromised by fecal contamination. It causes severe diarrhea, vomiting, chills, and fever that can last up to 3 days. Enteroinvasive *E. coli* is characterized by destruction of the mucus membrane of the intestine and also causes violent diarrhea, muscle pain, fever and chills. The enterotoxigenic strains

create enterotoxins as the bacteria multiply. Disease caused by these strains also include diarrhea and are easily transmitted in environments with poor hygiene standards. Enterohemorrhagic strains are responsible for causing bloody diarrhea in most cases, but do not usually cause fever (Larrie-Bagha et al., 2013; Schmidt, 2010). All of these pathogenic types contain a locus of enterocyte effacement (Schmidt, 2010). This pathogenicity island allows these strains to induce lesions that make successful gut-tissue colonization easier.

### 1.6 Iron Transport in *E. coli*

As previously discussed, siderophores are key to sequestering iron for utilization by both pathogenic and non-pathogenic bacteria. An entire transport system must be employed to bring the iron-siderophore complex into the cell. Although, iron passes across the OM through proteins, known as porins. These porins, like outer membrane porin F (OmpF), allow passive diffusion of polar molecules smaller than 600 Daltons (Cowan et al., 1995). Iron easily passes through these porins and into the cell under iron-replete conditions; it does so due to its concentration gradient, explained by Le Chatelier's Principle. Briefly, low iron concentrations inside the cell encourage the diffusion of iron from the outside, to reach an equilibrium concentration. However, diminished iron availability outside the

cell, renders this driving force a non-contributing factor and active transport becomes necessary.

### 1.7 Iron-Siderophore Complexes

Catecholates, hydroxamates, hydroxypyridonates, and aminocarboxylates comprise the four main classes of siderophores. Siderophores solubilize iron in its ferric state, making it available for microorganisms. Siderophores have a remarkable affinity of iron. The most stable siderophores involve hexadentate coordination with octahedral binding geometry, which is ideal for binding iron (Abergel et al., 2008; Raymond et al., 2003).

Once an iron-siderophore complex is brought into the cell, the iron must be released. This is achieved by either reduction of the ferric ion, leaving the siderophore intact, or degradation of the siderophore. Raymond and Carrano cleverly explain the two differing release mechanisms as the “European approach” and the “American approach” (Raymond et al., 2003). The monikers for microbial transport describe recycling or reuse of a siderophore for multiple rounds of complexation and transport versus disposal after a single use of the siderophore through degradation.

## 1.8 Ferric Enterobactin

Ferric enterobactin is the iron-complexed form of the siderophore enterobactin, secreted by the bacterium *E. coli.* Enterobactin is a catecholate iron chelator with catechol groups connected to a triserine ring through an amide linkage. Three catechol groups, also known as o-dihydroxybenzene groups, are responsible for the coordination of iron in ferric enterobactin. Once the siderophore binds iron, the structure changes to create a hexacoordinated cage around the iron atom, as shown in **Figure 1-2**. The weak acids of the catechol groups are deprotonated upon ferric iron binding and each give a dianion product. This is the key to conformational interconversion between the iron-unbound and iron-bound states. Coordination of the iron ion results in a net negative charge of -3. The affinity of enterobactin for ferric ion is the strongest documented chelation interaction ever recorded, with a rate of formation determined as $10^{52}$.

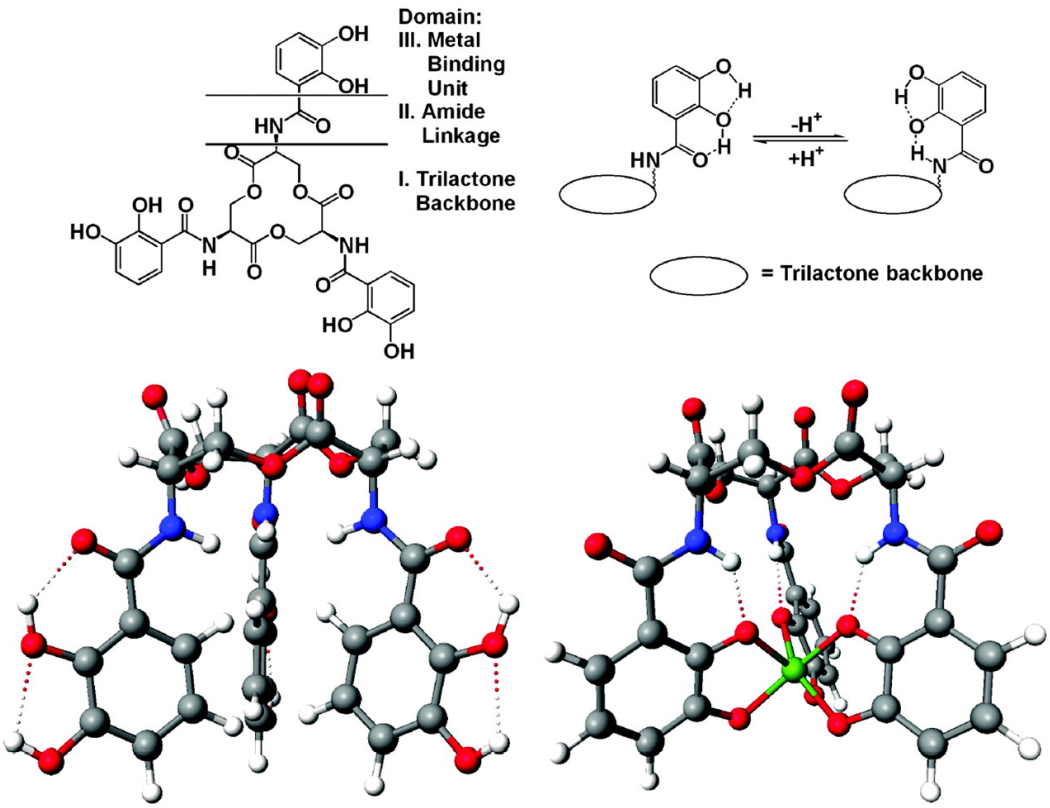


**Figure 1-2.** Raymond, K.N., Dertz, E.A., Kim, S.S., 2003. Enterobactin: an archetype for microbial iron transport. Proc. Natl. Acad. Sci. U. S. A. 100, 3584-3588. Copyright (2003) National Academy of Sciences, U.S.A. Published with the permission of National Academy of Sciences, U.S.A.

Shown above are representations of enterobactin and ferric enterobactin. The top portion shows a schematic of enterobactin's various features, while the lower portion depicts a space-filling cartoon of the molecule and its charge distribution.

## 1.9 The Need for Active Transport

Siderophores require transport systems to re-enter the cell. Scarce nutrients must pass through two barriers to reach the cytoplasm of Gram-negative bacteria. Specific transport proteins resident to each barrier mediate this passage (Annamalai et al., 2004). These transporters allow bacteria to accumulate iron against its concentration gradient. In the OM, ligand-gated transporters bind and translocate metal complexes, such as ferric siderophores, heme, and vitamin B12 from the extracellular environment (Udho et al., 2012).

These proteins are quite interesting for several reasons. Firstly, they are needed to facilitate translocation of iron into the cell against its concentration gradient. Although molecules smaller than 600 Da. diffuse through the OM without much resistance, objects larger than this molecular weight limit are size-excluded (Nikaido and Rosenberg, 1981). TonB-dependent transporters (TBDTs) also bind specific ligands and disallow other molecules from entering the cell, defining them as ligand-gated transporters. Due to their specificity and obligate active-transport mechanism, the transporters require energy input to translocate ligands. Despite energy requirements, the PMF generated by the same IM cannot be sustained by the OM (Bradbeer et al., 1978; Ferguson et al., 2002b). Porins in the OM allow small molecules (<600 Da) to diffuse into the cell also allows protons to freely equilibrate. This presents a complication for

larger molecules, however, an energy-transducing inner membrane protein, which spans the periplasm and directly interacts with TBDTs, alleviates the issue (Bassford et al., 1976; Braun and Endriss, 2007; Noinaj et al., 2010).

In E. coli, several proteins carry out iron uptake, including the outer-membrane transporter protein ferric enterobactin permease A (FepA) and the inner membrane protein TonB. The specific transport of FeEnt suggests that the globular domain acts as a gate rather than a pore and movement against a concentration gradient indicates an active transport process. Furthermore, a mechanism for specific coordinated movement of the globular domain requires an energy source.

Aside from nutrient availability, cell density has a substantial affect on the number of iron transport proteins expressed. Often, the general protocol for purifying or characterizing FepA from iron-starved cells requires cells grown in iron-deficient MOPS Minimal media until the cells reach an optical density of around 1.0 or slightly below. Iron transport proteins are expressed most abundantly when harvesting cells from late log growth in such conditions. The article "*The response of the TonB-dependent transport network in Anabaena sp.* PCC 7120 *to cell density and metal availability"* examined the dependence of TBDT gene and protein expression under iron, copper, or nitrogen starvation (Stevanovic et al., 2013). The authors found that high cell density caused *Anabaena* sp.

PCC 7120 metal transport genes to be upregulated under iron-deficient conditions (Stevanovic et al., 2013).

### 1.10 Ferric Enterobactin Permease A

FepA, the β-barrel ferric enterobactin (FeEnt) receptor and transporter located in the outer membrane (OM), transports the FeEnt complex into the periplasm. While it is widely accepted that FepA facilitates translocation of iron, its N-terminal globular domain occluding the FepA barrel complicates development of a working transport mechanism hypothesis. The globular domain creates a barrier to molecules other than FeEnt, while permitting transport of the siderophore. Together, the extracellular loops of the beta-barrel and the N-terminal globular moieties provide a ligand specific binding site. Although the globular domain is comparable amongst the various TBDTs, the beta barrel is “poorly conserved.” The varying composition of the barrel likely indicates a partial source of the observed specificity for a particular ligand. The specific transport of FeEnt suggests that the globular domain acts as a gate rather than a pore and movement against a concentration gradient indicates an active transport process.

Furthermore, a mechanism for specific coordinated movement of the globular domain implies a need for energy input. However, the OM is porous and therefore cannot sustain a proton gradient like that found

across the inner-membrane (IM), precluding conventional active transport and making IM proton motive force (PMF) the most likely energy source for active transport in the OM.

PMF favors hydrogen ion movement back into the cytoplasm, which ExbB and ExbD could harness to drive TonB motion (Zhai et al., 2003). Complicating this possibility is the periplasmic space (PS), which spans the distance between two membranes, makes utilization of this abundant energy source controversial and problematic. Considering these constraints, PMF requires an intermediary capable of coupling energy across the PS to OM proteins, a role likely fulfilled by the TonB-ExbB-ExbD complex.

### 1.11 TonB

TonB is central to the siderophore uptake process, evidenced by abolished transport activity in TonB deletion mutants (Bassford et al., 1976; Noinaj et al., 2010). Despite its well-documented participation, the specific role of TonB in the uptake mechanism is yet unknown. Particularly interesting questions being explored include the elucidation of any physical mechanism of interaction with ExbBD, as well as the TonB box and the precise mechanism of PMF energy transduction.

TonB is an inner membrane protein hypothesized to transduce energy to (OM) proteins that transport metals, mostly iron-binding proteins

and molecules (Noinaj et al., 2010). In 1976, TonB was first described as being part of a transport system in the paper "*Functional Organization of the Outer Membrane of Escherichia Coli: Phage and Colicin Receptors as Components of Iron Uptake Systems"* (Braun et al., 1976). The designation "ton" derives from phage T1 DNA dependence on TonA and TonB proteins for passage across the OM. It exists in Gram-negative bacteria, embedded in the cytoplasmic membrane, and consists of three functional domains. These domains include the cytoplasmic membrane-anchored N-terminal transmembrane domain, the flexible periplasm-spanning domain, and the TonB C-terminal domain that physically interacts with TBDTs (Jaskula et al., 1994; Larsen et al., 1994; Ollis et al., 2009; Postle, 1993). The Ton system is required for cell viability under iron-poor conditions. The C-terminal domain contacts OM transporters and has been crystallized (Braun, 2006). The crystal structure shows a three-stranded antiparallel β-sheet, positioned in front of two α-helices.

This region interacts with the TonB box domain of TonB-dependent OM transport proteins. The middle region of TonB is made up of two parts. Residues 103-149 are considered a flexible extension region to enable the C-terminal domain to span the periplasmic space and to find OM proteins. Residues 66 to 102 are mostly proline and glutamic acid followed by more proline residues alternating with lysine several times (Evans et al., 1986). Finally, an N-terminal membrane embedded region that spans the

cytoplasmic membrane as a helix, with 11 residues predicted in the cytoplasm. Although TonB has a membrane embedded region, a region that associates with OM proteins, and is capable of spanning the periplasm, transport of FeEnt does not occur without two other proteins (Jaskula et al., 1994).

TonB was previously isolated in association with two IM proteins, ExbB and ExbD, which are postulated to utilize energy available from the proton motive force. ExbB and ExbD interact with TonB and are postulated to function in energy transduction (Braun, 2006; Gresock et al., 2011; Skare and Postle, 1991). ExbB was first discovered while studying bactericidal proteins, to which mutations in *exbB* resulted in hyperexcretion of enterobactin (Guterman and Dann, 1973). Inner membrane proteins, ExbBD are homologous with MotAB, which serve as a stator and proton motive force-coupling unit for the flagellar motor protein complex. Several studies show the most homology between the two sets of proteins is found in the transmembrane domains. As concluded by Kampfenkel et al. (1993), sequence conservation likely indicates functional importance (Kampfenkel and Braun, 1993). Furthermore, having homology in the regions embedded in the IM supports claims of ExbBD utilizing PMF to deliver energy to TonB for transduction to TBDTs.

TonB-ExbBD, MotAB, and TolAQR are thought to harness PMF in a similar manner. To date, the most convincing evidence comes from

sequence homology with MotAB (Kampfenkel and Braun, 1993; Zhai et al., 2003). The arrangement of the Ton system proteins also suggests functional similarity among the three systems. Although the exact mechanism of energy transduction has not been conclusively shown, ExbBD appear to confer energy from the cytoplasmic PMF to TonB. The stoichiometry of TonB-ExbB-ExbD proteins in complex is not known, though experimental evidence supporting various models brings us closer to the answer. Some studies have provided evidence that there is a 1:2:7 stoichiometric ratios, however, there is still some disagreement among leading groups (Kaserer et al., 2008). There is also evidence that at least some of the TonB population acts as on TBDTs as a dimer (Chang et al., 2001; Freed et al., 2013; Koedding et al., 2004).

Homologous protein systems, like the proposed MotAB system and TolAQR, are also useful in understanding the roles of ExbB and ExbD (Zhai et al., 2003). For example, sequence homology between Mot, Tol, and Ton/ExbBD systems may indicate structural and functional homology. TolQR has 25% identity around 75% similarity with ExbBD. Up to 3 helical domains that span the cytoplasmic membrane are predicted within ExbB and the structure of ExbD appears to include one membrane spanning helix along with a C-terminal domain that extends into the periplasm (Garcia-Herrero et al., 2007). The proposed structural arrangement of

ExbBD is supported by several studies (Higgs et al., 2002a; Higgs et al., 1998; Khursigara et al., 2004).

TonB, ExbB, and ExbD likely interact physically based on evidence gathered in previous studies (Kampfenkel and Braun, 1993). In 1993 a protease protection study was performed to characterize the topology of TolQ (Kampfenkel and Braun, 1993). From that study, a three transmembrane domain model, in agreement with model for ExbB topology, was supported. In addition, the authors submitted, for the first time, that Ton system components, as well as, Tol system components, must interact in the cytoplasmic membrane. This conclusion was based on the homology between Ton and Tol systems and the fact that ExbB provided protection for the first 44 amino acids of TonB. Importantly, the membrane-spanning region of TonB is predicted to begin just after the 11$^{th}$ N-terminal residue. This evidence leaves only one possible conclusion, since the first 11 amino acid residues cannot span a very long distance. Therefore, ExbB must be closely associated with TonB for protease protection to occur. Vogel et al showed weak interaction between the C-terminal domain of ExbD and Glu-Pro region of TonB (Garcia-Herrero et al., 2007). The L132Q replacement in ExbD and also D25N in TonB resulted in loss of ExbD activity; suggesting that there is an important interaction between the periplasmic portion of ExbD and the transmembrane portion of TonB (Braun et al., 1996). This interaction

supports a model where ExbD influences periplasmic TonB movement similar to that seen in the MotA/B model (Zhai et al., 2003). In another study, residues involving both ExbD homodimeric interactions and TonB ExbD heterodimeric interaction were identified, in turn, suggesting that 2 ExbD are present in the functional complex.

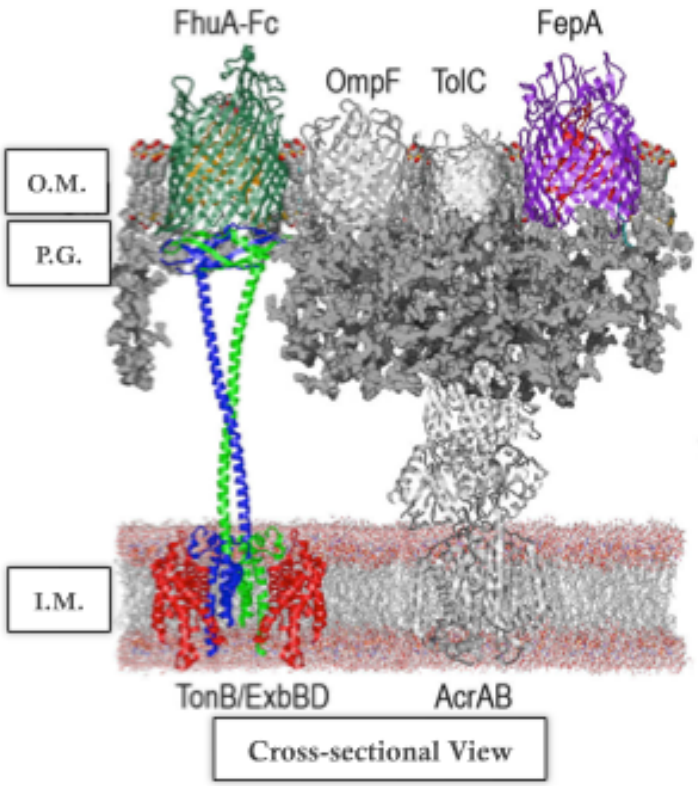


**Figure 1-3.** Published with the consent of the American Society for Microbiology. Kaserer, W.A., Jiang, X., Xiao, Q., Scott, D.C., Bauler, M., Copeland, D., Newton, S.M., Klebba, P.E., 2008. Insight from TonB hybrid proteins into the mechanism of iron transport through the outer membrane. J Bacteriol. 190, 4001-4016. Copyright American Society of Microbiology (2008).

Cartoon depiction of the TonB-dependent transport system. Outer membrane TonB-dependent transporters FhuA and FepA are shown in green and purple, respectively. TonB is shown as a dimer in blue and green, spanning the periplasmic space from the cytoplasmic membrane to the underside of FhuA. TolC and AcrAB are shown as a reference for the distance between the outer and inner membranes.

**Iron-siderophore Transport**

There are several models for ferric-siderophore complex uptake in Gram-negative bacteria (Ferguson and Deisenhofer, 2002; Ma et al., 2007; Noinaj et al., 2010). Generally, the ferric-siderophore must first bind to its respective TBDT. The specificity of this process is aided by the high affinity of these OM receptors for their ligands (Noinaj et al., 2010). Each of the TBDTs contains a beta-barrel comprised of the C-terminal portion of the protein and an N-terminal globular domain, which occludes the central portion of the barrel. A special sequence of amino acids, contained in the first 20 amino acids, is exposed upon ligand binding to the extracellular loops of the TBDT. This signal transmission is speculated to be a result of the receptors undergoing structural changes on the extracellular face of the OM that directly affect structural repositioning inside the N-terminal domain (Cadieux et al., 2000; Cadieux et al., 2003).

Further structural rearrangement of the tongue-like N-terminal domain is dependent on TonB interaction, facilitating transport of the ligand into the periplasmic space. A periplasmic binding protein finds the ferric-siderophore and binds it while in the periplasm. The journey of the ferric-siderophore complex culminates in transference from its periplasmic binding protein to its respective ABC-type permease, residing in the IM (Shea et al., 1991; Brickman and McIntosh, 1992).

## Clinical Relevance of TonB Research

The iron transport systems of Gram-negative bacteria are excellent targets for treating bacterial infection. Bacterial infections cause a wide range of diseases including the symptoms discussed earlier with regard to the various pathogenic forms of *E.* coli. Aside from the diseases induced by the efforts of bacteria during infection, the presence of bacteria triggers the host's immune system to sequester iron. The effects of the immune response can turn deadly if infection persists. One consequence of prolonged infection is the exponential growth of bacteria. Having more bacteria results in a larger, more drastic immune response.

# Chapter 2: Importance of Catecholate Siderophores During Infection

## INTRODUCTION

### 2.1 Rise of Antibiotic-Resistant Bacterial Threat

Bacterial infection is a serious threat to humans and livestock worldwide. In 2013, the Centers for Disease Control and Prevention released a detailed, 112-page report outlining the threat of antibiotic resistant infections in the US. The report estimates over 2 million illnesses were caused by antibiotic resistant infections alone. Of those antibiotic resistant infections, more than 23,000 cases resulted in human death (Guh et al., 2013). As antibiotic resistance increases, the need for novel and alternative treatments also becomes greater and more immediate.

Any threat or issue must first be identified if it is to be properly addressed. Our lab serves a critical role in identifying alternative strategies for the control and eradication of Gram-negative infections. As shown by many recent cases of infection, the realization of a world without effective antibiotics is happening now. Bacterial infections cause a wide range of diseases including the symptoms discussed earlier with regard to the various pathogenic forms of *E. coli*. Aside from the diseases induced by the efforts of bacteria during infection, recognition of triggering molecules from the pathogen, cause the host's immune system to sequester iron. The effects of the immune response can turn deadly if infection persists. With

the rise of carbapenem-resistant (CRE) bacteria, even mild infections can turn deadly without any recourse. Among these CRE bacteria are *Enterococcus faecium, Staphylococcus aureus, Klebsiella pneumoniae, Acinetobacter baumannii, Pseudomonas aeruginosa,* and various *Enterobacter* species. In consideration of these health concerns, the basic research pursued in my studies provides insight into an issue that will have far-reaching effects.

My first co-authored paper, “Role of Catecholate Siderophores in Gram-negative Bacterial Colonization of the Mouse Gut” article, shows the impact of catecholate siderophores. Specifically, it illustrates the effect of siderophores on *E. coli* virulence in a mammalian host system. This study comprehensively demonstrated the importance of iron as a virulence factor using a mouse model. Experiments were devised to test whether or not a siderophore, specifically FeEnt, was required for successful colonization of a murine host (Pi et al., 2012).

To achieve this end, the infectious ability of wildtype *E. coli* MG1655 was compared to that of newly mutagenized *E. coli* strains CAT0, CAT4, and CAT40. The gene for enterobactin synthesis, *entA*, was deleted in the strain designated *E. coli* CAT0. Since all native ferric catecholate transporters were still present in CAT0, catecholate iron sources could be readily utilized. CAT0 mutants were dependent on host iron sources and those chelators produced by competing bacteria because enterobactin is

the only siderophore secreted by *E. coli.* Conversely, in *E. coli* CAT4, genes were deleted for each of the receptors involved in translocation of ferric catecholate siderophores, including *fepA, cirA, fiu,* and *fecA*. This strain was unable to transport iron catecholate siderophores, though it was still capable of producing enterobactin under low-iron conditions. The characteristics of both CAT0 and CAT4 were present in the final strain used in this study, CAT40. This strain was unable to produce its own enterobactin or transport catecholate complexed iron.

## Materials and Methods

### 2.2 Bacterial Strains

All bacterial strains used were *E. coli*. Specific chromosomal deletions were made in strain BN1071 to remove all known OM iron-transporters (Ma et al. 2006). These deletions yielded target genes that included a chloramphenicol-resistance cassette, allowing a convenient method to transfer selected mutations to MG1655 using P1 transduction. Subsequently, a thermo-sensitive plasmid, pCP20, encoding a flippase gene was employed to remove the resistance cassette.

Multiple mutations were combined into MG1655 $str^R$ by introducing the deletions successively, removing all but the last cassette after each addition. The retention of a single chloramphenicol-resistance cassette helped to differentiate between our strain and prototrophic MG1655 $str^R$ in

competition studies. Strains were then grown in LB media containing appropriate combination of streptomycin 100 µg/ml), chloramphenicol (20 µg/ml), or ampicillin (100 µg/ ml). Bacterial isolation was achieved by diluting fecal samples in Tryptone broth and a small aliquot was spread on MacConkey agar plates with appropriate antibiotics.

### 2.3 *In vitro* Growth Rate Measurements

Overnight cultures grown in LB broth were subcultured into either new LB broth or iron-deficient MOPS minimal media (Smallwood et al., 2014). The absorbance of each culture was monitored every 30 min at 600 nm, beginning at t = 2hr and ending at t = 12 hr.

### 2.4 Mouse Colonization Studies

CD-1 male mice, at 6 weeks old, were administered drinking water containing streptomycin (5 g/L) for 24 hr to remove all endogenous gut flora present. The next day, the mice were not given food or water, in preparation for the study. Approximately $10^5$ colony-forming units (CFU) of *E. coli* strain MG1655 ($Str^R$ and $Nal^R$) and a mutant strain ($Sm^R$ and $Cm^R$) were delivered orally in a 1 ml 20% sucrose solution. Streptomycin-treated mice are more susceptible to colonization of the cecum, colon, and rectum (Pi et al., 2012). This allowed our laboratory to directly compare the amount of bacteria obtained from fecal samples to that of the colonized

portions of the intestinal tract. Post-ingestion, the mice were restored to their previous diet, including streptomycin-laced water.

Fecal samples were analyzed after 5 hr and 24 hr time points, every other day, for 15 consecutive days. Each sample was homogenized in Tryptone broth (1%) for serial dilution before plating on MacConkey agar including streptomycin (100 μg/ml) and nalidixic acid (50 μg/ml) to quantify the population of wild-type MG1655 strain. Fecal samples were also plated on MacConkey agar including streptomycin and chloramphenicol (30 μg/ml) to calculate the titer of the chromosomal deletion mutants. All colonization studies were repeated 2-3 times, with a detection limit of $10^2$ CFU/g feces.

### 2.5 *In vivo* Measurement of FeEnt

Mice studied for FeEnt content were sacrificed by $CO_2$ inhalation 12 days post-inoculation with the various strains of bacteria. The caecal mucus of 3 mice obtained from each group were collected and suspended in 200-μl $dH_2O$ and placed on ice. The samples were then subjected to centrifugation. The resulting supernatant was collected in 100-μl aliquots and 10-μCi of $^{59}FeCl_3$ was added. The solutions were incubated on ice for a total of one hour, allowing complexation by apo-enterobactin.

Sodium phosphate buffer (5-mM, pH 6.9) containing 0.25-μmols of $^{56}$FeEnt was added to samples and each was subjected to column

chromatography on a Sephadex LH20 column with 0.5 cm diameter and 10 cm height. Fractions were limited to 0.5 ml and were analyzed by spectroscopic and radioisotopic measurements. A Packard Cobra gamma counter was used to measure radioactivity counts from each fraction. Relative protein concentration was quantified using $A_{280}$ UV measurements. The samples were further determined to contain ferric enterobactin by visual confirmation of the distinctive red color and observation of an absorbance peak at 495 nm using spectroscopy.

### 2.6 P1 Transduction

100 µl of P1 phage lysate was added to an overnight culture of the donor strain, which was diluted 100-fold with fresh LB including 5mM $CaCl_2$ and 0.2% glucose and then shaken for 1hr at 37 $^{o}$C, 250 rpm. This mixture was then shaken an additional 1-3 hr until lysis occurred. Several drops of chloroform were subsequently added to the lysate, followed by centrifugation to remove cell debris. The resulting supernatant was decanted and stored at 4 $^{o}$C.

Recipient strains were grown in LB overnight, harvested using centrifugation, and resuspended in the same volume of LB with 100 mM $MgSO_4$ and 5 mM $CaCl_2$ included. This suspension was then mixed with either undiluted or diluted (1:10) P1 lysate, 100 µl each, and incubated for 1 hr at 37 $^{o}$C. To arrest the transduction process, 100 mM sodium citrate,

pH 5.5 was added and cells were spread on chloramphenicol (20 µg/ml) containing LB plates. PCR was used to verify chromosomal deletions in colonies observed post-transduction.

### 2.7 Siderophore Nutrition Assay

We inoculated and allowed desired strains to grow overnight. Subculture was performed with (1:100) 50 microliters of cells in 5 ml of Nutrient Broth and grown for 3.5 hours. Nutrient Broth Top Agar was melted and placed in a 42$^{o}$C water bath, such that the agar is in a liquid state, but not boiling. Afterwards, 3ml of Nutrient Broth Top Agar was added to glass test tubes and place in water bath. The appropriate antibiotics were also added to each test tube (ex. 6 microliters of Cm). Next, we added 6 microliters of bipyridal to test tubes and poured each test tube into a different well. Finally, 10 microliters of 50 µM FeEnt was loaded onto a paper disc and place a disc into each well. Incubate several hours in 37$^{o}$ C. The well plates were purchased from Falcon, product # 35 3224. Description: Tissue Culture Plate, 6 well, Flat Bottom with low evaporation lid.

### 2.8 Regeneration of Nickel-NTA Resin

Regeneration of nickel-NTA resin was performed and the purification of FepA was attempted using the regenerated nickel-NTA resin. The resin

was restored using the procedure outlined in the Qiagen handbook. The FepA to be purified was from a pass that was run mid-July. This pass was found to have all of the FepA from the last purification performed, since almost none of the FepA stuck to the nickel column and mostly all of the protein eluted in the pass. The nickel-NTA column was run this week using the regenerated nickel-NTA resin and the pass from the previous purification attempt. A continuous gradient of imidazole from 10mM-200mM in 50mM Tris/2% Triton was used to elute the protein from the column. 36 fractions of approximately 2 ml each were collected. An SDS-PAGE was run to check which fractions contained the desired protein, FepA.

### 2.9 Ethics Statement Regarding Animal Usage

The recommendations contained in the *Guide for the Care and Use of Laboratory Animals* distributed by the National Institutes of Health were strictly adhered to while performing all experiments. All protocols were reviewed and approved by the Institutional Animal Care and Use Committee of the University of Oklahoma. The University of Oklahoma has a documented statement of Animal Welfare Assurance with the Office of Laboratory Animal Welfare (IACUC approval # A-3240-01). This statement is effective until July 1$^{st}$ of 2013. To the knowledge of all researchers involved, there is no reasonable *in vitro* alternative to the animal

experiments performed. No discomfort was brought to the animals during the experiments and they were sacrificed by method of $CO_2$ asphyxiation, in accordance with the recommendations of the Panel on Euthanasia of the American Veterinary Medical Association.

## RESULTS & DISCUSSION

### 2.10 Construction of Mutants

Appropriate deletion strains were necessarily designed and created to begin the experiments. Mutations were added by P1 transduction to various host strains possessing a chloramphenicol cassette. These strains included *E. coli* OKN10, OKN2, OKN3, OKN5, and OKN9. Cells from *E. coli* OKN10 were used for P1 transduction of *ΔentA::Cm*.

Whereas CAT0 only required one round of P1 transduction, CAT4 required four separate transductions in succession. The deletions of *fecA, fepA, cirA,* and *fiu* were carried out by growing P1 lysates on OKN2::Cm, OKN3::Cm, OKN5::Cm, and OKN9::Cm successively (see materials and methods section). Chloramphenicol cassettes were removed in the first 3 transductions in CAT4, using pCP20 transformation. The final cassette from *ΔfecA::Cm* was inserted into the chromosome without further modification. *E. coli* CAT40 was made by combining elements from CAT0 and CAT4. In this case, the last chloramphenicol cassette was removed from the CAT4 *ΔfecA marker* and the lysate was added to CAT0 cells. The

resulting strains could be easily selected by growing the cells with chloramphenicol containing media.

### 2.11 Verification by SDS-PAGE

To verify the deletion of outer membrane catecholate siderophore-bound iron transporters, we used SDS-PAGE analysis. Cells from wildtype *E. coli* MG1655, CAT4, and CAT40 were fractionated using a French Press apparatus. The purified OM fractions were added to sample buffer, boiled for 5 minutes, and applied to a polyacrylamide gel containing sodium dodecyl sulfate (SDS). The gel was then subjected to electrophoresis until the dye-front cleared the bottom of the gel.

The resulting protein bands were identified using a molecular weight ladder that was run alongside the membrane fractions (shown in lane 4 of Figure 2-1). MG1655, corresponding to lane 1 in **Figure 2-1**, presented 3 bands not seen in lanes 2 or 3, which represented CAT4 and CAT40, respectively. The bands for Fiu, FepA, and Cir, appeared at 82 kDa, 81 kDa, and 71 kDa, as expected. OmpC/F and OmpA, at 37 kDa and 31 kDa, were used as reference bands. The three bands belonging to the deleted catecholate siderophore transporters are absent in lanes 2 and 3, thus confirming their successful deletion.

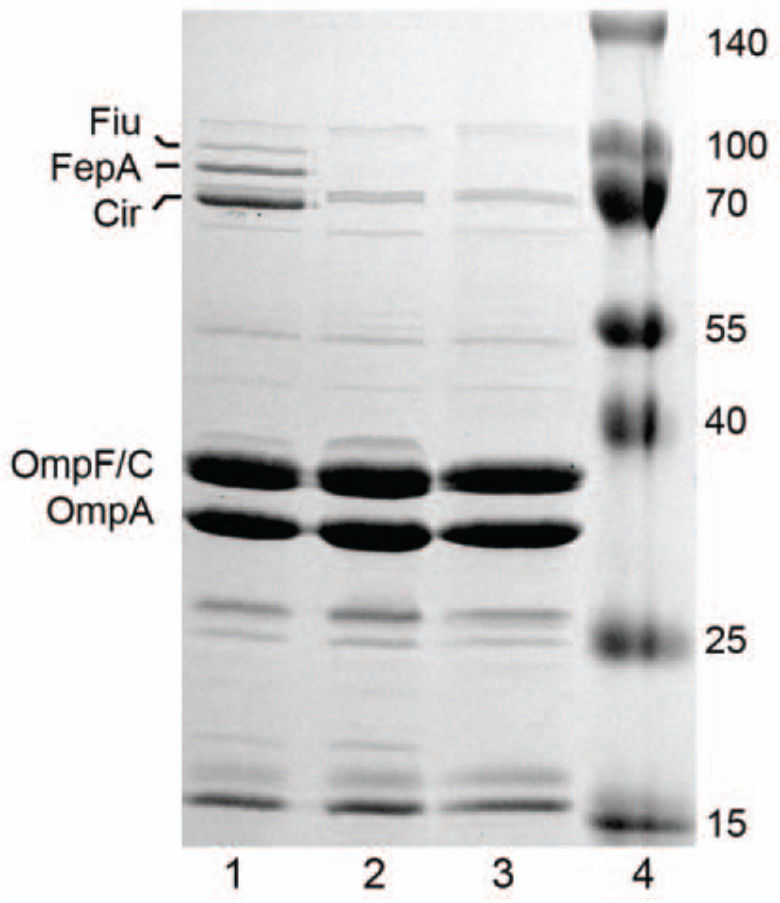


**Figure 2-1** (Pi et al., 2012). In the gel shown above, MG1655, CAT4, CAT40, and a molecular weight ladder appear in lanes 1, 2, 3, and 4, respectively. Bands for Fiu, FepA, and Cir are clearly present in the first lane, representing *E. coli* MG1655 wildtype. While in lanes 2 and 4, the bands are not observed. This gel clearly illustrates the successful deletion of targeted OM iron-siderophore transporters.

| Table 2-1 *E. coli* strains and plasmids (Pi et al., 2012) | |
|---|---|
| MG1655 | Wild type strain used in colonization study CGSC #7740 |
| MG1655 $Sm^r$ | MG1655 mutant with spontaneously acquired resistance to streptomycin |
| MG1655 $Sm^rNal^r$ | MG1655 $Sm^r$ mutant with spontaneously acquired resistance to nalidixic acid |
| BN1071 | F-, rpsL trp, B1, entA |
| BN1071/pKD46 | Initial strain used for Datsenko mutagenesis |
| OKN10::Cm | Donor for *entA* |
| OKN3::Cm | Donor for *fepA* |
| OKN2::Cm | Donor for *fecA* |
| OKN5::Cm | Donor for *cir* |
| OKN9::Cm | Donor for *fiu* |
| pKD3 | Template plasmid for Cm-cassette amplification |
| pCP20 | Thermo-sensitive plasmid for excision of Cm-cassette |
| CAT0 | MG1655 $Sm^r$ Δ*entA::Cm* |
| CAT4 | MG1655 $Sm^r$ Δ*fiu,* Δ*fepA,* Δ*cirA,* Δ*fecA::Cm* |
| CAT40 | Δ*fiu,* Δ*fepA,* Δ*cirA,* Δ*fecA,* Δ*entA::Cm* |
| ΔTonB | " " Δ*tonB* |

**Table 2-1** (Pi et al., 2012). Comprehensive list of all strains used and shows the genotype for each strain.

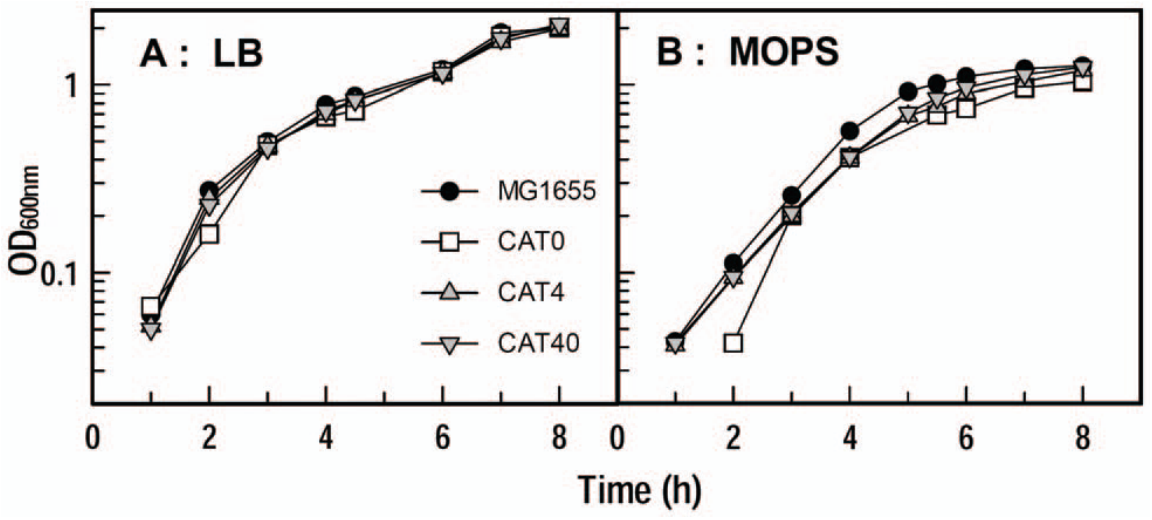


**Figure 2-2** (Pi et al., 2012). Plot showing the growth curves of strains MG1655, CAT0, CAT4, and CAT40 in both LB broth and MOPS Minimal Media.

## 2.12 Competition Studies

The next step was to determine whether the constructs had any growth defects. The growth of MG1655, CAT0, CAT4, and CAT40 was monitored in LB broth and in MOPS Minimal Media over an 8 hour time period. An absorbance reading taken at 600nm was recorded every hour. The resulting curves are shown **(Figure 2-2)**. These curves provided a baseline for the performance of each strain. There was very little difference between the four strains in iron-deficient media growth experiments. These conditions were analogous to the low iron supply found in the mouse gut.

The findings, depicted in **Figure 2-2**, indicated that all strains were capable of obtaining sufficient amounts of iron to support growth under iron-limited conditions. Furthermore, they illustrate the performance of each strain in a non-competitive environment. No difference should be observed if there is no dependence on siderophore mediated iron uptake. An iron-replete environment would not present a challenge to any of the strains. However, it was hypothesized a mouse-gut environment lacking much free iron would cause competition between bacterial strains for the host's supply. In each competition experiment, the wildtype strain produced enterobactin and competed for resultant ferric enterobactin. Due to the high number enterobactin molecules secreted and its extraordinary affinity for iron, any available ions were immediately scavenged and

sequestered. This setting created a situation where the only available iron was catecholate bound.

Competition experiments were performed and analyzed by counting colony-forming units recovered from fecal samples over a 15-day period. Mice were either untreated or treated with streptomycin to eliminate endogenous gut flora prior to inoculation with test strains. In each case, wildtype *E. coli* MG1655 was introduced along with either *ΔtonB*, CAT0, CAT4, or CAT40 for competition studies (results shown in **Figure 2-3**). The first frame in **Figure 2-3** shows that the TonB- strain is unable to compete with wildtype MG1655 and after 5 days, *ΔtonB* cells present in such low concentrations that there was no reasonable argument to collect further data points. The data from *ΔtonB* cells suggested the strain was unhealthy and unable to bring in enough nutrients to colonize gut tissues. Although data from the *ΔtonB* strain is shown in panel one, it was tested against MG1655 in a separate experiment from CAT0. Generally, strains deficient for TonB expression show lower viability under iron-starvation conditions, so it was not surprising to observe insignificant colony counts after a few days. Still it was necessary to establish the impact of a functioning TonB on cell viability. Without functional TonB-dependent systems cells are unable to colonize immune competent mouse hosts.

In panel 2 of **Figure 2-3**, MG1655 and CAT0 strains show comparable growth, with CAT0 showing a slightly lower number of

colonies, likely due to its inability to create its own siderophores. Lacking the ability to secrete its own siderophores, CAT0 could only compete for the siderophores secreted by MG1655. When siderophores are secreted, they diffuse into the surrounding media. Diffusion rates are much lower in the mucosal layer of gut tissues, so one may expect higher concentrations of ferric enterobactin local to the secreting bacterium. This FeEnt would likely be imported before it was able to diffuse far enough for an encounter with a competing organism. Which causes the CAT0 strain to compete directly for siderophores made by MG1655.

Notably, the number of colony forming units started to decrease over time for both strains and the ratio gap between MG1655 and CAT0 narrows. This trend is explained with consideration of iron as a limited resource. As the bacteria use up their limited resource there is less to scavenge and less to compete for. Eventually, both strains should have an equal likelihood of finding FeEnt and they should contribute equal amounts of colony forming units. All of these considerations aside, the competition between MG1655 and CAT0 showed that secretion of enterobactin alone is not necessary for virulence.

The second frame shows MG1655 outcompeting CAT4 by a large margin and reduction of CAT4 growth. The blue curve, indicating the number of CAT4 colony forming units, trends downward after day 1. In contrast the red curve representing wildtype trends upward and starts to

level off just above 5 log CFU after day 8. Since CAT4 cannot import catecholate-bound iron sources, all of the secreted enterobactin was available for utilization by MG1655. Ultimately, the death of outcompeted cells would also contribute to the nutrient supply for MG1655; although, panel 3 and another factor must be considered. In Panel 3, results for MG1655 and CAT40 are shown. The results are similar to panel 1 for the first 8 days; however, at day 9 numbers of wildtype and CAT40 colony-forming unit counts start to diverge. The colony counts for wildtype trend upward and CAT40 counts trend downward. Also, unlike panel 2, the wildtype trend is not as steep, which indicated another variable was likely to be involved.

Overproduction of enterobactin was considered, since iron transport mutations caused overproduction of enterobactin *in vitro*. An experimental study showed that *exbB* mutations resulted in hyperexcretion of enterobactin (Guterman and Dann, 1973). Since ExbB is known as an essential component of the TonB-dependent transport system. This prompted an investigation into the concentration of enterobactin secreted by the colonizing strains.

### 2.13 Quantification of Secreted Enterobactin

Consideration of the competition experiment results prompted the testing of enterobactin concentrations present in the mouse gut system.

Elevated levels of enterobactin were found in the gut mucous of mice inoculated with CAT4, shown in **Figure 2-4**. These results suggested that the upward trend observed in **panel 2** of **Figure 2-3** was not only due to the lack of competition for catecholate-bound iron, but also due to the excess enterobactin contributing to the available iron pool. Synthesis of enterobactin is an energy-intensive process that costs cells valuable resources. It is only because of a "sensed" benefit that bacteria devote resources to this process.

The histogram in **Figure 2-5** shows levels of enterobactin production *in vivo* for each strain. The amounts of protein found in mucosal samples from the mouse gut were used as a standard for normalizing enterobactin levels for comparison relative to each strain. The CPM enterobactin was divided by the $A_{280}$ reading.

Under normal conditions of infection, there are many more bacteria in the gut and each species/strain secretes siderophores, which can be used by *E. coli*. These conditions allow *E. coli* to avoid production of its own siderophore, until the competition becomes fiercer. At that point, it is much more advantageous to synthesize enterobactin. The fact that enterobactin is not reused after is of no consequence to the bacteria because it is the only way to retrieve enough iron to sustain a habitable environment. Essentially, Raymond's "American approach" has enough of a competitive edge that degradative release of iron is more beneficial than

conservation of resources. Furthermore, the point that *E. coli* does not synthesize any reusable siderophores of its own may be considered. It is conceivable that evolutionary pressure has pushed *E. coli* toward a single iron chelator due to its high affinity and efficiency.

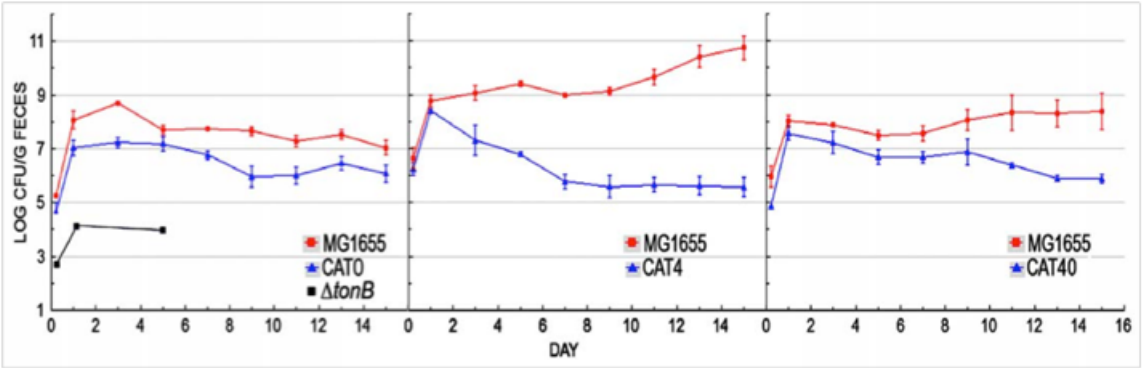


**Figure 2-3:** Wildtype MG1655 appears in the figure above, along with CAT0 and *ΔtonB* mutant in the first panel. The second panel features data from wildtype MG1655 competition with CAT4. Finally in the third panel, data from MG1655 competition with CAT40 are shown. As previously noted, CAT0 does not produce enterobactin, CAT4 has no iron transporters present in the outer membrane, CAT40 has no iron transporters and is unable to produce enterobactin, and the ***Δ****tonB* strain does not express TonB protein.

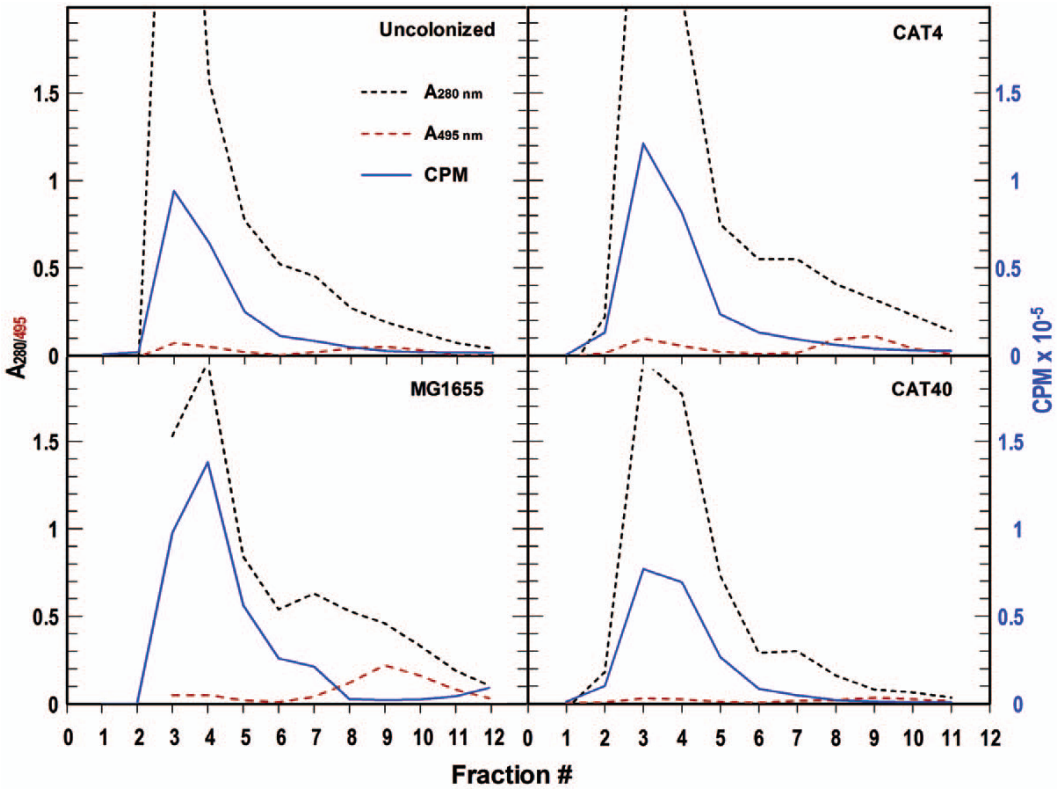


**Figure 2-4** (Pi et al., 2012). *In vivo* quantification of enterobactin was achieved by evaluating caecal mucus from mice, that were inoculated on days 0 and 12 and either colonized or uncolonized b MG1655, CAT4, or CAT40. Five mice were used from each experimental group yielding a combined sample of 100 microliters, after discarding debris. 10 mCi of $^{59}FeCl_3$ was added to the sample, which was put on ice and chromatographed afterwards.

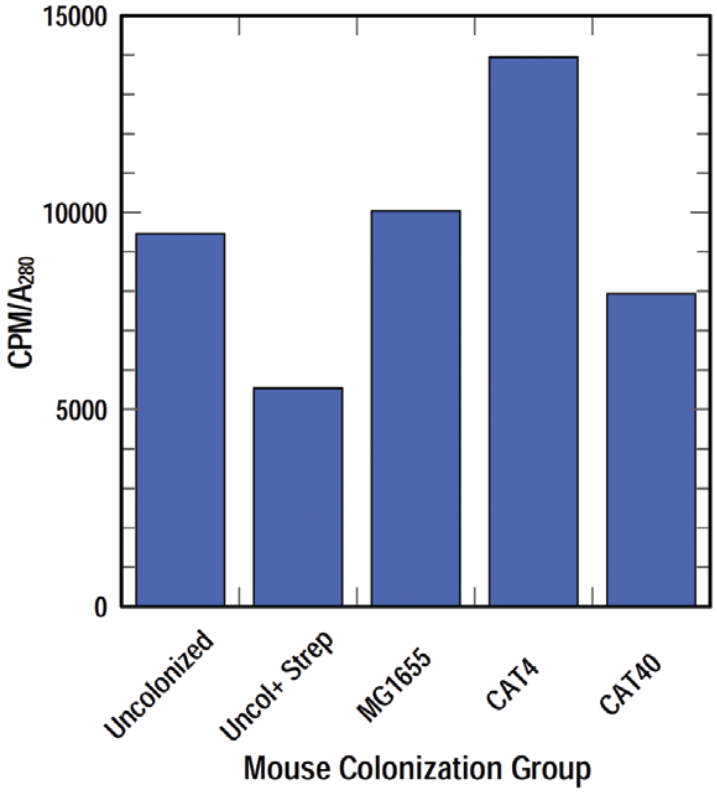


**Figure 2-5** (Pi et al., 2012). Histogram of quantified levels of enterobactin production *in vivo*. Caecal samples from 5 mice from each test group were combined and analyzed for enterobactin concentration, using radioisotopic quantification.

# Chapter 3: GFP-TonB Fusion Studies

## 3.1 Introduction

Like all known Gram-negative bacteria, *E. coli* acquires iron-siderophore complexes using TonB-dependent outer membrane transporters (TBDTs). As discussed in Chapter 1, these transporters require TonB, likely due to its proposed ability to transduce energy from the PMF to the outer membrane. In order to achieve this proposed transduction, TonB is hypothesized to interact as a TonB–ExbBD inner membrane complex, conferring a physical force onto the TonB box of TBDTs and initiating the energy-dependent portion of the siderophore transport process. Presented in this chapter is evidence of ExbBD participation in PMF energy transduction through TonB and characterization of TonB motion.

## 3.2 Fluorescence

According to the IUPAC Gold Book, fluorescence is “luminescence which occurs essentially only during the irradiation of a substance by electromagnetic radiation.” Luminescence in the sense relevant to this work is the spontaneous release of a photon from an electronically excited species as it returns to a ground state. The emission lifetime of fluorescence occurs in less than 10 ns and is often confused with

phosphorescence, which has a lifetime range of milliseconds to full seconds (Albrecht, 2008).

### 3.3 Green Fluorescent Protein

Green fluorescent protein (GFP) played a critical role in our lab's work to improve understanding of TonB involvement in siderophore transport. In *Energy-dependent Motion of TonB in the Gram-negative Bacterial Inner Membrane*, GFP fusion proteins were used to infer steady state TonB motion. In microscopic studies, GFP-TonB fusions revealed the localization of TonB during FeEnt, raising new questions about the role of TonB in energy transduction. A short review of this powerful tool is warranted, given its proven utility and central role in our investigation of TonB.

Researchers, Morin and Hastings coined the term "green fluorescent protein" in 1969; several years after Dr. Osamu Shimomura first isolated it along with aequorin (Shimomura, 2009). Together the two proteins confer the glowing green fluorescence exhibited by *Aequorea victoria*. In 1979, Dr. Shimomura characterized the chromophore comprising the helix, centered inside the beta-barrel of wild-type GFP. In the early 1990s Dr. Roger Tsien took Dr. Shimomura's work even further and revolutionized the field of biochemistry with new mutant GFP, possessing various beneficial characteristics (Tsien, 1998).

Since the use of GFP in *C. elegans,* many new GFP derivatives were created. We used SuperGlo GFP (sg-GFP) in our studies of TonB motion through monitoring TonB-GFP fusion proteins for changes in fluorescence polarization. The protein sg-GFP has substitutions at F64L, S65C, and I167T. It was obtained from from QbioGene, Irvine, CA was used to create the constructs pTpG, pGT, pGGT, pGBT, and pGBΔ40T.

## Materials and Methods

### 3.4 Fluorescence Anisotropy

Isotropy is derived from Greek roots of *isos* and *tropos*, roughly translated as “equal” and “way”, respectively. Taken together, the word’s meaning is defined as “uniformity in all orientations.” Anisotropy (R) is therefore the opposite of isotropy and describes an inequality amongst all possible orientations. With respect to small molecule/protein tumbling events, anisotropy is a measure of bias toward a particular orientation. With regard to the probability of fluorophores being maximally affected by an excitation beam, the IUPAC Goldbook states that “anisotropy is the existence of transition moments for absorption and emission that lie along specific directions within the fluorophore structure.” In this case, more plainly, anisotropy indicates the extent of restricted motion experienced by a given molecule.

Measurements of the fluorescence polarization (FP) or the fluorescence anisotropy (FA) of fluorescent molecules are achieved by preferentially and selectively exciting randomly oriented fluorophores. This is achieved by induction of an “oscillating electric moment” that results in photon absorption, according to the IUPAC Goldbook. The amount of absorption is based on the transition moment **M** and the distance it samples, from the initial dipole moment (i) to the final dipole moment (f), over the time it takes to absorb/excite the fluorophore. The probability of photon absorption increases as the cosine square of the angle between the $\mathbf{M}_{if}$ and the propagating electric field tends toward 90 or 180 degrees.

In summary, there is a difference in the extent to which a fluorescent molecule is excited as it reorients in solution. Those whose transition dipole moment is aligned with the incident linearly polarized light, of the proper excitation wavelength, are selectively excited. During such phenomena, fluorophores absorb incoming radiation to the extent that their dipole moments align with the electric field of the excitation beam.

Fluorescence anisotropy and fluorescence polarization measure the same phenomenon, however, FA is the preferred comparison of light components. By accounting for both perpendicular planes, FA represents the ratio of the parallel component of light to the total emitted light present (Eq. 2.1). This is in contrast to FP, which only accounts for one perpendicular plane (Eq. 2.2).

**Equation 3.1**

$$P = (I_{VV} - I_{VH}) / (I_{VV} + I_{VH})$$

**Equation 3.2**

$$R = (I_{VV} - I_{VH}) / (I_{VV} + 2I_{VH})$$

**Equation 3.3**

$$R = (I_{VV} - GI_{VH}) / (I_{VV} + 2GI_{VH})$$

The resulting fluorescence intensity is proportional to the amount of light absorption experienced by the fluorophore. Molecules with transition dipole moments aligned with the excitation beam absorb the most light and therefore emit with the highest intensity. Those fluorophores with transition dipole moments exactly perpendicular to the excitation beam are not directly excited and therefore have minimal emission intensity. Further, the emitted light retains the angle of the dipole moment at the time of emission. Detectors are used to record the intensity of emitted light. One detector collects fluorescence intensities from light emitted in parallel with the incident beam and another detector collects fluorescence intensities of light emitted in perpendicular to the incident light. This is achieved with a beamsplitter located in the emission light path just before couplers for each

detector. The dipole moment is considered depolarized if the excited fluorophore reorients before emission. Quicker reorientation of the molecule, results in greater depolarization, or greater isotropy, since it should therefore sample non-parallel orientations more frequently.

Generally, one may use the equation 2.1 to calculate the anisotropy value (R) of a specific molecule in a given medium. In this equation, $I_{VV}$ is the intensity of emitted fluorescent light, parallel to the excitation beam and $I_{VH}$ represents the components perpendicular to the excitation beam. There are a total of 3 components of light, the X, Y, and Z planes, to consider regarding spatial orientation of a given fluorophore in reference to the excitation beam. Since the experiments presented in this chapter were performed with linearly plane-polarized light, only one plane contributes to the parallel component and two planes contribute to the perpendicular component. Hence, a coefficient of 2 is required for the $I_{VH}$ component.

The 3 planes can further be broken down into their positive and negative reflections. Moreover, the Z plane allows four extra components, which include the positive and negative reflections of ZX and ZY. Altogether, there are 10 components, which contribute to the maximum anisotropic value of 1.0, or R = 1.0, representing the total emitted light. Dividing the total light by the number of components yields a value of 0.1 for each component. A total of 4 components represent the excitable plane, $Y^{+/-}$ and $YZ^{+/-}$ or $X^{+/-}$ and $XZ^{+/-}$, and the remaining 6 vectors comprise

perpendicular planes. With this consideration, 0.4 is the highest possible anisotropic value for an isotropic population of fluorophores. Alternatively, one may recall that the probability of absorption is proportional to the $\cos^2\theta$. Given this relationship, the population of transition dipole moments, capable of excitation, is oriented such that their angles oscillate around vector Z.

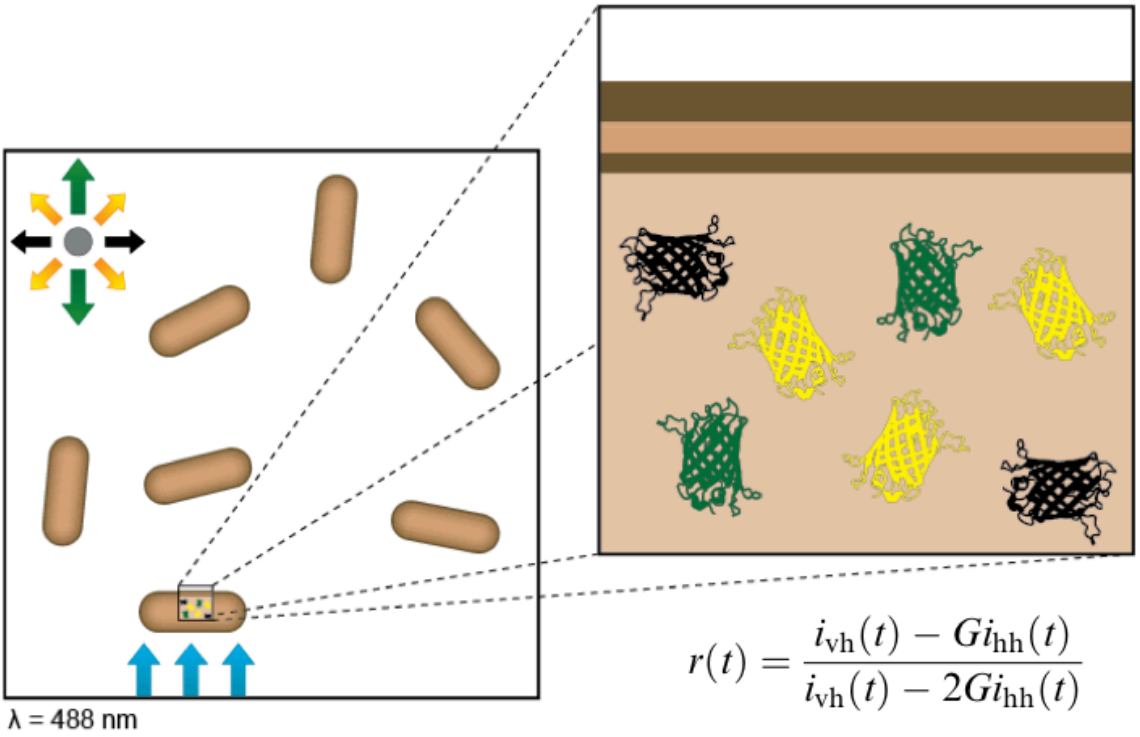


**Figure 3-1** Simplified representation of *E. coli* pTpG control. Linearly polarized light excites GFP oriented parallel to the incoming beam. Fluorescent molecules perpendicular to the light are not excited. In this case, separate detectors gather parallel and perpendicular light. Using the equation above, one can find the anisotropy (r) of the fluorescent molecules within the field of excitation. An average R-value is calculated for each strain and compared.

One important value, worth consideration is the so-called “magic number,” where anisotropy is lost. An average $\cos^2\theta$ equal to $54.7^O$ is one-third the total possible excitation angles. Recalling equation 3.3, a parallel component equal to one third of the total fluorescence causes the numerator to go to zero. In other words, if on average a fluorophore reorients by $54.7^O$, the fluorophore will exhibit depolarization. Additionally, a $\cos^2\theta$ greater than $54.7^O$ results in a negative anisotropy.

The term G symbolizes a correction factor for discrepancies between the emission channels for $I_{VV}$ and $I_{VH}$. These differences are intrinsic to the instrumentation and can vary from experiment to experiment, depending on the source. Possible R-values range from 0 to 1 in oriented samples and 0 to 0.4 in random non-oriented samples. An R-value of 0 signifies completely isotropic motion, while a value of 1 represents completely anisotropic motion.

In order to obtain an anisotropic value, at least two orientations of the molecule being studied must be identified and differentiated. Furthermore, it is essential to monitor the change in orientation. Fluorescence polarization is a technique that achieves both and is based on the specific activation of fluorophores by polarized light. Fluorophores in parallel with the excitation beam are excited and undergo a fluorescence emission shortly thereafter. During this nanosecond time frame, before their fluorescence emission, the fluorophores have an opportunity to

reorient. If reorientation occurs quickly, the parallel fluorescence intensity ($I_{VV}$) will decrease and the anisotropic value will tend toward 0. Conversely, a slow reorientation would result in a value closer to 0.4, non-oriented molecules and 1 for oriented molecules.

### 3.5 General Instrument Setup

In our experimental scheme, plane polarized light was directed onto a sample chamber containing living *E. coli* cells adhered to the bottom surface of the chamber. This incident light of wavelength 488 nm was used to excite fluorophores harbored by the cells, which then emitted light at 519 nm. Splitting the emitted light and monitoring it in two separate channels facilitated fluorescence polarization measurements.

Additionally, two separate detectors were required to observe and record the fluorescence intensity of each channel. The ratio of intensities between these channels was used to establish the anisotropic value, and thereby the relative motion of our fluorophore of choice. Using this technique, our lab monitored green fluorescent proteins attached to the N-terminus of TonB, allowing us to infer the anisotropy of TonB.

### 3.6 Sample Preparation

Custom sample chambers were constructed from plastic cuvettes and “clean” glass coverslips. All coverslips needed to be completely free

from organic substances and other foreign particles, requiring sonication in an acetone bath for 30 min, followed by 3 washes with Millipore $dH_2O$ and sonication in NaOH for 30 min. The coverslips needed to be thoroughly rinsed of NaOH, 5 times with $dH_2O$, before the final 30 min sonication in $dH_2O$. After drying with compressed air, the coverslip was adhered to a custom-cut cuvette using an epoxy and allowed to dry 20 min before use. Subsequently, 300 µL of poly-L-lysine hydrobromide, MW 225.19 (8.33 mg/mL; 37 µM) was added to the chamber for 15 min and discarded.

Cell samples were taken from iron-deficient MOPS media cultures in the late-exponential growth phase, to ensure full induction of our proteins of interest. A 1 O.D. sample of the cells was sedimented and resuspended in TBS. A 100-µl volume of these cells was added to the sample chamber and allowed to adsorb to the coverslip for 10-15 min, then rinsed twice with TBS, pH 7.0, to remove weakly adsorbed bacteria. Finally, 500 µl of TBS containing 0.4% glucose was added to the chamber.

Once in focus on the microscope stage, the sample was allowed to settle for a 10 min period because of the change in distance resulting from oil compression between the coverslip and objective. To minimize the variation in polarization measurements between samples and increase the reliability of comparisons drawn from raw data, only sample measurements gathered on the same day were analyzed together. Trends were then evaluated among the overall R-values for each day. By analyzing the

change in anisotropy of the samples, the issue of light scattering due to the cell membranes was alleviated.

Differences in temperature, detector alignment, and laser intensity could have contributed to variation in measured light intensities between days. Variations in the R-value between samples were a result of differences in cell morphology, pixel selection, reproducibility of focal plane. During the study, all efforts were made to minimize the effects of each variable. Once the cells were ready for viewing, the objective was again focused and the viewing field was scanned. Once the field was scanned, fluorescence intensity was observed on the computer monitor and assessed for scan quality. If the fluorescence intensity imaged matched the area on the camera monitor, spots were chosen to gather transient polarization data. If not, the stage was reset and the field was scanned again.

### 3.7 Signal-to-Noise Ratio

The background fluorescence values were negligible, with values less than 10 a.f.u. in areas without cells. Data was collected from single pixels with initial intensities representative of the average a.f.u. for the particular cell being measured. Each pixel represents an area of 0.01 $\mu m^2$. The pixels selected for analysis were usually chosen from areas near the center of each cell imaged. Data from the $I_{VV}$ and $I_{VH}$ pathways was

collected, generating hundreds of individual intensity measurements over a period of 5-15 s.

### 3.8 Cell Selection

Cells were chosen based on several criteria including cell shape, apparent growth stage, proximity to surrounding cells, quality of fluorescence scan image, extent of immobilization, and orientation with respect to the glass coverslip. Cells with more round morphologies comprised a small portion of the sample population and were generally excluded from measurements. The decision was made to avoid non-representative cells, although, several measurements were taken on the round cells prior to that decision. Those measurements appeared similar to measurements obtained from average cells, however, a separate comparative statistical analysis was not performed.

### 3.9 Variability in Polarization Measurements

A noticeable difference in anisotropy is observed when comparing the average R-values of ExbBD(-) and pGT strains, or even the same strain to itself, from day to day. These variations can be attributed to several factors affecting the individual experiments. Some of the contributing factors include cell shape, pixel selection, sample size, detector alignment, reproducibility of the focus, laser intensity, the

concentration of fluorescein used to obtain the G-factor, and temperature. All of these factors were considered and an attempt to minimize each of their effects was made during the study.

### 3.10 Cell Morphology and Pixel Selection

The cell's shape may vary in thickness from one position to another depending on how round the cell is. Not all of the cells have identical morphologies, so an attempt was made to select cells of comparable size and shape within the same sample. To avoid biasing the results, only cells with an excessively round shape or those that were present in large clusters were avoided. Pixel selection refers to the point on each cell selected for sampling. The middle of each cell was selected for consistency, since this area tended to possess the highest intensity.

### 3.11 Sample Size

Sample size was considered for each experiment to improve statistical analysis. Experiments done on the same day included similar numbers of samples measured. Statistical comparison of equal sample amounts using Student's T-test is generally viewed as more accurate. Experiments were performed with this convention in mind.

### 3.12 Detector alignment

Two detectors were used to collect the light intensity emitted from the samples. The alignment of the fiber optic cable, which funnels the light beam into the detector, may change slightly due to vibrations in the environment. If the light path or intensity of one detector (or both to varying extents) is affected, the R-value can be impacted. The G-factor allows us to account for intrinsic bias in the light paths and normalize the difference in intensities between the two detectors.

Reproducibility of the focus was also considered. The microscope objective must be refocused for each sample, so minor variation may occur during data collection. If the objective focus is different from sample to sample the point of laser focus will also vary. This is not favorable because a small, focused beam is ideal for interrogation of a single spot on the cell. Whether the laser focus is slightly above or below the cell's surface, the beam spot will be larger and the intensity of emitted light will be impacted.

### 3.13 Variations in Light Path

The laser intensity at the stage varied slightly from day to day due to losses in efficiency throughout the optical path. Small vibrations may affect the fine-tuned position first coupler, which sends light into a fiber optic cable and to the sample.

### 3.14 Fluorescein Concentration

Fluorescein is used to obtain the G-factor. Since it is a small, highly mobile fluorescent molecule, its R-value should be very close to 0. After collecting intensity data on fluorescein, we use the intensity difference between the detectors to determine the G-factor, which allows the normalization of results obtained by the detectors. Approximately 10 µmols fluorescein was added to the sample chamber after cell measurements were obtained. Polarization measurements were then taken for the freely diffusing fluorescein molecules. The anisotropy values for the fluorescein served as a baseline from which a G-factor could be derived and used to calculate the anisotropy of the cell samples.

### 3.15 Bacterial Strains and Plasmids

OKN3 (ΔfepA), OKN1 (ΔtonB), OKN13 (ΔfepA, ΔtonB), and BN1071 (F-, entA, pro, trp, B1) from which they were created, were used as host strains for pTpG, pGT (Kaserer et al., 2008). These plasmids were derived from the low-copy vector pHSG575. The plasmid pTpG expresses cytoplasmic GFP, while pGT expresses the GFP-TonB fusion protein. The hybrid protein expressed by pGT possessed wild-type ferric siderophore uptake and colicin sensitivity (Kaserer et al., 2008). Additionally, OKN3/pGT and OKN13/pGT with pFepAS271C were transformed. The

plasmid pFepAS271C, is a pUC18 derivative which expresses fepAS271C controlled by its natural fur promoter ((Ma et al., 2007)).

### 3.16 Fluorescence Microscopy

Strains were grown in LB broth at 37 $^{o}$C overnight, followed by a 1:100 subculture into iron-deficient MOPS minimal media. Both media contained appropriate antibiotics, including streptomycin (100 µg/ml) and chloramphenicol (20 µg/ml). After subculture, the strains were shaken at 37 $^{o}$C for 5-6 hr until they reached late log phase. A 1 O.D. aliquot, usually 1 ml, was taken from the MOPS culture and washed with Tris-buffered saline (TBS).

### 3.17 *In vivo* Cysteine Labeling

Experiments involving fluorophore labeled BN1071/pGT/ pFepAS271C, required additional steps. In that instance, cells were washed once, followed by a resuspension with NaHPO4 buffer (50 mM, pH 6.5). This same solution allowed the engineered cysteine, FepA S271C to be specifically labeled using either Alexafluor 555 (AM555) or Alexafluor 680 (AM680) maleimide. The fluorophore was added to 5 µM and incubated with cells at 37 $^{o}$C for 15 min. One wash was performed followed by resuspension with $NaHPO_4$ (50 mM, pH 6.5) buffer.

### 3.18 Confocal Studies at the University of Oklahoma

Confocal fluorescence microscopy was used for the many benefits offered over the conventional fluorescence microscope available in our laboratory. Such benefits included an upgraded software package, which controlled various microscope functions, such as zoom and optimization settings for the lasers. Although, *E. coli* samples are rather small scale, the confocal microscope offered Z-stacking that allowed us to capture slices of the bacteria at different depths.

Cells from strain OKN3 *fepA*S271C/pGT were grown in iron-deficient MOPS minimal media, labeled with either AlexaFluor maleimide 555 or 670. The latter dye was favored, since its absorption spectra was further from the tail-end of the GFP emission spectra, ending around 536 nm. Additionally, LacY-GFP fusions, expressed from a plasmid in the OKN3 host strain, were prepared. Images were captured using an Olympus 122 FluoView FV1000 (Olympus American, Inc; Center Valley, PA). All cell images were captured using a 100X objective.

### 3.19 Confocal Studies at Kansas State University

Fluorescence microscopic experiments were carried out on a Zeiss LSM 700 confocal laser-scanning microscope. Cells harboring a TonB N-terminus linked GFP and a single cysteine substitution at residue S271C in FepA, were labeled with AlexaFluor 546 and observed microscopically for

changes in fluorescence after introduction of ferric-enterobactin. GFP was excited with 488 nm laser light and AlexaFluor546 was excited with 555 nm laser light consecutively, with a total scan time of 20 seconds.

The images were taken using a 100X magnification objective. Cells were grown in iron deficient MOPS minimal media for 5-6 hours, labeled at an OD of 1.0, and resuspended in PBS (pH 7.4). Cells were adhered by poly-L-lysine and viewed in an 8 well micro-slide manufactured by Ibidi. Approximately $5^{x}10^{8}$ cells (120 microliters of $5^{x}10^{9}$cells/ml) were observed before and after addition of 10nM FeEnt (20 microliters 500nM FeEnt) into 200 microliters of PBS (340 microliters total). Images were collected over a time course of 22.5 minutes.

### 3.20 Anisotropy Studies: Laser and Light Path

Fluorescence polarization measurements were obtained using a custom-built sample-scanning microscope. A *Thor Labs* floating table, the legs of which possessed air cushions with pneumatic feedback for stabilization, supported the instrument. The light source and optics associated with the excitation beam path were set up on the floating table. A darkroom curtain surrounded the instrument setup and both the excitation and emission pathways were enclosed in lightproof *Plexiglas* to help shield the sample chamber from environmental light.

### 3.21 Light Source

We used an argon ion laser source with fan cooling in our anisotropy experiments. An excitation light beam of wavelength 488 nm was attained with this source, a prism, and an aperture to block unwanted wavelengths. After selecting a wavelength, we needed to adjust the circularly polarized light to plane-polarized light. We achieved plane-polarized light by modulating a quarter-wave plate, placed in the beam path. Plane polarized light allowed biased excitation of fluorophores parallel to the excitation beam.

### 3.22 Excitation Beam Optics

The beam was directed into a coupler, using a 10x lens, which funneled light into a single-mode fiber optic cable of a 3.3-μm diameter. This cable was then connected to a second coupler, allowing the beam to exit into the backside of the microscope. Before sending the light into the microscope, however, the light was first collimated with a second 10x lens and sent through a half-wave plate. The degree selected on the half-wave plate allowed us to control the angle of the plane-polarized light hitting the sample.

### 3.23 Microscope

The microscope was based on the Nikon TE-200 inverted microscope platform and included a nano-positioning stage with feedback for precise sample location. The intensity of the light beam was easily modified by the addition of neutral density filters placed just before the first coupler. A CCD camera was placed along a selectable emission beam-path, in order to more easily calibrate the microscope and associated optics for polarization measurements. The CCD camera path was selected by positioning a “flip-up” mirror after the exit port for the emission path. When this mirror was upright, it directed light from the focused sample to the camera.

### 3.24 Metabolic Inhibitor Exposure

Cells harboring the *gfp-tonB* fusion gene, pGT, were exposed to energy poisons to determine the energy-dependence of TonB. The microscope was focused on a single immobilized cell for each group of polarization measurements. After the first intensity measurements were taken, an effective concentration of each metabolic inhibitor was added to the sample chamber containing 500-µL of PBS.

The final concentration for the inhibitors was 1mM for carbonyl cyanide m-chlorophenyl hydrazone (CCCP), 2 mM for dinitrophenol (DNP), and 10 mM for sodium azide. The poisons were allowed to equilibrate in

solution for a period of 10 minutes before the polarization was again measured and recorded. Administration of the energy poisons was made to the entire sample chamber; thus disallowing more than a single pair of measurements per sample preparation.

## Experimental Results and Discussion

### 3.25 Characterization of TonB-GFP

The GFP-TonB hybrid was studied using confocal microscopy. Fluorescence microscopic characterization of GFP-TonB hybrid proteins exhibited compartmentalized localization of the GFP-TonB fluorescence, as shown in **Figure 3-2**. Restricted movement has previously been reported for OM proteins, however, no evidence of compartmentalization has been shown for the IM proteins (de Pedro et al., 2004). Additionally, fluorescence anisotropy characterization performed in vivo on the GFP-TonB fusion protein, revealed an energy-dependent motion within the IM. Its energy-dependence was determined by measuring fluorescence polarization in the presence and absence of several energy-depleting inhibitors. The motion of GFP-TonB was slower in the presence of the inhibitors, while GFP-TonB ΔExbBD motion remained unaffected by loss of PMF. Furthermore, the observed motion of GFP-TonB was higher overall than that of the ΔExbBD mutant. This observation strengthened our hypothesis that ExbBD directly affects the way energy is delivered to TonB

from the PMF. Taken together, the results of this study suggest a model for the mechanism of interaction between TonB and TBDTs during the ligand uptake process.

### 3.26 Confocal Images of TonB in the Cell Envelope

FepA is dispersed uniformly throughout the OM (Jordan et al., 2013) and there is much evidence that all FepA proteins participate in FeEnt transport. As established, the TonB C-terminus or termini directly interact with the "TonB box" of TBDTs in order to complete energy-dependent translocation of their ligands. Despite evidence of necessary physical interaction with FepA (Braun and Endriss, 2007), we observed TonB residing primarily at the central regions of the cell and is largely absent from the poles.

### 3.27 Localization of GFP-TonB

Two GFP constructs were studied using confocal fluorescence microscopy, to verify localization of TonB within the IM (Kaserer et al., 2008). GFP-TonB, with the Super Glo GFP gene (*sggfp)* inserted upstream of wild-type TonB and under the same promoter, was characterized and shown to be membrane associated. A cytoplasmic GFP (pTpG) construct was also characterized to control for non-membrane-associated GFP

fluorescence (Kaserer et al., 2008). Upon investigation of images obtained with confocal microscopy, localization of GFP-TonB was discovered in the central regions of most cells, with fluorescence absent from the poles (**Figures 3-2, 3-3, and 3-4**). Understanding the method of energy coupling of PMF to active transport through TBDTs, has presented many challenges for nearly 40 years (Hancock and Braun, 1976). The bacterial cell envelope is not known to have any compartmentalization, yet fluorescence from GFP-TonB hybrid proteins exhibited localization that was restricted to the central regions of

Experiments involving Alexfluor-labelled FepAS271C, showed a fluorescence signal throughout the OM. Likewise, GFP-LacY mutants residing in the IM, exhibited fluorescence signal throughout the cell. To test the hypothesis of ExbBD involvement with regard to TonB localization, the ΔExbBD strain was also imaged and analyzed. ΔExbBD cells did not show a difference in the distribution of GFP-TonB fluorescence.

Regardless of the relationship between TonB and ExbBD, TonB is needed for transport of TBDT ligands. Our laboratory's proposed mechanism for TonB-dependent transport takes into consideration the centralized distribution of TonB. It is not possible for TonB to be in physical contact with all TBDTs simultaneously, so we suggested a surveillance model (Jordan et al., 2013). In this model, TonB is in constant motion and drags along the underside of the OM.

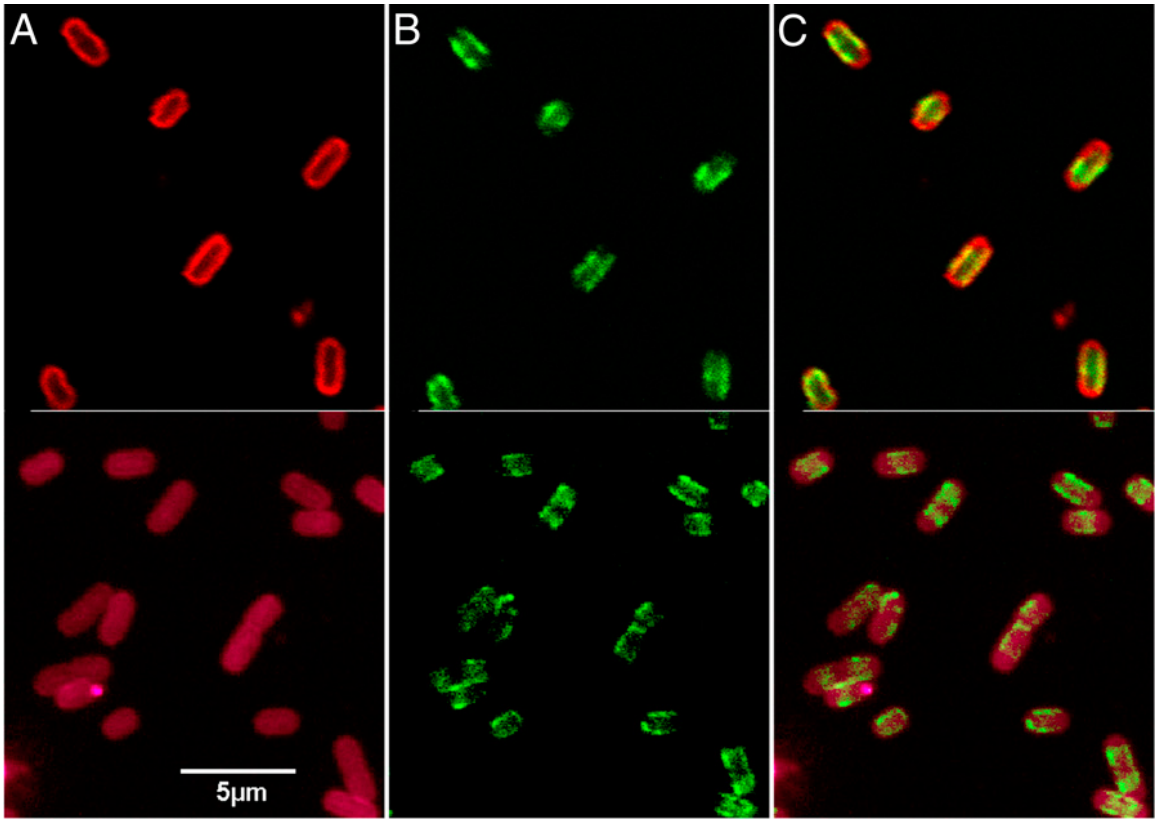


**Figure 3-2** (Jordan et al., 2013). Localization of FepA, in red, and TonB in green, shown in the *E. coli* cytoplasmic membrane. **(A)** Fluorophores in the strain OKN3 pFepAS271C/pGT were excited using using 680 nm light and observed at 700 nm (shown in top **panel A)**. The lower part of **panel A** shows cells excited with 553 nm light observed at 570 nm. **(B)** Shows GFP-TonB fusion protein excited with 488 nm light and observed at 520 nm. **(C)** Shows an overlay of **panel A** and **panel B.**

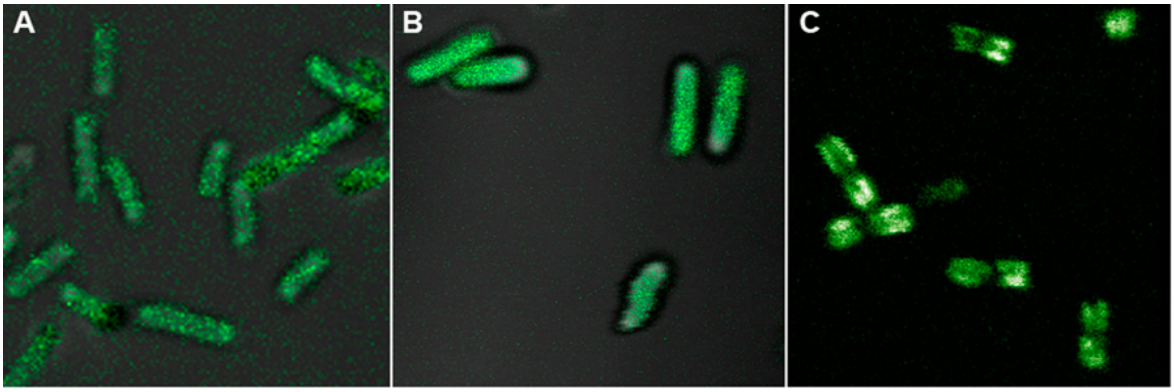


**Figure 3-3** (Jordan et al., 2013). (A) Image showing the cellular distribution of *E. coli* T184/pT7GFP-LacY, provided by Dr. Xiaoxu Jiang, Department of Physiology, UCLA School of Medicine, Los Angeles, California). The LacY production was induced using isopropylthiogalactoside (IPTG). (B) Shows the distribution of freely diffusing GFP in the cytoplasm of BN1071 pTpG cells. (C) Shows the centralized localization of GFP-TonB fusion proteins in the cytoplasmic membrane of BN1071 cells harboring pGT.

### 3.28 Measurements of TonB Motion

Fluorescence polarization was measured for three GFP constructs to determine anisotropic values for TonB motion in vivo. First, we established the baseline anisotropy for pGT, our GFP-TonB construct, by comparing polarization readings from pTpG, our construct expressing free GFP in the cytoplasm. Next, we showed the impact of PMF on TonB motion. The polarization for both constructs was measured to determine the anisotropy of TonB in cells lacking proton motive force. Moreover, we examined these same conditions in cells lacking ExbBD, to establish the role of ExbBD in transduction of energy to TBDTs.

The characterization of pGT and pTpG anisotropy implied a lower level of motion in pGT than in pTpG. The anisotropy values for pGT and pTpG were 0.16 and 0.22, respectively. These values are generated when GFP reorients after excitation, so they indicate the fraction of fluorophores undergoing detectable motion over the sampling interval. For pGT, the reorientation of GFP directly represents the changing position of TonB on a nanosecond timescale. Common protein movements within a cell membrane include translational diffusion, lateral diffusion, and rotational diffusion (Nenninger et al., 2014). Translational diffusion occurs. Molecular rotation is the only reasonable motion observable within our sampling interval because TonB is inserted into the cytoplasmic membrane.

The sampling time-scale in this anisotropy study was appropriately

selected to exclude sampling of motion influenced by lateral or translational diffusion. The lifetime of fluorescence emission for GFP is approximately 3 nanoseconds (Biophysical Journal). The direction of fluorescence polarization cannot be impacted by reorientation due to lateral diffusion, which takes place in milliseconds. On the other hand, rotational diffusion occurs on a nanosecond time-scale and can impact fluorescence polarization. Our measurements were taken over microsecond intervals, allowing enough time for excitation, rotational reorientation, and fluorescence emission of fluorophores in parallel with the excitation beam.

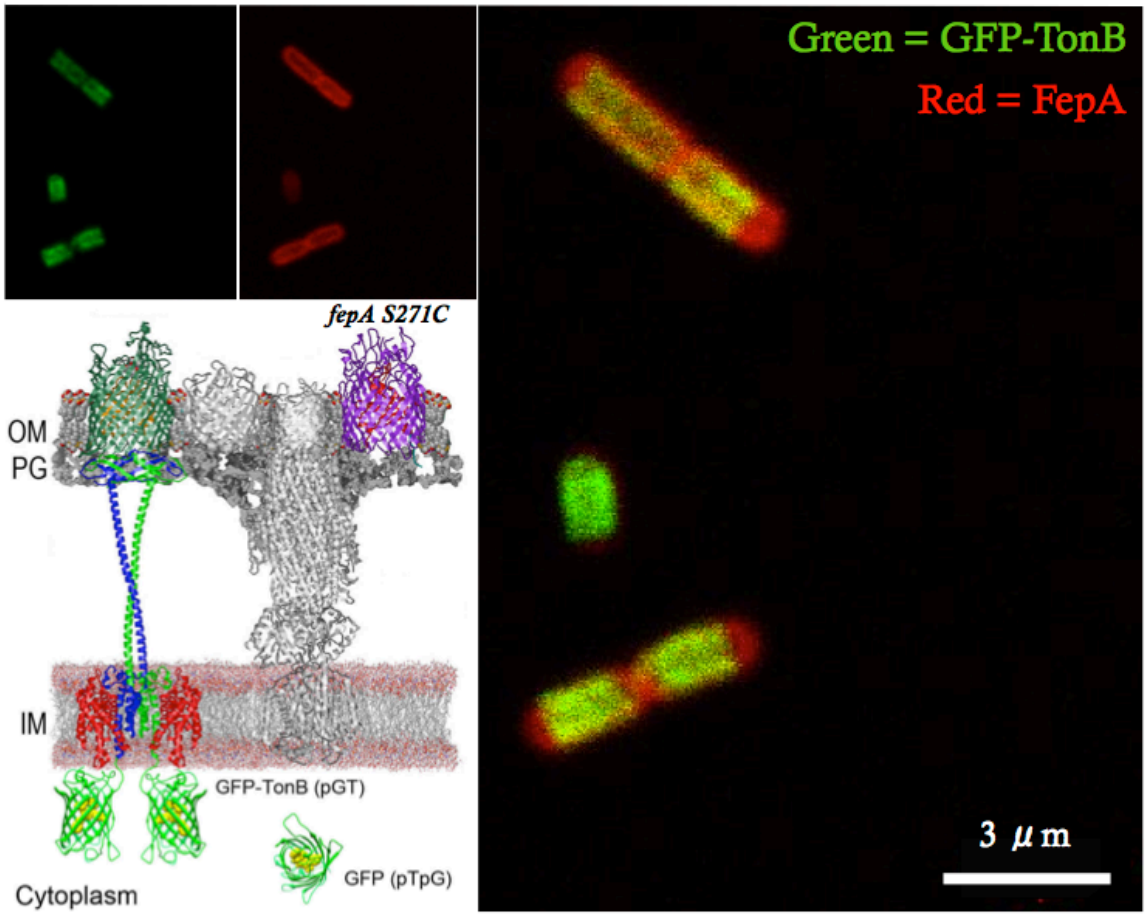


**Figure 3-4** (Adapted from (Jordan et al., 2013). Top left panels show high-resolution images of OKN13 p*fepA*S271C/pGT excited with 488 nm and 553 nm light, respectively. The lower left cartoon depicts a representation of the OKN13 p*fepA*S271C/pGT and OKN13 p*fepA*S271C/pTpG constructs.

The observed changes in polarization were not aberrant. A significant portion of fluorophores must reorient during the sampling time. Otherwise, depolarization would occur and the minor portion of anomalous molecules would be indistinguishable from photons emitted by the major population. As predicted, the strain expressing GFP (pTpG) in the cytoplasm presented lower R-values than the one expressing a GFP-TonB fusion (pGT). Average R-values of 0.16 and 0.22 were determined for pTpG and pGT, respectively. Measurements for both values were taken over 50 different samples and were found statistically significant when subjected to the Student's T-test.

The intensity of GFP fluorescence is dependent on the pH of its environment (Tsien, 1998). At low pH the fluor emits at a lower wavelength than at neutral and high pH (Kneen et al., 1998). This has a direct affect on intensity. Though the pH dependence of GFP leaves it vulnerable to fluctuations in pH, fluorescence anisotropy experiments are not influenced by these phenomena. Intensities from light emitted in parallel and perpendicular to the incident beam are detected concurrently, so changes in the pH of the sample did not impact anisotropy.

### 3.29 Effect of Metabolic Inhibitors on TonB Motion

TonB has long been assumed to rely on the proton motive force to energize the TonB-dependent transport process. Since alternate energy

sources have not been found in the OM, the proton motive force was the most likely candidate in the IM. Establishing the energy source for TonB was perhaps the most important step in building a model for its involvement. Our lab set out to confirm whether TonB did, in fact, rely on the energy of the proton motive force in the IM. To achieve this end, we introduced several energy poisons, aimed at disrupting the proton gradient. Carbonyl cyanide m-chlorophenyl hydrazone (CCCP), dinitrophenol (DNP), and sodium azide were tested for their effects on TonB polarization measurements in pGT, pGT delta ExbBD, and pTpG.

### 3.30 Effects of CCCP

Introduction of CCCP depolarizes the inner membrane by binding protons and due to its amphipathic nature, freely diffusing across the inner membrane. In this way, a gradient cannot build, especially at high concentrations of CCCP. As proton pumps work to translocate protons and build an electrical potential, the ionophore saps away the energy competitively by equilibrating across the membrane. Fluorescence polarization measurements were recorded from *E. coli* BN1071 pGT, BN1071 pTpG, and BN1071 pGT *ΔexbBD* cells. Measurements were taken as described in the Materials and Methods section at the beginning of the chapter. Briefly, the cell sample chamber was placed on the microscope stage and cells were measured before and after addition of

energy poison. Around 50 samples were measured in this way, yielding an average change in anisotropy of just fewer than 12%.

Although analysis of transient data showed anisotropic values varied from day-to-day, there was a positive increase in every measurement post-inhibitor addition. Given the pTpG control cells in **Figure 3-7** show that CCCP had almost no affect on anisotropy values, TonB motion was almost certainly slowed by addition of CCCP. This result is supported with statistical confidence level greater than 95%.

### 3.31 Effects of Sodium Azide and DNP

In an attempt to identify the exact type of cellular energy utilized by the TonB-ExbBD transport system, two more energy poisons were tested for their effects on the cells. Azide targets the electron transport chain and specifically blocks cytochrome oxidase activity in Gram-negative bacteria. Dinitrophenol (DNP) is a protonophore that binds positively charged protons, in contrast to CCCP, which indiscriminately binds ions.

The anisotropy of GFP-TonB increased in every case where metabolic inhibitors impacted the PMF. When FeEnt was used in lieu of energy poisons, the anisotropy was not affected to a significant extent, though there was a small positive change in R. Decreased motion after the addition of metabolic inhibitors indicated that TonB motion is energy dependent and that its activity is disrupted by removing the PMF.

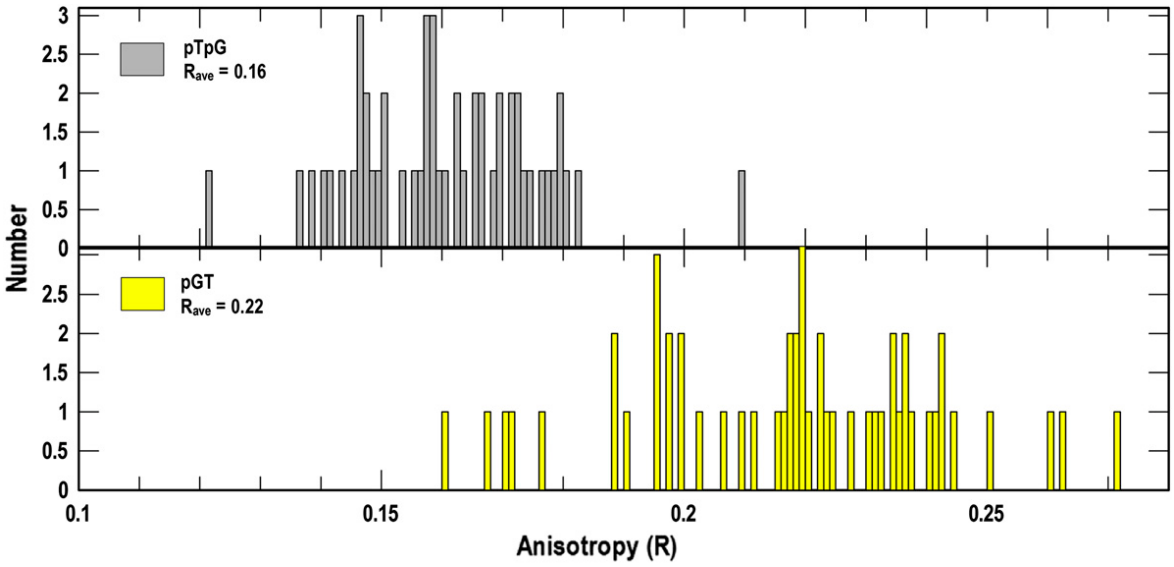


**Figure 3-5** (Jordan et al., 2013). Data from analysis of polarization measurements, showing the anisotropy of BN1071 cells harboring either pTpG or pGT.

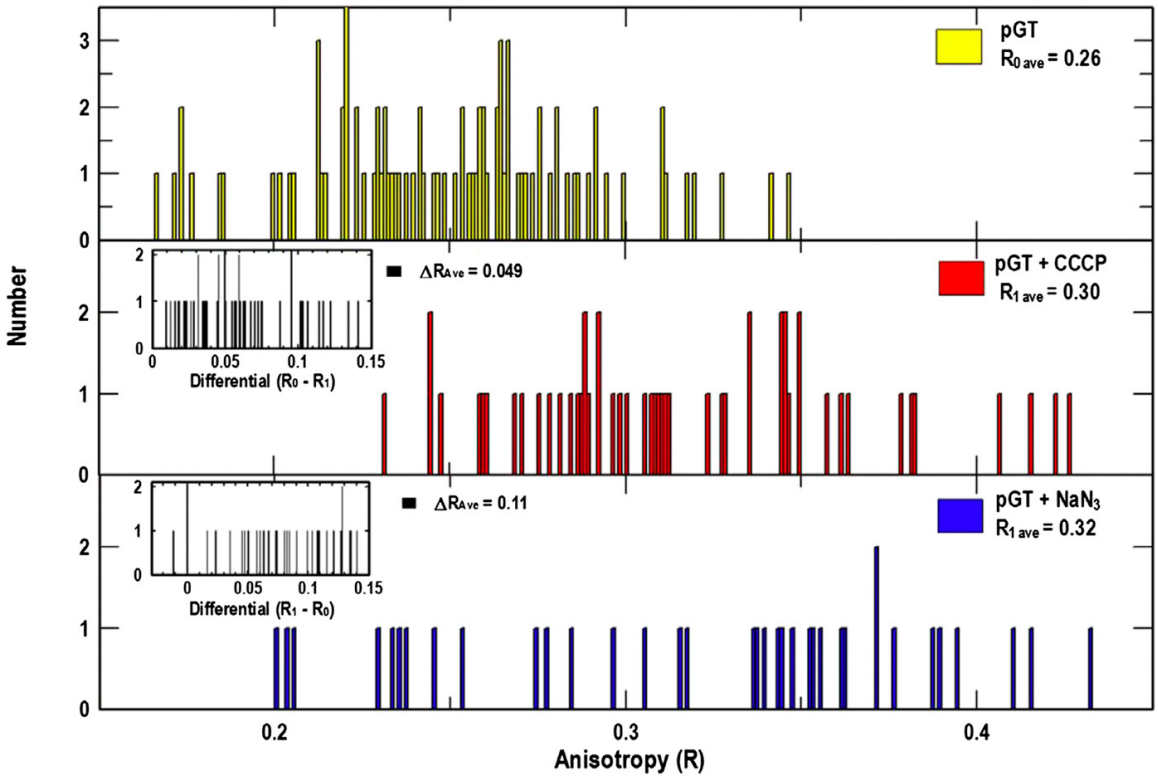


**Figure 3-6** (Jordan et al., 2013). Data from analysis of polarization measurements, showing the anisotropy of BN1071 pGT cells before and after exposure to either CCCP or $NaN_3$.

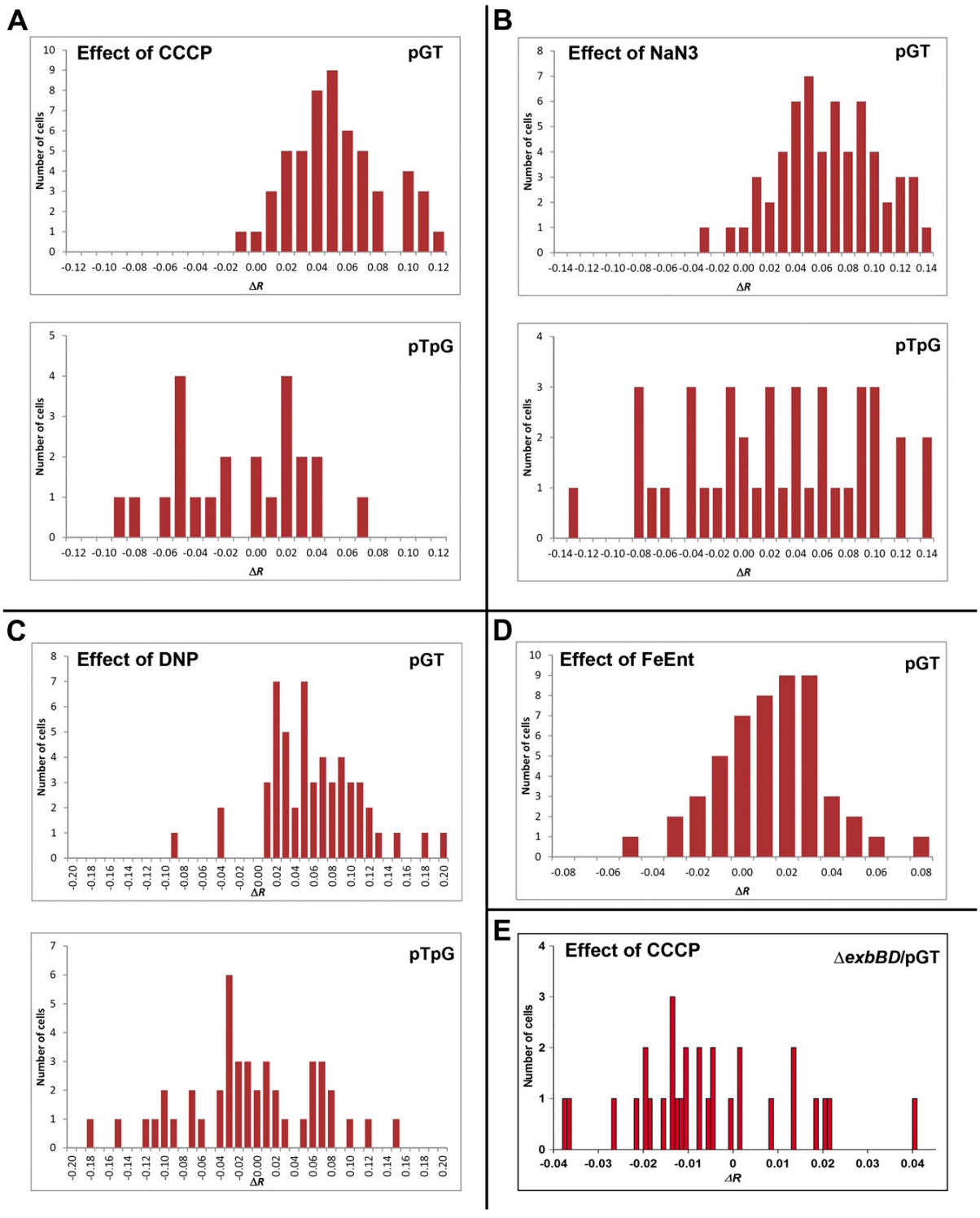


**Figure 3-7** (Jordan et al., 2013) Histograms showing the effect of CCCP, DNP, sodium azide, and ferric enterobactin on the change of anisotropy.

| *Construct* | *Agent* | *Sample Size* | *$\Delta R_{avg}$* | *SD* | *z* | *90 %* ¥ | *95 %* € | *99 %* ₹ |
|---|---|---|---|---|---|---|---|---|
| BN1071/pGT | CCCP | 52 | +0.047 | 0.0302 | +11.3172 | Pass | Pass | Pass |
| BN1071/pTpG | CCCP | 23 | -0.015 | 0.0431 | - 1.6627 | Fail | Fail | Fail |
| *ΔexbBD*/pGT | CCCP | 30 | -0.005 | 0.0177 | +0.052 | Fail | Fail | Fail |
| BN1071/pGT | $NaN_3$ | 58 | +0.060 | 0.0371 | +12.3404 | Pass | Pass | Pass |
| BN1071/pTpG | $NaN_3$ | 40 | +0.019 | 0.0674 | +1.7975 | Fail | Fail | Fail |
| BN1071/pGT | DNP | 53 | +0.056 | 0.0512 | +7.9198 | Pass | Pass | Pass |
| BN1071/pTpG | DNP | 44 | -0.012 | 0.0717 | - 1.0806 | Fail | Fail | Fail |
| BN1071/pGT | FeEnt | 51 | 0.008 | 0.0240 | +2.3815 | Pass | Pass | Fail |

**Table 3-1** (Jordan et al., 2013). Anisotropy measurements were taken using cells grown in MOPS minimal medium and subsequently resuspended in PBS. The BN1071 host strain was used for each construct shown. Cells were immobilized on a glass coverslip and a single cell was chosen for experiments involving metabolic inhibitors. *Z*-tests were conducted for sample groups performed on the same day and statistical significance was analyzed after obtaining anisotropy values.

(¥) Statistically significant value, if $|z| > 1.960$

(€) Statistically significant value, if $|z| > 2.241$

(₹) Statistically significant value, if $|z| > 2.807$

| | BN1071/pGT | | | BN1071Δ*exbBD*/pGT | | | | |
|---|---|---|---|---|---|---|---|---|
| Study # | $R_{avg}$ | SD | n | $R_{avg}$ | SD | n | T-test | Null |
| 1 | 0.547 | 0.100 | 12 | 0.298 | 0.179 | 24 | 4.92 | <0.0001 |
| 2 | 0.493 | 0.142 | 36 | 0.311 | 0.080 | 24 | 5.72 | <0.0001 |
| 3 | 0.414 | 0.166 | 26 | 0.306 | 0.053 | 31 | 3.42 | 0.0012 |
| 4 | 0.377 | 0.160 | 29 | 0.173 | 0.096 | 37 | 6.55 | <0.0001 |
| 5 | 0.459 | 0.198 | 50 | 0.281 | 0.153 | 49 | 4.99 | <0.0001 |

**Table 3-2** (Jordan et al., 2013). Five sets of anisotropy data from BN1071/pGT and BN1071*ΔexbBD*/pGT were compared. $R_{avg}$ represents the mean anisotropy value, n is the number of samples taken for the corresponding experiment, "T-test" refers to the resulting score after statistical analysis using Student's T-test, and Null represents the null hypothesis probability. The results strongly indicate that BN1071/pGT, the GFP-TonB construct, was more mobile than the *ΔexbBD* mutant in all cases.

# Chapter 4: Concerted Loop Motion Triggers Induced Fit of FepA to Ferric-enterobactin

## 4.1 Introduction

Structural transitions due to ligand binding events are a hallmark of TonB-dependent outer-membrane transporters (Braun et al., 1998). These conformational changes are comparable to those described in the Induced Fit Theory that models enzyme-substrate interactions leading to catalysis. The induced fit model traditionally concerns a phenomenon observed during enzyme-substrate interactions. Daniel E. Koshland Jr. first introduced the “Induced Fit Theory” in 1958, effectively changing the way biochemists viewed enzymatic reactions. Koshland described three characteristics to define his theory. From his 1958 paper, “a) the precise orientation of catalytic groups is required for enzyme action, b) the substrate causes an appreciable change in the three-dimensional relationship of the amino acids at the active site, and c) the changes in protein structure caused by the substrate will bring the catalytic groups into the proper alignment, whereas a nonsubstrate will not.”

His words imply that the enzyme is not initially in its catalytic conformation and that substrate association expedites change to said conformation. This is a process by which small positive substrate interactions contribute to a specific structural reorientation of the enzyme.

The resulting conformation accommodates and stabilizes the transition state of the substrate and thereby promotes catalytic action. Aside from providing an alternative to the Key-Lock Theory, his Induced Fit Theory maintains a simple and elegant explanation for substrate specificity of enzymes and more broadly, macromolecules.

Ligand-gated transporters, like FepA, are presumed to undergo similar conformational changes to facilitate ligand translocation across membranes. Specificity for a particular ligand is well established (Cao and Klebba, 2002; Chakraborty et al., 2003; Scott et al., 2001; Thulasiraman et al., 1998), though the details of binding events are yet unclear. In this study we provided evidence that the extracellular loops of FepA close around FeEnt in an ordered fashion during binding. Moreover, we showed that all labeled FepA proteins transport FeEnt, which was unexpected. In a previous study (Jordan et al., 2013), TonB was undetectable in roughly a third of the cell; whereas, FepA was evenly distributed throughout the OM.

Previously, our lab investigated whether there was clear evidence to support either the “Transient Pore Model” or the “Ball-and-Chain Model” for FeEnt transport through FepA, **Figure 4-1** (Ma et al., 2007). That study led to the conclusion that the latter model was substantiated, though more recent work has evidenced a contrary understanding of FepA transport dynamics. Although many insights were gleaned, perhaps the most beneficial aspect of that study was the mutant library generated as a result

(**Figure 4-2**). The cysteine-modified residues associated with that study provided a starting point for the experiments detailed in this chapter.

**Figure 4-1.** Published with the consent of the Journal of Bacteriology. Copyright Journal of Bacteriology 2007. Ma, L., Kaserer, W., Annamalai, R., Scott, D.C., Jin, B., Jiang, X., Xiao, Q., Maymani, H., Massis, L.M., Ferreira, L.C., Newton, S.M., Klebba, P.E., 2007. Evidence of ball-and-chain transport of ferric enterobactin through FepA. J Biol Chem 282, 397-406.

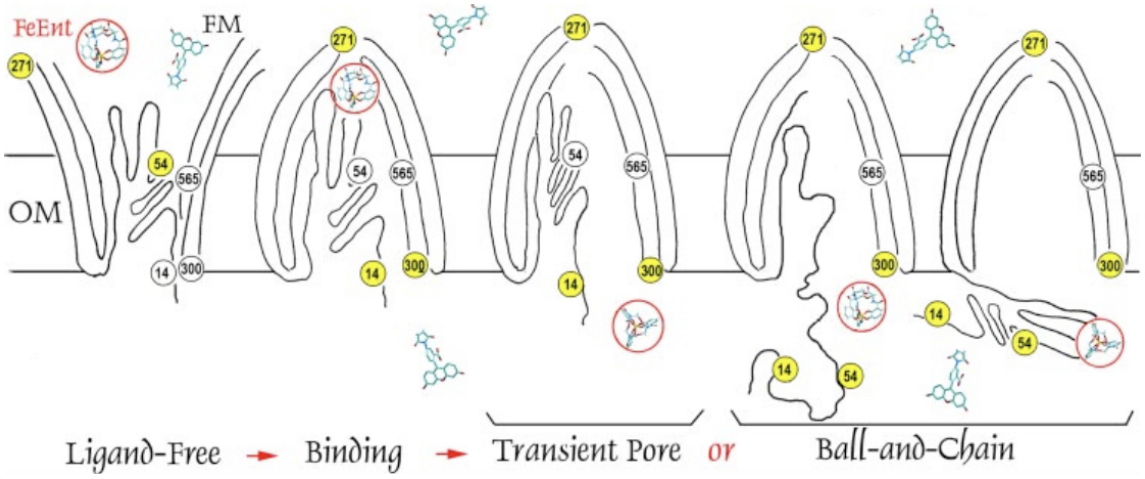


Diagram depicting two prevalent models regarding FeEnt translocation through the TonB-dependent transporter, FepA. Ligand transport through the beta-barrel is hampered by the presence of an occluding “plug domain,” which is assumed to accommodate ligand import through an energy-dependent process. The two models depict the plug domain moving to the side of the barrel, unwinding from the bottom of the barrel, or partially unwinding to pivot out of the barrel, like a hatch. The fluor, fluorescein maleimide (FM), is indicated in accordance with its ability to access both sides of the outer-membrane (OM).

In the localization studies of Jordan et al., 2013 and the spectroscopic assays of (Smallwood et al., 2014) we used the free sulfhydryl group of the engineered cysteines on FepA, were specifically labeled with 5μM fluorescein maleimide (FM). The low concentration of FM, along with a pH of 6.5 and incubation period of 5 minutes at 37 $^{o}$C, allowed specific labeling of FepA cysteines with minimal non-specific labeling of proteins within the periplasm or cytoplasmic surface. Furthermore, there are not many free sulfhydryls available to the fluorophore for labeling. Firstly, the majority of proteins do not contain cysteines. Secondly, the proteins that do contain cysteines, mostly reside in the cytoplasm. There is a considerable bias toward an even number of cysteines within proteins residing in the outer membrane and periplasmic space. Of the cysteine-containing proteins exported to the periplasm or inserted into the OM, most contain an even number of cysteines (Dutton et al., 2008). Therefore, many of the cysteines were present in a disulphide bond form and unable to react with FM. Upon addition of FeEnt, the fluorescein maleimide attached to an engineered cysteine on one of the extracellular loops (dependent on the particular mutant) was quenched.

## Materials and Methods

### 4.2 Bacterial Strains and Plasmids

OKN3 and OKN13 (BN1071 *ΔfepA* and BN1071 *ΔfepA*, *ΔtonB*, respectively) (Ma et al., 2007) were derived from the parent strain BN1071 (F- pro, trp, B1) (Klebba et al., 1982). The low-copy plasmid pHSG575 (Hashimoto-Gotoh et al., 1986) carrying wild-type $fepA^+$, was used to make pITS23 (Ma et al., 2007) and pITS47 (Smallwood et al., 2009). Mutations in the $fepA^+$ structural gene were made using a QuikChange kit (Agilent Technologies) allowing site-directed Cys residues (Ma et al., 2007; Smallwood et al., 2009) to be introduced in the expressed gene product.

### 4.3 Spectroscopic Experiments

Strains were grown in LB broth at 37 $^oC$ overnight, followed by a 1:100 subculture into 3-(N-morpholino) propanesulfonic acid (MOPS) minimal media. Both media contained appropriate antibiotics, including streptomycin (100 μg/ml) and chloramphenicol (20 μg/ml). Importantly, the MOPS buffered minimal media was iron-deficient to promote activation of the fur operon and transcription of the desired proteins. After subculture, the strains were shaken at 37 $^oC$ for 5-6 hours until they reached late log phase. The cells were then harvested by centrifugation at 8,000x g at 4 $^oC$ for 10 min. The ferric enterobactin (Klebba et al., 1982) used was purified from *E. coli* AN102 (Cox et al., 1970). The purified FeEnt was stored at 0

$^{o}$C for 2-3 weeks, after which the solution became oxidized or degraded and was again purified by chromatography on Sephadex LH-20 (Wayne and Neilands, 1975). The concentration was spectrophotometrically measured using its extinction coefficient and peak absorbance at 495 nm.

### 4.4 Selection of Cysteine Modification Sites

Possible sites for cysteine modification studies were identified on the basis of accessibility and labeling efficiency. Previously introduced cysteine substitutions (Liu et al., 1994; Jiang et al., 1997; Payne et al., 1997; Cao et al., 2003; Ma et al., 2007; Smallwood et al., 2009) were considered, along with recent mutations in loops 3, 4, 7, and 10 (S275C, G327C, S490C, and G640C & T648C, respectively). Fluorescence spectroscopy revealed differences in the labeling efficiency for each cysteine mutation-fluorophore maleimide pairing, which helped in selection of preferred mutations.

### 4.5 Fluorescent Modification of Cysteine Residues

Site-directed mutagenesis was performed to introduce modifiable cysteine residues into the loops of FepA (Ma et al., 2007; Smallwood et al., 2009). From these studies, we learned that certain sites were more accessible to labeling than others. A screen was performed in order to determine which sites would be most useful for investigation by

fluorescence spectroscopy. After the screening, residue S271C was selected for preliminary studies and assay optimization.

Cells were prepared by growing strains in 10 mL of LB broth overnight, cells were subcultured into 10 mL of iron-deficient MOPS Minimal media and grown to an optical density of 1.0. Cells generally required a 12-hour incubation with shaking, to reach stationary phase. Subsequently, cells were collected using centrifugation and resuspended in labeling buffer (50-mM $Na_2HPO_4$, 0.9% NaCl, pH 6.5, at 0 $^oC$), after one wash.

Cells were then incubated with either 5-μM fluorescein maleimide or Alexa Fluor 488 maleimide at 37 $^oC$ for 5 minutes. The labeling reaction was quenched using β-mercaptoethanol, at 100 mM concentration. Afterward, cells were collected by centrifugation, washed once, and finally, resuspended in sample buffer (0.4% glucose in PBS). Fluorescence intensity of each sample was monitored using an SLM AMINCO 8000 fluorescence spectrometer, made by SLM Instruments. The spectrometer hardware and software was refurbished and upgraded by OLIS. Data was gathered using OLIS SpectralWorks software.

The assay included fluorescent labeling of FepA residue S271C, *in vivo*, using fluorescein maleimide. Once labeled, the cells were observed spectroscopically. The fluorescence intensity of wildtype cells was weak, approximately 0.2 – 0.3 A.F.U., while labeled cells exhibited much higher

intensities. The number of cells to buffer ratio per cuvette was tested to avoid turbidity of the sample. The S271C cells consistently gave readings around 0.7 – 0.8 A.F.U., which verified the cells were properly labeled. We then added FeEnt to the sample and observed fluorescence quenching of more than 30 percent. Recovery of fluorescence intensity was observed with lower concentrations of FeEnt. Several experiments were run to adjust the duration of recovery time.

**Figure 4-2.** Published with the consent of the Journal of Biological Chemistry. Copyright Journal of Biological Chemistry (2003). Cao, Z., Warfel, P., Newton, S.M., Klebba, P.E., 2003. Spectroscopic observations of ferric enterobactin transport. J Biol Chem 278, 1022-1028.

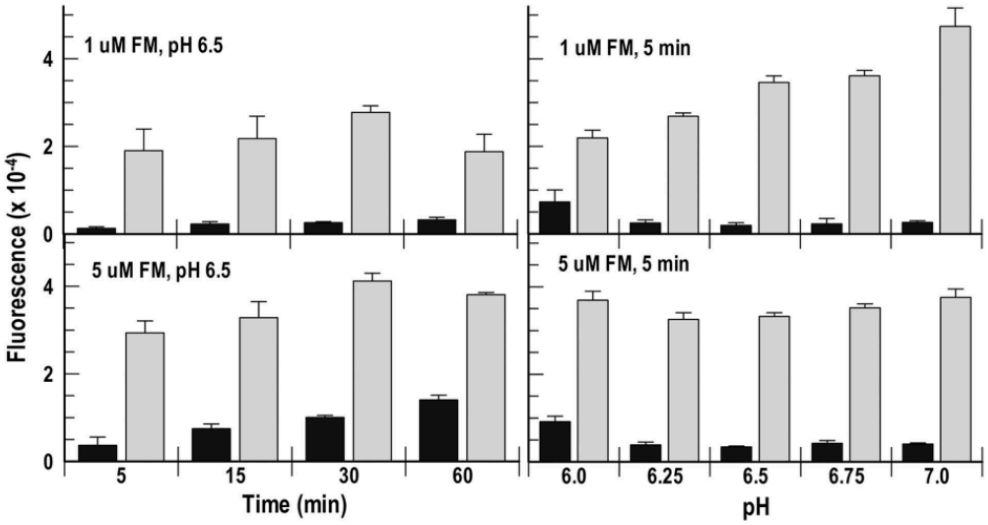


**(Cao et al., 2003; Smallwood et al., 2014)** Shown are histograms representing the relative efficiencies of labeling at different times and pH values. Black bars represent *E. coli* OKN3/*pfepA-S271C* and gray bars represent OKN3/*pfepA-S271C* after labeling. Fluorescence intensities were measured on an OLIS-SLM8000 fluorometer at wavelength 520 nm, with an excitation beam of wavelength 488 nm. Error bars are indicative of the standard deviation of each mean value.

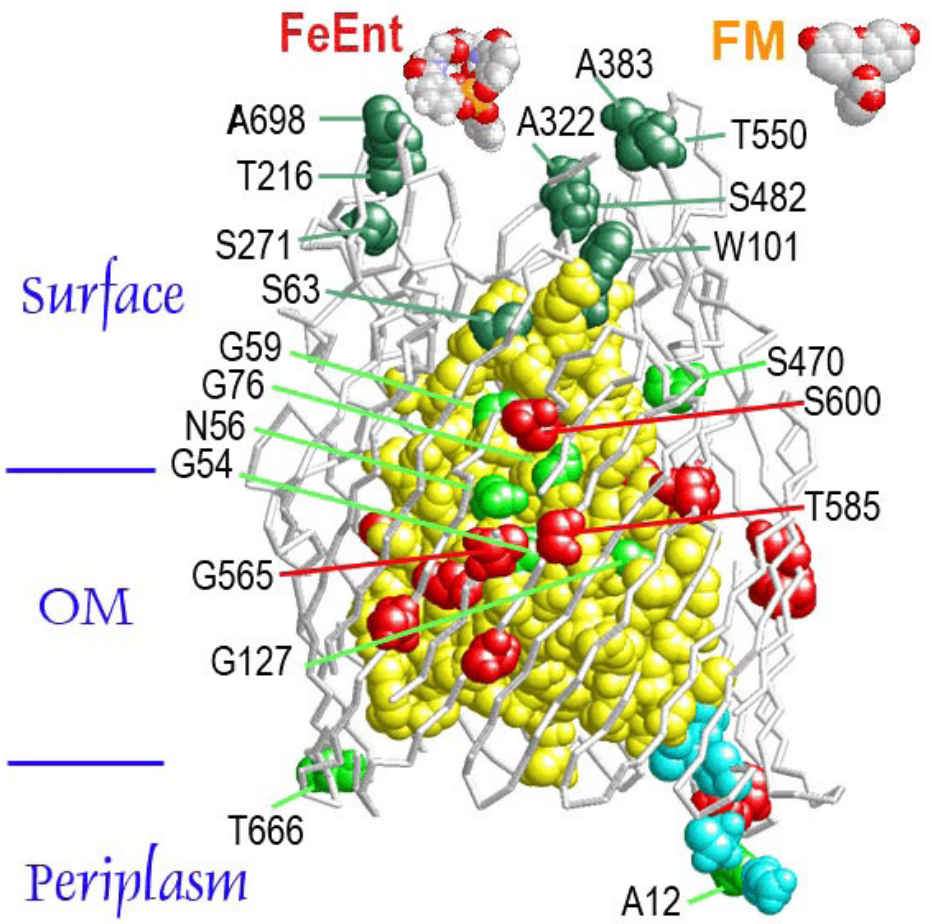


**Figure 4-3** (Smallwood et al., 2014)**.** Cartoon depiction of FepA in the outer membrane. The backbone of the β-barrel domain is shown as tubes, shown in white. The N-terminal plug domain is shown in a yellow space-filling representation and engineered cysteine residues of interest are highlighted in either red, dark green, or light green, while the TonB box is highlighted in cyan. Above are space-filling models of ferric enterobactin (FeEnt) and fluorescein maleimide (FM). Highly reactive cysteine substitutions are labeled dark green. Less intensely labeled cysteines are colored light green. Red colored spheres represent cysteine residues that were unreactive.

## 4.6 Cell Fractionation

Outer-membrane fragments were isolated to perform analysis of OM receptor-ligand binding kinetics. The cells were broken at a pressure of 14,000 psi, using a French press. This procedure presented a convenient way to isolate the OM from the IM, yielding “vesicle-like structures” (Smit et al., 1975) for study of FepA proteins in their native environment. The resulting OM fractions were then analyzed in an OLIS-SLM8000 fluorometer using stopped-flow rapid mixing for kinetics data.

## 4.7 Stopped-flow Quenching Experiments

FeEnt was added to 200 nM final concentration in a 4 mL sample volume containing 2.5 x $10^7$ cells. Samples were continuously stirred at a constant temperature of 2 $^oC$, throughout the observation period. Binding kinetics experiments were measured at 0 $^oC$ using an OLIS attachment in conjunction with the SLM fluorescence spectrometer. The stopped-flow attachment rapidly mixed components and allowed for the acquisition of kinetic information from the first few moments of interaction between the fluorescently tagged receptor and FeEnt.

Analysis was performed using GraFit 6.011, made by Erithacus Software. The data was fitted to either a single or double exponential decay with equations of $A(t) = A_0 e^{-kt}$ + offset and $A(t) = A_{0(1)} e^{-k1t} + A_{0(2)} e^{-k2t}$ + offset, respectively (Payne et al., 1997). The recovery curves, derived

from fluorescence intensity changes during FeEnt transport, were fitted with to a single exponential decay; which yielded the half times for the motion of modified loops.

### 4.8 Binding and Transport using $^{59}Fe$

In a previous study (Newton et al., 1999), transport rates of labeled and unlabeled FepA strains were measured and compared for activity. The $K_d$ and capacity values were obtained by measuring binding at 0 $^{o}C$ and fitting the resulting data with the bound-versus-total equation, supplied by GraFit 6.011 software. For $K_M$ and $V_{max}$ values, the enzyme kinetics equation was used to analyze data taken from cells in grown iron-deficient MOPS media with 0.4% glucose added before measurements at 37 $^{o}C$.

### 4.9 SDS-PAGE

SDS-PAGE was used to separate proteins for analysis and preparation for nitrocellulose transfer (Ames, 1974; Newton et al., 1999). Samples were prepared in sample buffer containing SDS and 3% β-mercaptoethanol. The samples were then boiled for a period of 5 minutes and loaded into an SDS-polyacrylamide gel, along with a molecular weight ladder to help identify resulting bands during analysis. Samples were then subjected to electrophoresis at room temperature until the dye-front reached the bottom of the gel. After electrophoresis the gels were either

stained using Coomassie Brilliant Blue stain or prepared for immunoblotting.

### 4.10 Fluorescence Imaging

Labeling efficiency was quantified by comparing fluorescence intensity levels to the level of FepA expression using a Typhoon fluorescence imager, manufactured by GE Healthcare. The cells used were grown to late log in iron-deficient MOPS Minimal media. Then 5 x $10^8$ cells were collected by centrifugation and resuspended in 150 µl of SDS-PAGE sample buffer. The cells were then boiled for 5 minutes and SDS-PAGE was run using 30 µl of the cell suspension for each sample. After electrophoresis, the gel was rinsed with water and scanned for fluorescence on a Typhoon imager.

### 4.11 Fluorescence Quenching

Fluorescence quenching is most easily described as a decrease in fluorescence intensity. This decrease can be attributed to physical transference of energy, fluorescence resonance energy transfer (FRET), or through a return from an excited state to the ground state by another nonradiative path. Each of which results in a reduction of emitted light. Lastly, perhaps the most often overlooked form of quenching is mitigation of the excitation beam (Albrecht, 2008). Attenuation of the light source can

occur when an absorbing molecule or side-chain, as in the case of our experimental study of FepA extracellular loop motion, physically blocks the incident beam from reaching the fluorophore. In the FepA system, the observed drop in fluorescence intensity for each loop had a characteristic rate, which offered insight into mechanistic changes in the loop environment.

Next we investigated the effects of FeEnt on the fluorescence intensity of various fluorescein maleamide-labeled extracellular loops of FepA. We hypothesized that upon binding of FeEnt, the loops of FepA must close in around the ligand to completely achieve or assist in the binding process. Our hypothesis was based on previous papers that evidenced a direct interaction of ligand and receptor loops during binding (Smallwood et al., 2009). Therefore, we expected a drop in the fluorescence intensity due to physical interaction between the ligand and the cysteine-modified sites within the loops of FepA.

### 4.12 Quantitative Immunoblot

Expression levels of FepA were determined with quantitative immunoblot analysis. Samples were prepared and subjected to SDS-PAGE as in the fluorescence protocol; however, the gels were transferred to nitrocellulose paper for identification with immunochemistry. Unexposed sites on the paper were blocked with TBSG pH 7.5 (50 mM Tris chloride,

0.9% NaCl, and 1% gelatin). TBSG was poured off and blots were incubated for 1 hr with mouse anti-FepA antibodies 41 and 45 (0.5%; Murphy et al., 1990), suspended in TBSG. Antibody solution was poured off and blots were washed 5 times with 0.05% Tween 20 in TBS for 5 minute intervals.

Next, the blot was incubated with [$^{125}$I] protein A for 1 hour, shaking at room temperature. After incubation period, [$^{125}$I] protein A solution was poured into a radioactive waste container. The blot was washed once with tap water, which was also poured into a radioactive waste container. Subsequently, the blot was washed twice more with tap water and air-dried.

The emissions from the radioactive decay were captured using a phosphorescent screen. The screen was exposed to the blot for a minimum of 3 hours and scanned using the storage phosphor setting on the Typhoon imager. The amounts were easily quantified using ImageQuant software and a standard curve for FepA concentration. The standard curve was obtained from FepA standards that were run alongside the samples of unknown concentrations.

### 4.13 Confocal Microscopy Studies

A confocal Carl Zeiss LSM 700 (laser scanning microscope) was used to study fluorophore-labeled OKN13/pGT/p*fepA*S271C (Jordan et al.,

2013). The Confocal Microfluorometry and Microscopy Core Facility at Kansas State University granted microscope usage. Cells were grown in iron-deficient MOPS Minimal media to mid-log (5-6 hr), labeled with AlexaFluor 546 using previously mentioned in vivo labeling protocol, and resuspended in PBS (pH 7.4).

An 8-well microslide, made by Ibidi Inc., was prepared with a coat of poly-L-lysine to immobilize the cells for viewing. A sample containing 5 x $10^9$ cells in 350 µl of PBS was added to a single well and observed under 100x magnification. A fluorescence scan of the sample at 488 nm was performed, immediately followed by a scan at 555 nm. Once initial scans were complete, 5 nM FeEnt was added to the sample well and images were recorded over a 23-minute time period.

## Results

### 4.14 Spectroscopic Measurements of Loop Motion

Quenching of fluorescence intensity, due to changes in the immediate environment of the fluorophore maleimide tag was observed previously by our lab (Cao et al., 2003; Scott et al., 2002; Smallwood et al., 2009). In this study, cysteine mutations on seven of the eleven surface loops of FepA were selected for spectroscopic measurements. These loops were monitored for fluorescence intensity until a stable baseline was established (approximately 100 s), at which point, FeEnt was quickly

added to the sample cuvette. The sample was continuously monitored for approximately 600 s, after FeEnt addition.

Fluorescence quenching assays were performed on each mutant possessing a site-directed cysteine modification. The cysteines were engineered on several extracellular loops of FepA, with one modification per strain. These modified sites, labeled with fluorescein maleimide, were monitored for 1500 seconds. At 300 seconds, ferric enterobactin was introduced and quenching was observed (**Figure 4-4**). The change in fluorescence intensity was different for each mutant strain. This resulted from the different environments of the cysteine mutants, which directly impacted how the fluorophore interacted with FeEnt and the other loops (**Figure 4-6**).

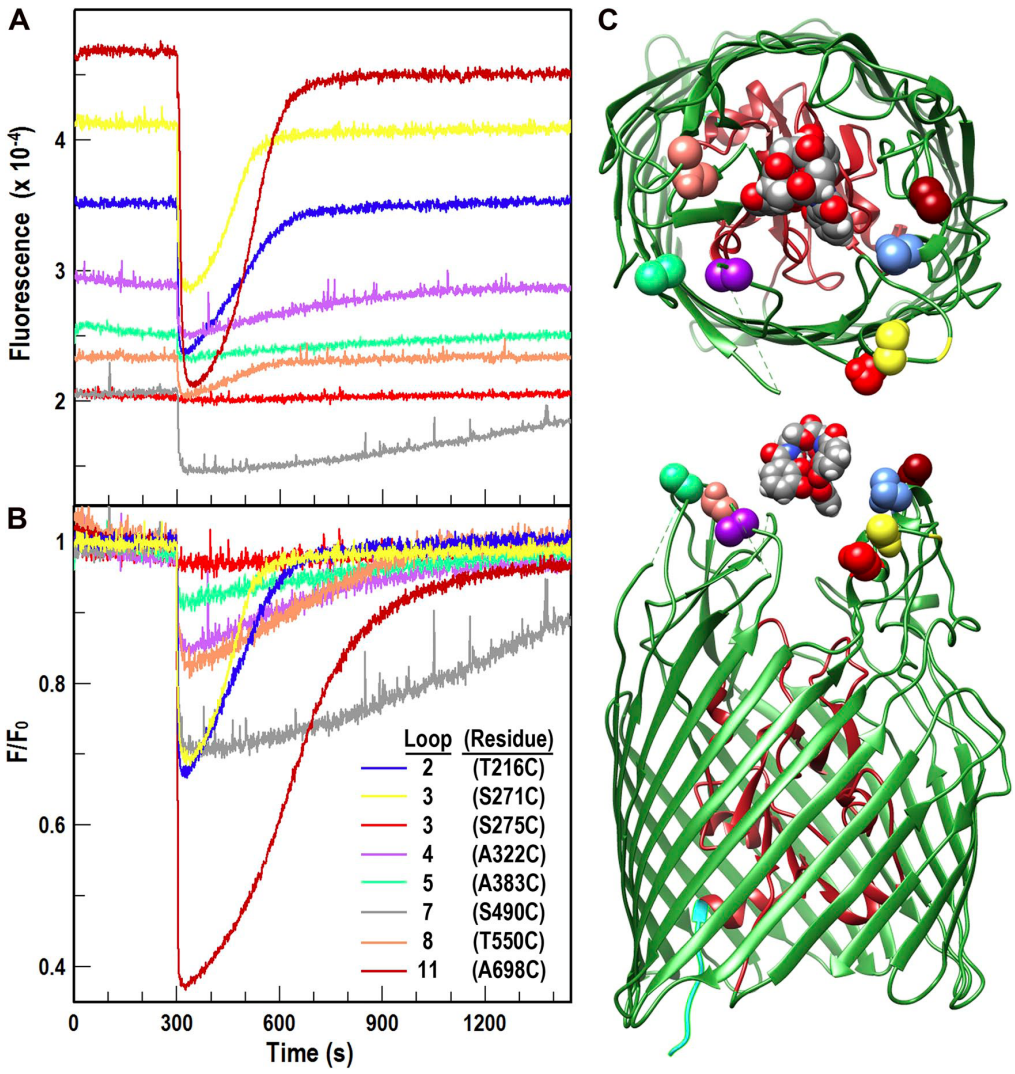


**Figure 4-4** (Smallwood et al., 2014). **(A)** Raw fluorescence data from labeled cysteine residues.

**(B)** Fluorescence data corresponding to those in **panel A**, normalized with such that the average baseline reading is set to 1.0 a.f.u. Each color represents a different cysteine modified residue.

**(C)** Depiction of FepA from two perspectives. (Top) Depiction of FepA as viewed from the extracellular environment looking down on the OM.

(Bottom) Depiction of FepA from side-view perspective. FepA backbone is shown as ribbon diagram with the β-barrel colored green and the N-terminal plug domain in red. Engineered cysteine residues are shown as spheres and correspond to the colors listed in **panel B**.

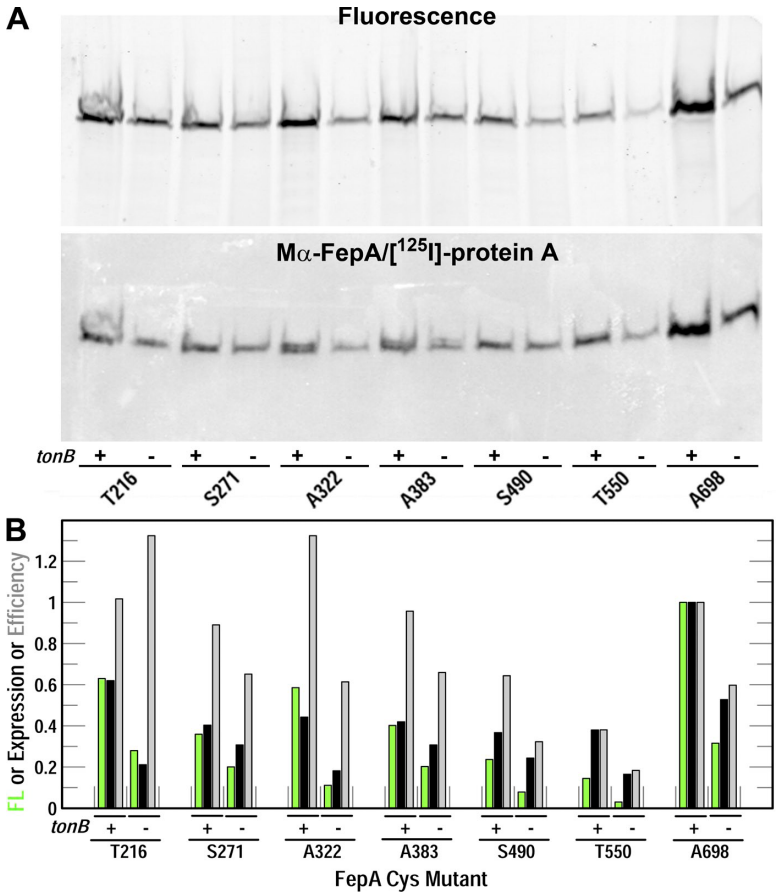


**Figure 4-5** (Smallwood et al., 2014). (**A) Top:** Gel image showing fluorescence of FepA proteins resolved by SDS-PAGE. of FepA in cells expressing TonB from a plasmid and *ΔtonB* cells. **Bottom:** Immunoblot of gel shown in top panel. An immunoblot using the primary antibody Anti-FepA mAbs 41/45 was used to evaluate the amount of expression and fluoresceination of FepA proteins. **(B)** Shows expression levels of FepA, relative to *fepA A698C*. The green bars represent the relative amount of labeling by fluorescein maleimide. Black bars represent the relative expression levels, while gray bars represent the relative labeling efficiency for each strain.

**Table 4-1**. Published with the consent of the Journal of Bacteriology. Copyright Journal of Bacteriology 2007. Ma, L., Kaserer, W., Annamalai, R., Scott, D.C., Jin, B., Jiang, X., Xiao, Q., Maymani, H., Massis, L.M., Ferreira, L.C., Newton, S.M., Klebba, P.E., 2007. Evidence of ball-and-chain transport of ferric enterobactin through FepA. J Biol Chem 282, 397-406.

*Summary of FepA Cys substitution mutant phenotypes*

| | N domain | | | | | | | | | | C domain | | | | | | | | |
|---|---|---|---|---|---|---|---|---|---|---|---|---|---|---|---|---|---|---|---|
| **Location** | **TonB-box** | | **Periplasm** | | | **Interior** | | | **Loops** | | **Loops** | | | | | | | | **Periplasm** |
| Residue | **12** | **14** | **30** | **32** | **33** | **54** | **59** | **127** | **63** | **101** | **216** | **271** | **280** | **322** | **383** | **482** | **550** | **698** | **666** |
| Expression[1] | **100** | 100 | 100 | 100 | 100 | 100 | 100 | 60 | 100 | 100 | 100 | 100 | 100 | 100 | 100 | 100 | 100 | 100 | 100 |
| Functionality of Cys substitution mutants before fluoresceination | | | | | | | | | | | | | | | | | | | |
| Binding[2] | 25 | 100 | 100 | 100 | 100 | 60 | 40 | 25 | 40 | 30 | 47 | 88 | 100 | 59 | 82 | 10 | 48 | 100 | 100 |
| Transport[3] | 20 | 40 | 100 | 100 | 100 | 100 | 30 | 0 | 20 | 10 | 77 | 84 | 100 | 62 | 45 | 0 | 28 | 100 | 100 |
| Susceptibility to fluoresceination at 0°C | | | | | | | | | | | | | | | | | | | |
| 5 μM[4] | 50 | 25 | 52 | 44 | 38 | 63 | 45 | 13 | 25 | 100 | 125 | 100 | 35 | 50 | 75 | 38 | 13 | 100 | 50 |
| 300 μM[5] | 75 | ND | 90 | 88 | 60 | ND | ND | ND | ND | ND | ND | 100 | 100 | ND | ND | ND | ND | 100 | 75 |
| Susceptibility to fluoresceination at 37°C | | | | | | | | | | | | | | | | | | | |
| 5 μM[4] | 30 | 10 | 60 | 52 | 20 | 20 | 15 | 20 | 120 | 90 | 80 | 100 | 45 | 120 | 100 | 65 | 70 | 80 | 20 |
| 300 μM[5] | 90 | ND | 100 | 100 | 90 | ND | ND | ND | ND | ND | ND | 100 | 100 | ND | ND | ND | ND | 100 | 100 |
| Functionality of Cys substitution mutants after fluoresceination | | | | | | | | | | | | | | | | | | | |
| Binding[2] | 17 | 83 | 100 | 90 | 83 | 33 | 40 | 7 | 13 | 13 | 43 | 81 | 100 | 21 | 19 | 10 | 67 | 87 | 90 |
| Transport[3] | 7 | 53 | 100 | 100 | 100 | 53 | 27 | 0 | 13 | 0 | 37 | 60 | 100 | 19 | 32 | 0 | 26 | 86 | 100 |

Chart summarizing the phenotypes of individual cysteine substitutions. Light gray boxes represent mutations that could only be labeled by fluorescein maleimide, rather than larger AlexaFluor maleimides. Dark gray boxes represent mutations that were labeled by fluorescein maleimide and AlexaFluor maleimides.

### 4.15 Hierarchy of Loop Motion

The rate of decay for each of the loops was of particular interest, since our lab previously observed biphasic fluorescence decay in a strain containing a FepA mutation in A280C (Payne et al., 1997). In this study, we used a stopped-flow attachment for the fluorometer to observe the rate of fluorescence decay in cysteine-modified FepA mutants, after exposure to FeEnt. This was first performed using whole cells, however, we achieved smaller standard deviations using outer-membrane fractions; which were prepared using the French press lysis technique. These fractionated membranes showed the same kinetics as those observed in the whole cell samples and offered lower turbidity, along with higher fluorescence intensity **(Figure 4-6)**.

Our kinetics experiments using a stopped-flow device showed a faster binding rate than previously reported (Payne et al., 1997; Smallwood et al., 2014). The rates revealed a hierarchy of loop motion, with L3 > L11 > L7 > L2 > L8 > L5, and > L4.

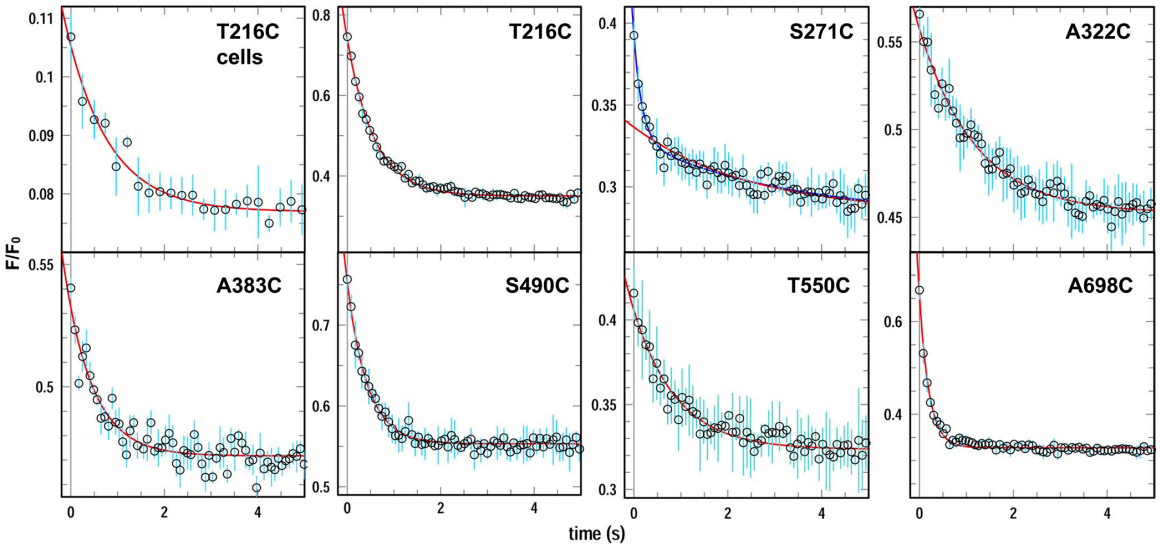


**Figure 4-6** (Smallwood et al., 2014). Stopped-flow measurements were taken on OKN3 cells containing cysteine-modified *fepA* genes, expressed from pHSG575-derived plasmids. Using an OLIS-SLM8000 fluorometer, 2 ml of 200 nM FeEnt was rapidly mixed with the same volume of $10^{10}$ cells, resuspended in PBS. Panels show various rates of fluorescence quenching, resulting from addition of FeEnt, for tested residues on each loop. The first panel is an example of rates obtained from whole cells, while subsequent panels show rate data gathered from OM fractions

*Rates of FM quenching in different surface loops of FepA during FeEnt binding*

| Mutant | Loop | k (SE) | $t_{1/2}$ | Rank |
|---|---|---|---|---|
| | | $s^{-1}$ | $s$ | |
| T216[a] | 2 | 1.08 (0.08) | 0.64 | 7 |
| T216 | 2 | 1.73 (0.04) | 0.40 | 4 |
| S271C[b] | 3 | 5.72 (0.81); 0.31 (0.04) | 0.12; 2.23 | 1 |
| A322C | 4 | 0.84 (0.05) | 0.83 | 8 |
| A383C | 5 | 1.64 (0.15) | 0.43 | 5 |
| S490C | 7 | 2.32 (0.13) | 0.30 | 3 |
| T550C | 8 | 1.09 (0.06) | 0.64 | 6 |
| A698C | 11 | 4.90 (0.18) | 0.14 | 2 |

**Table 4-2** (Smallwood et al., 2014). Chart detailing the results of stopped-flow experiments, where equal volumes of suspended OM fragments (containing FM-labeled FepA receptors) and 200 nM FeEnt, were rapidly mixed. ([a]) *In vivo* measurements in cells expressing FepAT216C-FM. ([b]) Biphasic decay observed with single exponential kinetics displaying amplitude of 0.063 and a double-exponential kinetic profile of 0.047.

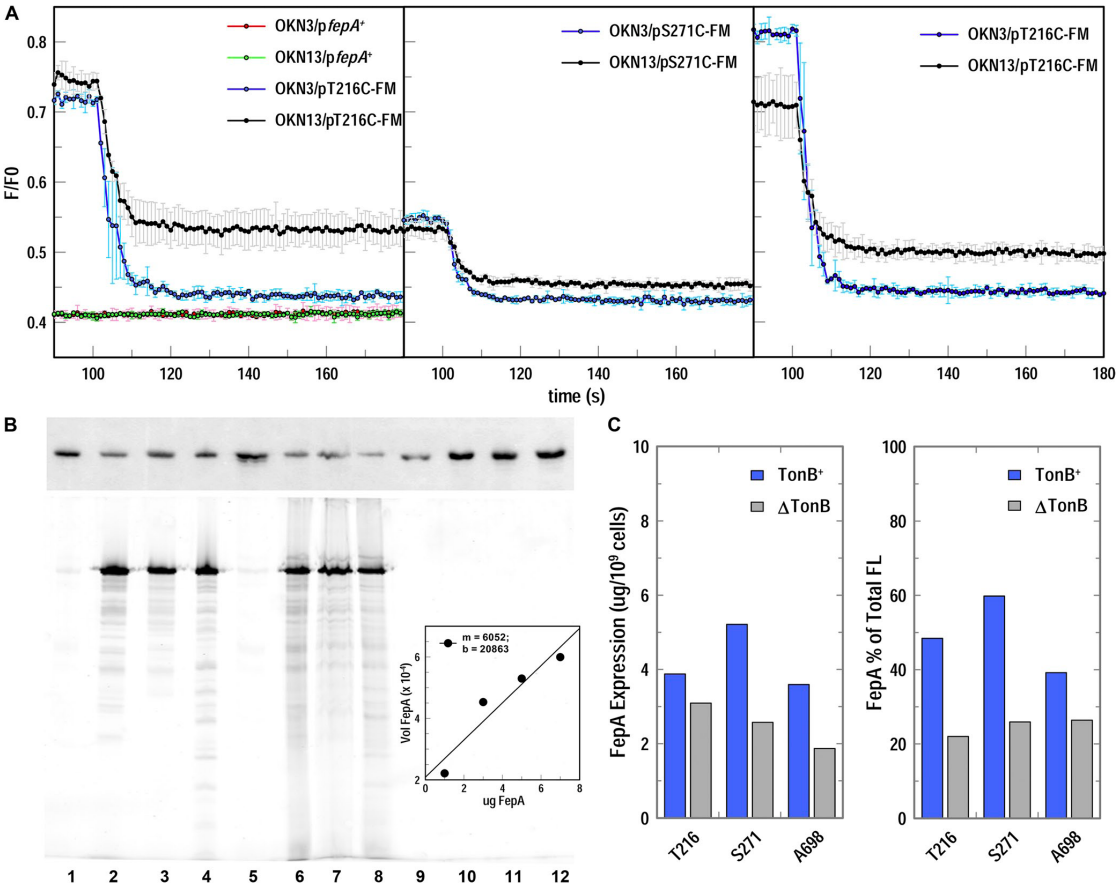


**Figure 4-7** (Smallwood et al., 2014). **(A)** The first panel shows the fluorescence intensity of labeled OKN3/p*fepA*S271C and OKN13/p*fepA*T216C, as well as unlabeled controls, before and after addition of FeEnt. The second and third panels show residues S271C and A698C, respectively, under the same conditions as panel one. The ferric siderophore always quenched fluorescence more in *tonB*+ (blue curves; gray SD) than *ΔtonB* (blackcurves; cyan SD) bacteria. The bottom right panel summarizes the different mean extents of quenching from two averaged experiments.

**(B)** The top panel shows an immunoblot of the SDS-PAGE gel shown (below). The immunoblot was performed using anti-FepA mAbs 41/45/[$^{125}$I] protein A. Phosphoimaging of the immunoblot was achieved using a Typhoon scanner. The bottom panel shows OM proteins from OKN3

strains in lanes 1-4 and those from OKN13 strains in lanes 5-8. Lanes 1 & 5; 2 &6; 3 & 7; and 4 & 8, expressed $FepA^{+}$, FepAT216C, FepAS271C, and FepAA698C, respectively. To serve as a standard, purified FepA was added in amounts of 1, 3, 5, and 7 μg to lanes 9-12. **(C)** Relative expression and labeling of FepA is shown for residues T216C, S271C, and A698C.

### 4.16 TonB-GFP and FM-Labeled FepA Evaluation Microscopically

Confocal fluorescence microscopy was used to determine whether all FepA receptors evenly distributed across the OM of the cell envelope were transporting, or if transport was restricted to the transporters colocalized with TonB. In Jordan et al, a centralized localization of fluorescence signals from TonB-bound GFP was observed. Further to this data, the spectroscopic quenching assay using the S271C residue encouraged investigation of any differences between labeled FepA before and after introduction of FeEnt.

Fluorescence microscopy was performed on strains containing a cysteine point mutation in the *fepA* gene and the pGT construct in one strain. Strain OKN13 was used as a host strain for the two plasmids, one high copy number plasmid carrying the *fepA S271C* mutation and pGT, the latter of which derived from the low copy plasmid pHSG575. OKN13 has two deletions; the chromosomal gene for FepA and the chromosomal gene for TonB were removed. Our lab monitored the location and status of FepA and the location of TonB microscopically *in vivo*, by adding the *fepA S271C* mutation and pGT plasmids. Once the strain was prepared, it contained a GFP attached to TonB and free cysteine in FepA that could be labeled using fluorophore maleimides. Specifically, AlexaFluor maleimide 546 was used to label FepA in the OM. We used a Zeiss 700 Confocal Laser Microscope, which was made available to our lab by the Kansas

State University Confocal Core Facility, to study fluorophore-labeled cells. All cells were studied at 100x magnification.

A time lapse of labeled OKN13/*fepAS271C*/pGT, bound to the surface inside an Ibidi slide well using poly-L-lysine, is shown from 0 to 9 minutes in panel A of **Figure 4-8**. In the top frames, two immobilized cells are shown in images captured during excitation with wavelength 488 nm laser light. Bottom frames are images of the same two cells, however, they were captured during excitation with wavelength 555 nm laser light. Excitation with 488 nm light selectively induces a fluorescence phenomenon in the GFP, whereas AlexaFluor 546 is selectively excited using 555 nm light (Albrecht, 2008; Cao et al., 2003; Jordan et al., 2013; Kaserer et al., 2008; Smallwood et al., 2014; Smallwood et al., 2009).

The addition of FeEnt resulted in fluorescence quenching of AM-labeled FepA, however, the fluorescence intensity of TonB-associated GFP remained the same throughout the experiment. All of the labeled FepA receptors were quenched, upon addition of FeEnt and fluorescence intensity rebounded for each fluorophore. This indicated that FeEnt was bound by all available receptors and that TonB-dependent transport occurred for each of them, round after round.

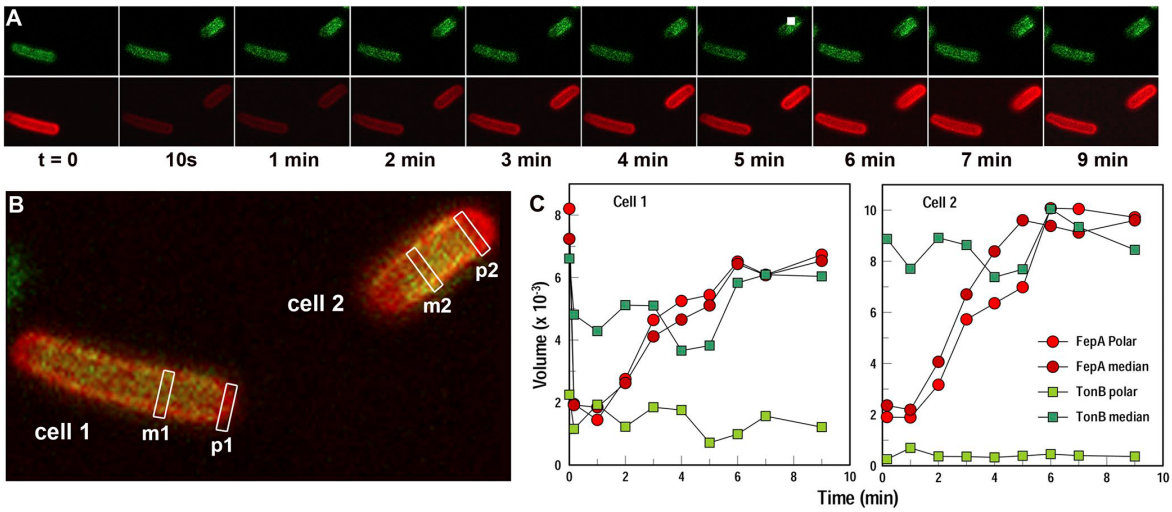


**Figure 4-8** (Smallwood et al., 2014). **(A)** Time-lapse sequence of *E. coli* OKN13/*fepA*S271C/pGT cells with GFP-labeled TonB shown in green (Top) and AlexaFluor546-labeled FepA shown in Red (Bottom). **(B)** Enhanced view of the two cells monitored in **A.** The rectangular boxes labeled m and p correspond to the middle and pole regions of the cells, respectively. **(C)** Plots supporting the conclusion that all FepA receptors bind and transport FeEnt, even though TonB is absent at polar regions of the cell.

# Chapter 5: Investigation of TonB Rotational Model

## 5.1 Introduction

Observations from TonB anisotropy studies (Jordan et al., 2013) led to a new mechanistic model in which the motion of TonB is central to energy transfer to TBDTs. Assuming the rotation is mechanically causing an unwinding of the TBDT plug domain, as in the ball-and-chain mechanism (Ma et al., 2007), the rotational diffusion rate of TonB should affect the rate of FeEnt transport through the OM.

With that rationale in mind, the speed of TonB rotational diffusion was expected to decrease with the addition of more mass, thereby increasing the size of the cytoplasmic portion of the TonB fusion protein. Although the additional cytoplasmic mass alone should not hamper the mobility of a membrane protein, additional size was thought to increase non-specific interactions with various cytoplasmic proteins. This chapter details the efforts made to further investigate TonB motion and to uncover whether rotational diffusion is the key to TonB energy transduction.

## 5.2 Reduced Motion in the Inner Membrane

Although proteins with a single-pass transmembrane topology freely diffuse within the lipid bilayer, there are several mechanisms by which their motion may be retarded. It is reasonable to expect a particular protein's

motion to correlate with the free diffusion rates of similar proteins, however, it is also prudent to consider various factors disallowing unrestricted diffusion. TonB is predicted to possess a single transmembrane domain, but there is evidence that other aspects of its topology play a large role in its mobility (Higgs et al., 1998; Skare and Postle, 1991).

Generally, free diffusion can be complicated by three common cellular phenomena. For instance, protein motion can be restricted if the protein is bound to an immobile matrix. Since the TonB membrane-spanning region is able to interact with TBDTs, it is likely to also contact the peptidoglycan layer below the OM. In our model, contact with the peptidoglycan matrix can slow TonB or even confine its movement transiently. In addition to immobile cellular structures, formation of homodimers or inclusion in a multimeric complex can also significantly reduce protein diffusion rates. Another common way free diffusion is often complicated is by direct, physical interaction with soluble proteins moving about in the cell.

There are many proteins in the in the cell. In the OKN3/*fepA*S271C cell line, there are approximately 50,000 copies of the OM transporter FepA, alone. There are many more proteins in the periplasmic, IM, and cytoplasmic regions of the cell. Accordingly, there should also be many more chances for collisions between proteins and transference of

momentum. This transference would alter the motion of both proteins involved in the collision and potentially slow the motion of at least one of the proteins.

## MATERIALS & METHODS

### 5.3 Site-directed Mutagenesis

Mutagenesis was used to add a PstI restriction enzyme site into the plasmid pGT derived from the low-copy vector pHSG575. The PstI site was added after the XhoI site present between *gfp* and *tonB* genes. Additionally, we created a mutant possessing a beta-galactosidase monomer, expressed as part of the fusion protein. The beta-galactosidase gene was inserted between *gfp* and *tonB* genes, in the same way the second GFP was added in pGGT. The resulting plasmid was named pGBT. Since beta-galactosidase is naturally expressed as a tetramer, we chose to create another fusion protein without the ability to tetramerize. The active site is comprised of the different domains of their respective monomers, but a loop from domain 2 of its paired monomer (A & D; B & C) completes the active site. This yields 4 active sites per tetramer. Additionally, two complimentary monomers must be associated for enzymatic activity to occur. A literature search provided valuable insight regarding alpha-complementation and reported evidence that deletion of the first 40 amino acids results in loss of the enzyme's ability to tetramerize

(Juers et al., 2012). With this information, we designed and created a deletion in pGBT to yield pGBd40T.

### 5.4 PCR

PCR was used to amplify the beta-galactosidase gene from wildtype *E. coli* strain MG1655 and GFP from OKN3 pGT. PCR was also used to confirm the presence of inserted and mutagenized genes. Once the PCR was finished running, the samples were run on a 1% agarose gel to compare fragment sizes and determine whether the fragment was, in fact, the product of interest.

### 5.5 Sequencing

Each construct was verified by sequence analysis through Molecular Cloning Laboratories (MCLAB; South San Fransisco, California). The sequences were again checked using FinchTV sequence viewing software.

### 5.5 Transformation

*E. coli* host strains DH5α, XL-1 Blue, OKN3, OKN1, and OKN13 were used to create various OKN1 pGGT, OKN1 pGBT, and OKN1 pGBd40T.

## 5.7 Siderophore Nutrition Test

Strains were inoculated and grown overnight. Cells were then subcultured (1:100) 50 microliters of cells in 5 ml of Nutrient Broth and grow for 3.5 hours. Molten Nutrient Broth Top Agar was placed in a water bath, and occasionally stirred such that the agar is in a liquid state, but not boiling. Added 3ml of Nutrient Broth Top Agar to glass test tubes and place in water bath. The appropriate antibiotics were added to each test tube (example: 6 microliters of chloramphenicol). Added 6 microliters of bipyridal to test tubes and pour the each test tube into a different well. Micropipette 10 microliters of 50 μM FeEnt onto a paper disc and place a disc into each well. Incubate several hours in 37$^{o}$ C.

## 5.8 Post-uptake Binding

PUB is a technique that measured the proportion of FepA molecules that were actively transporting the siderophore. First the cells were fully coated with non-radioactive FeEnt at 0 C. Temperature was quickly shifted to 37 C for 1 minute allowing transport. Binding with radioactive FeEnt allowed measurements of the number of receptors that transported the siderophore during the 37 C incubation.

### 5.9 SDS-PAGE/Immunoblot

Strains OKN1, OKN1 pT23, OKN1 pGT, OKN1 pGGT, OKN1 pGBT, OKN1pGBT/*fepA*S271C, and OKN1 pGBΔ40T were used. Cells were grown in LB media overnight and then subcultured into iron-deficient MOPS minimal medium. Either whole cell samples or OM fractions were prepared with sample buffer and 2% BME and loaded onto SDS-PAGE gels that were then subjected to electrophoresis. They were subsequently transferred to nitrocellulose paper for identification with immunochemistry.

Unexposed sites on the paper were blocked with TBSG pH 7.5 (50 mM Tris chloride, 0.9% NaCl, and 1% gelatin). TBSG was poured off and blots were incubated for 1 hr with mouse anti-TonB and mouse-anti β-galactosidase antibodies suspended in TBSG. Antibody solution was poured off and blots were washed 5 times with 0.05% Tween 20 in TBS for 5 minute intervals. Next, the blot was incubated with [$^{125}$I] protein A for 1 hour, shaking at room temperature. The blot was washed three times with tap water and air-dried.

### 5.10 Immunoblot Analysis

The emissions from the radioactive decay were captured using a phosphorescent screen. The screen was exposed to the blot for a minimum of 3 hours and scanned using the storage phosphor setting on the Typhoon imager. The amounts were quantified using ImageQuant

software and a standard curve for FepA concentration. The standard curve was obtained from FepA standards that were run alongside the samples of unknown concentrations.

**Figure 5-1**

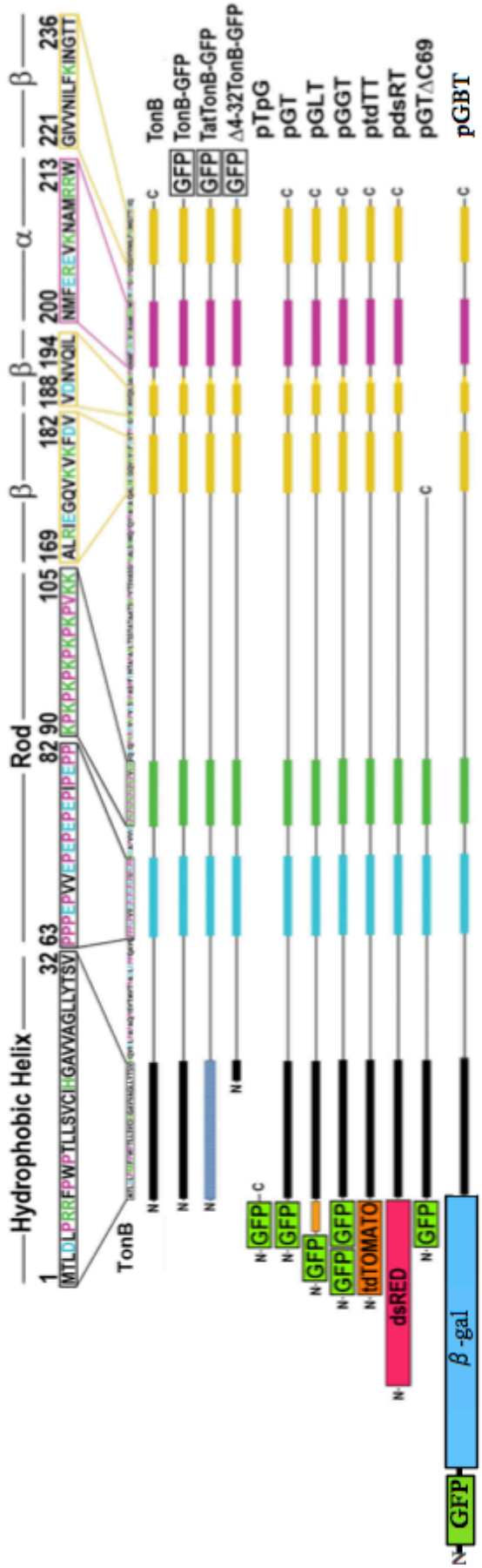
Hydrophobic Helix
Rod
TonB
TonB-GFP
TatTonB-GFP
Δ4-32TonB-GFP
pTpG
pGT
pGLT
pGGT
ptdTT
pdsRT
pGTΔC69
pGBT
GFP
tdTOMATO
dsRED
β-gal

**Figure 5-1** Adaptation published with the consent of the American Society for Microbiology. Kaserer, W.A., Jiang, X., Xiao, Q., Scott, D.C., Bauler, M., Copeland, D., Newton, S.M., Klebba, P.E., 2008. Insight from TonB hybrid proteins into the mechanism of iron transport through the outer membrane. J Bacteriol. 190, 4001-4016. Copyright American Society of Microbiology (2008).

At the top of the figure is an amino acid sequence magnified and labeled with secondary structure characteristics. Beneath the sequence is a color-coded visual representation of each region of secondary structure for each of the TonB constructs created by Dr. Phillip Klebba's research group. A linker region is depicted in orange in the pGLT construct. Additional elements, like fluorophores, have their common names written within their respective boxes.

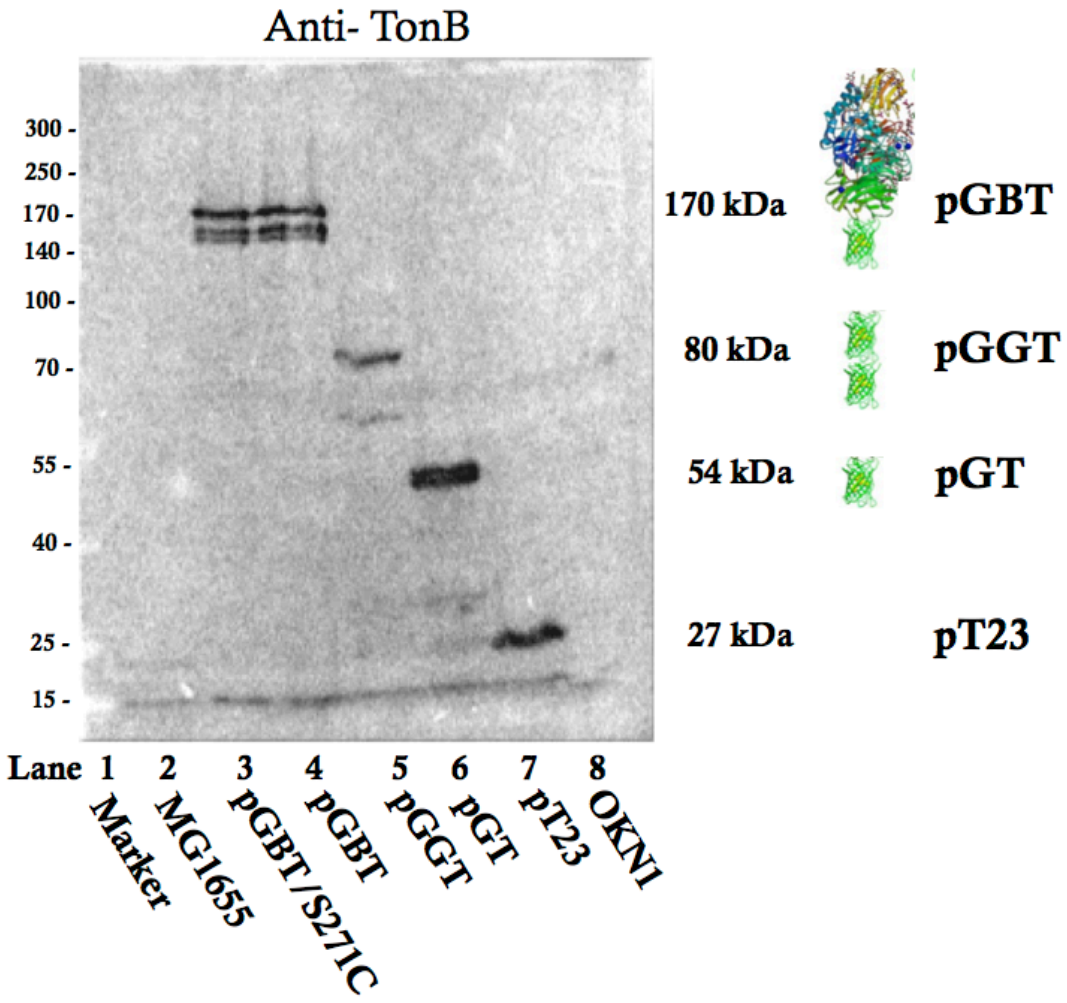


**Figure 5-2.** Shows a scanned image of an immunoblot, using mα-TonB/[$^{125}$I] protein A. Proteins encoded by the various constructs appear at appropriate molecular weights. Immunoblot was achieved using whole cells. Wildtype MG1655, in lane 2, was not iron starve and served as a control for the presence of beta-galactosidase. Beta galactosidase expression was induced using 0.1 mM IPTG. As expected, the host strain (lane 8) shows no TonB present.

## Results

### 5.11 TonB-Double GFP

To explore whether additional size would impact the motion of TonB, a TonB-double GFP construct was made by adding another sg-*gfp* gene to pGT. That construct was dubbed pGGT. Prior to mutagenesis, pGT only contained an XhoI between the *sg-gfp* and *tonB* genes. Originally, two approaches were attempted to make the pGGT construct. The first approach used the unaltered pGT vector. The XhoI site between *sg-gfp* and *tonB* was selected to receive the additional *sg-gfp* insert. Accordingly, the insert was mutagenized to include an XhoI site on either side of the gene.

A second approach was pursued in order to ensure proper orientation of the additional *sg-gfp* and avoid an extraneous screening process. In that instance, the pGT sequence was modified just after the first *sg-gfp* to include a PstI site. We were able to introduce directionality by using two restriction enzyme sites. An s*g-gfp* fragment was mutagenized using a thermocycler. Primers were constructed to include a PstI site at the beginning of the fragment and an XhoI site at the end. In this way, s*g-gfp* 5' → 3' was the only possible orientation for insertion into the mutagenized pGT vector.

The second approach was more desirable because subsequent constructs would be much easier to create in the future. The non-directional drop-in tactic was a less favorable alternative because it would involve a more thorough colony screening. Fortunately, the directional approach proved successful and assays characterizing the functionality of pGGT were commenced. Siderophore nutrition tests showed some slight differences between the faint halos of pGT and pGGT, however post-uptake binding (PUB) and transport experiments showed pGGT behaved similarly to pT23, which is *tonB*$^{+}$. The next step was to characterize the anisotropy of pGGT.

Experiments investigating the anisotropy of pGGT were performed as in the investigation of pGT and pGT *ΔexbBD* in Jordan et al., 2013. Five separate experiments were completed on pGGT; however, no significant difference was observed between pGT and pGGT. Consultation with Dr. Wai Tak Yip and Dr. Ken Ritchie yielded valuable insight regarding the major forces affecting the motion of TonB. For instance, forces exerted by cytoplasmic proteins could impact the motion of the GFP-TonB fusion protein. By increasing the size of fusion protein's cytoplasmic domain, those collisional forces could increase in frequency and may well reduce the efficiency of TonB-dependent transport.

## 5.12 Alternative Fluorescent Protein Constructs

Other fluorescent proteins were considered to address various concerns going forward. For instance, tdTomato was considered because of its natural tendency to homodimerize. Other GFP derivatives offered options such as brighter fluorescence, different colors, and higher stability than *sg-gfp.* However, the newly mutagenized pGT vector, used in the creation of pGGT, provided a convenient opportunity to insert a large protein between GFP and TonB.

With a GFP fluorophore already available, we only needed to decide the large, non-interacting protein and add the appropriate restriction sites to either side. Beta-galactosidase was chosen because it fulfilled the condition of being rather large, at 116 kDa, and it was very well characterized. Furthermore, fusions of beta-galactosidase have been previously studied (Benson et al., 1984).

## 5.13 Beta-galactosidase

Beta-galactosidase is a large, homotetrameric protein that is regulated by the *lac operon*. Each monomeric unit is 1023 amino acids long, with a DNA sequence of 3075 bp (Matthews, 2005). The monomer has five domains, including an active site contained within the α/β barrel of domain 3 (Matthews, 2005). Impressively, beta-galactosidase tetramers can catalyze up to 38,500 reactions per minute (Juers et al., 2012). The

protein is capable of three different enzymatic actions: cleavage of disaccharide lactose into glucose and galactose, catalyzing the transgalactosylation of lactose to allolactose, and finally, cleavage of allolactose to yield glucose and galactose.

Due to its natural tendency to tetramerize, we chose create a mutant version of pGBT, where beta-galactosidase was truncated to prevent tetramerization. Data from siderophore nutrition test assays showed that OKN1 pGGT, OKN1 pGBT, and OKN1 pGBd40T were all functional and able to transport ferric enterobactin **(Figure 5-3)**.

Although these constructs were created and confirmed, analysis by anisotropy was not yet possible for the beta-galactosidase fusion proteins. This was due to limitations in accessing necessary instruments. We have considered further analysis through one of our collaborators and are taking steps to move the project forward without my direct involvement.

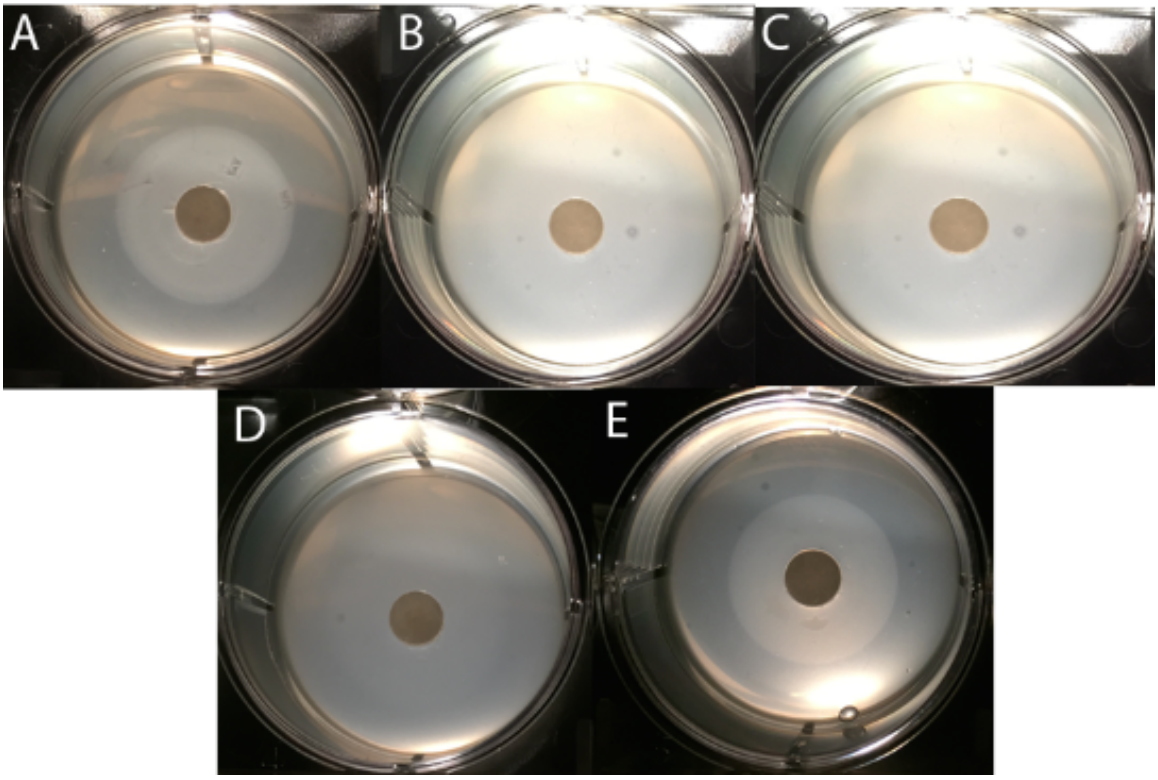


**Figure 5-3**. Siderophore nutrition test: **A)** OKN1 pT23 shown as a control with unmodified TonB expressed from plasmid. **B)** OKN1 pGT. **C)** OKN1 pGGT. **D)** OKN1 pGBT. **E)** OKN1 pGBd40T.

# Chapter 6: Discussion

## Significance

The central goal of the doctoral research described was to understand the role of TonB in ferric enterobactin transport. TonB-dependent metal transport systems hold the potential for a major advantage in the fight for dominance over Gram-negative bacteria. Thus far, we have shown the importance of catecholate siderophores as a virulence factor, established a working model for TonB motion in the cell, and characterized the intricate motions of FepA binding its ligand. We helped demystify a biological process that underlies the persistence of an imminent threat to human health and identified which new questions should be addressed next. This work exemplifies the fundamental purpose of scientific exploration: to identify and understand complexities in the world around us.

## 6.2 Discussion of Mouse-gut Colonization Study

Animals, including humans, benefit from a symbiotic relationship with bacteria that do not cause disease under “normal” circumstances (Alekshun and Levy, 2006). These types of bacteria are essential to many daily processes often taken for granted and are known as commensals. Commensal bacteria serve as a kind of protection from pathogenic

bacteria by filling an ecological niche, an effect commonly referred to as competitive exclusion (Callaway et al., 2008). This effect arises because established colonies use nearly all of the nutrients available. With limited nutrients, new and potentially pathogenic bacteria are often unable to compete. Commensal bacteria also directly aid in the digestion of food. On average, there are greater than 2,000 different species of bacteria present in the guts of most animals (Callaway et al., 2008). The various commensal species release enzymes, toxins, and siderophores into their environment, the host body, in order to gain an advantage over competing organisms.

Although competition is ongoing, the host's bacterial community becomes relatively stable. In the digestive tract, this stable community of bacteria is known as the "normal" gut flora. Sometimes, commensals are also "opportunistic pathogens," meaning, they take advantage of situations where the host immune system is compromised. While competing against a normal immune response, these wolves in sheep' clothing are innocuous, however, shifts in resource availability or even hormones can trigger their change.

A major way commensal and pathogenic bacteria battle for nutrients is the use of siderophores. The article, "Role of Catecholate Siderophores in Gram-negative Bacterial Colonization of the Mouse Gut", showed the impact of catecholate siderophores, specifically, on *E. coli* virulence in a

mammalian host system (Pi et al., 2012). This study comprehensively demonstrated the importance of iron as a virulence factor using a mouse model. Experiments were devised to test whether or not a siderophore, specifically FeEnt, was required for successful colonization of a murine host (Pi et al., 2012).

Our study found that catecholate siderophores drastically affect the colonization effectiveness of *E. coli* in the gastrointestinal tracts of mice. Mutant strains of *E. coli* with no ability to transport iron, but retaining the ability to make enterobactin (CAT4), showed the most interesting results (Smallwood et al., 2014).In competition with wildtype MG1655, CAT4 fecal CFU counts decreased more rapidly than did CAT0 and CAT40. CAT0 could not make enterobactin, but could transport enterobactin and CAT40 could not make enterobactin or transport FeEnt and other catecholate siderophore complexes. The wildtype strain also increased more rapidly in competition with the mutant strain CAT4. After analysis of the FeEnt concentration in mouse gut samples, we found that CAT4 was overproducing enterobactin. This overproduction was depleting the resources of CAT4 cells and as they were unable to utilize any FeEnt, there was no competition for wildtype cells. Thus, there is a significant sacrifice of resources when making enterobactin. Furthermore, FeEnt import is a critical step in colonization.

### 6.3 Mechanistic Analysis of TonB-dependent Transport

There are currently three major models for energy transduction via TonB: the rotational/propeller model, pulling model, and the periplasmic binding protein model. A fourth model, known as the "TonB shuttle hypothesis," was completely refuted by Wallace Kaserer (Kaserer et al., 2008). The mini review "TonB or not TonB: is that the question?" by Krewulak and Vogel describes all four models and gives an overview of the TonB-Exb system (Krewulak and Vogel, 2011).

The pulling model is based on the fact that a globular N-terminal domain blocks OM-TBDTs. As stated previously, this domain must move to allow transport of siderophore complexed iron. There are two main hypotheses regarding a pulling action by TonB. The "Ball and Chain" model describes the globular domain of the TonB-dependent transporter being pulled out of its barrel by TonB as one unit. On the other hand, the "Transient Pore" model describes TonB pulling the globular domain out as a string unraveling. The paper *Evidence of Ball-and-chain Transport of Ferric Enterobactin through FepA* strongly supports the former.

Transport of ferric enterobactin through FepA is not possible without an energy source or TonB. It is hypothesized that TonB acts on the N-terminal domain of OM transporters in a mechanical fashion in order to achieve transport. The region TonB interaction on the N-terminal domain of TBDTs is commonly referred to as the “TonB-box.” This TonB box consists

of a short sequence of amino acids, near the N-terminus of TBDTs, that impacts the transport efficiency when substitutions are introduced. Yet, when deleted entirely, the TonB box appears unnecessary for translocation of iron-containing siderophores. Deletion of the entire plug domain still results in TonB-dependent transport, albeit lowered efficiency (Braun et al., 1999).

The once prominent theory, the "TonB Shuttle Hypothesis" suggested that TonB was visits an "energized" conformation that leaves the cytoplasmic membrane completely in order to associate with TonB-dependent outer membrane proteins, subsequently returning to the cytoplasmic membrane to repeat the process (Gresock et al., 2011). However, this scenario was not a likely biochemical process and was not well substantiated (Kaserer et al., 2008).

### 6.4 Basis for Hypothesis

The rotational model for TonB energy transduction is based on homology with MotA and MotB, major components of the flagellar motor system. The question of whether or not the areas of homology correspond to functionally relevant regions of the proteins is one of particular importance. Since evidence supports MotAB as the main elements of the flagellar motor system, the TonB-ExbBD system is widely believed to function in a similar manner. MotAB are believed to impart flagellar

rotational capability to E. coli. Homology between MotA/MotB and ExbB/ExbD has been shown in regions that are believed to be important to the function MotA/MotB function.

Bacterial cell motility is governed by attraction and repulsion to various substances in the extracellular environment. In the absence of either an attractant or repellent, the bacteria frequently change direction; an event called tumbling. Food and nutrients are among the substances that attract bacteria, while noxious chemicals repel. The structures responsible for propelling bacteria, flagella, often spin in unison counter-clockwise. Protein discs, including MotAB, is used to achieve movement of the flagella. These discs contain a motor, stator, and rotor, all of which are powered by either a sodium or proton ion gradient, as opposed to nucleotide triphosphates. Although the mechanism of rotation is not fully understood, it has been proposed that MotA and MotB are responsible for providing a stator and an ion channel to harness PMF (Roujeinikova, 2008; Zhai et al., 2003).

### 6.5 Pal-Tol system in *E. coli*

Extensive studies have been performed regarding the interactions between the peptidoglycan-associated lipoprotein (Pal) and Tol system components. OM-spanning OmpF, OM-anchored Pal, periplasmic TolB, and IM anchored TolAQR participate in stabilizing the cell's structural

integrity and are also required for Group A colicins to enter the cell (http://www.york.ac.uk/res/kleanthous/research.html). The current model for Group A colicin killing includes TolB presenting a Tol box to TolA. More specifically, the colicin binds to a TBDT and an unstructured region of the colicin snakes through the OmpF porin, simultaneously disrupting the TolB-Pal interaction and making contact with TolB on the other side. Once an association with TolB is achieved, TolB recruits TolA with a TolA box and a cell death signal is communicated.

The TonB-ExbBD system, which has homology to the TolAQR system, is required for Group B colicins to enter and kill the cell. TonB-ExbBD system is also responsible for energy transduction from the inner membrane to TBDTs for translocation of siderophore complexes. Similarities between the Ton and Tol systems transcend sequence homology into function. For instance, only double deletions/mutations in *exbB* and *tolQ* or *exbD* and *tolR* caused significant reduction of H8 bacteriophage activity, which further suggests that TolQ can supplement the role of ExbB.

### 6.6 Model for Transport

Although our lab has developed a surveillance model for TonB selection of and interaction with TBDTs, our current model does not address two key phenomena. The first unexplained issue is the

discrepancy between the sheer number of OM TBDTs and the number of TonB-ExbBD complexes. TonB is expressed at approximately 1,000 copies per cell, while many more TBDTs are present in the OM. For FepA alone, there are approximately 50,000 copies, all of which have been observed binding and transporting FeEnt (Smallwood et al., 2014). The second unexplained issue was revealed in Jordan et al., 2013, when our lab discovered an anomalous centralized localization of TonB-GFP fluorescence. If TonB is localized in the central regions of the cell, there is another challenge to the model, which includes an obligate physical interaction between TonB and all of the FepA receptors.

Regardless of the relationship between TonB and ExbBD, TonB is needed for transport of TBDT ligands. Our laboratory's proposed mechanism for TonB-dependent transport takes into consideration the centralized distribution of TonB. It is not possible for TonB to be in physical contact with all TBDTs simultaneously, so we suggested a surveillance model (Jordan et al., 2013). In this model, TonB is in constant motion and drags along the underside of the OM, due to constant energy input by the PMF. We expect that ExbBD help transfer PMF energy to TonB and a TonB dimer is then driven to rotate inside a stator formed by ExbBD.

The issues not addressed by our model, along with the dual role of the TonB-ExbBD system, and homology with TolAQR, inspired the creation of a new hypothesis that attempts to incorporate our lab's

rotational model and merge it with elements that may explain TonB energy-transduction to all “loaded” FepA receptors.

Crossover of TolI and Ton protein involvement in the same system may offer an explanation for some of the most complicated aspects of TonB-dependent transport. The enigmatic process by which FeEnt transport occurs through the blocked FepA barrel, and likelihood that colicin entry mechanisms have some similarity to siderophore transport, both support similar action of TonB. Adding weight to the latter point, two other TBDTs, FecA and FhuA, possess a short alpha helix that unwinds into a flexible strand upon ligand adsorption (Ferguson et al., 2002a). TonB is known to associate with a variety of proteins and has been shown to have differential action, dependent on the TBDT (Sauter et al., 2003).

In our developing model, TonB proteins could potentially affect transport in all 50,000 FepA receptors over a short time-span. Upon FeEnt adsorption to FepA, the TonB box relocates to hang beneath the central area of the receptor and signal a loaded FepA molecule for TonB recruitment. As TonB continuously surveys the underside of the OM, it would do so as a dimer and by interaction with peptidoglycan, via lysin domains. The region between amino acids 33-239 of TonB was shown to associate with other TonB proteins as a dimer, using electron pulse resonance (EPR) to detect double electron-electron resonance (DEER) (Freed et al., 2013). Another study, using the same technique, proposed

that this dimeric interaction between the proline rich regions of TonB could lend itself to the propeller model described in Kaserer et al., 2009.

Interaction with peptidoglycan is essential for TonB surveillance action, since the flexible region of TonB would otherwise hamper its efficiency in finding the TonB box and the association of TonB with peptidoglycan would help it to move to new regions. Without interaction with the peptidoglycan layer, TonB would diffuse like an unanchored buoy in a vast ocean. Further, the extreme C-terminus of dimeric TonB is approximately the same diameter as the putative hexagonal openings in the peptidoglycan matrix (Koch, 1998; Vollmer et al., 2008).

TonB has long been known to associate with the IM and OM to almost equal extents, despite its N-terminal cytoplasmic membrane anchor domain. This fact was often attributed to its function of transducing energy to OM proteins. During a “loaded” state, TBDTs signal TonB recruitment with exposed TonB box regions, which relocate to the central barrel region. This causes an increase in TonB association with OM fragments. However, through crosslinking experiments, Higgs et al. showed that TonB association with OM components was not dependent on its interaction with ligand-loaded TBDTs (Higgs et al., 2002b). A *fepA* deletion showed no difference in the ratio of OM-associated TonB, nor did degradation of peptidoglycan with lysozyme. The one treatment that greatly affected TonB distribution was the introduction 4 M salt. The authors concluded that

TonB, must therefore, be interacting with nonreceptor OM-associated proteins.

Upon location of a TonB box at the center of the barrel of a TBDT, the TonB dimer would then dissociate and a single TonB would impart energy to the TBDT for ligand translocation. This mechanistic aspect is supported by evidence that binding of the TonB C-terminal domain to the FepA TonB box causes TonB to lose elements of its secondary structure. The observed decrease in C-terminal ordered structure was also previously suggested to lend itself to interactions with the barrel domain of TBDTs (Peacock et al., 2006). Evidence of physical interaction of the TonB C-terminal region physically interacting with OM TonB-dependent transporters was reported (Endriss et al., 2003; Pawelek et al., 2006). The publication *Insight from TonB Hybrid Proteins into the Mechanism of Iron Transport through the Outer Membrane*, Kaserer et al. describes a peptidoglycan-binding motif (lysin domain) in the sequence of TonB (Kaserer et al., 2008).

Given the discrepancy of expression levels between TonB and TBDTs, there have been questions raised regarding physical interaction of TonB. However, it is possible that each TonB is able to affect around 50 TBDTs, within a short time frame. The quenching studies performed using confocal microscopy, showed gradual recovery of fluorescence over 9 minutes, with 1 min intervals after the first minute. This method is not

sensitive enough to detect simultaneous transport of FeEnt and is somewhat limited. With that point in mind, one might also consider that transport takes approximately 15-20 seconds and the diffusion rate of TonB is on the microsecond timescale. Additionally, the small nature of bacteria makes it difficult to resolve single fluorophores close to each other using microscopy. This information points toward the possibility of TonB transferring energy to one TBDT and quickly diffusing to transfer energy to another TBDT. In this way, the limiting factor for servicing all TBDTs is the rate of ligand transport.

## References


Abergel, R.J., Clifton, M.C., Pizarro, J.C., Warner, J.A., Shuh, D.K., Strong, R.K., Raymond, K.N., 2008. The siderocalin/enterobactin interaction: a link between mammalian immunity and bacterial iron transport. J Am Chem Soc. 130, 11524-11534. doi: 11510.11021/ja803524w.

Albrecht, C., 2008. Joseph R. Lakowicz: Principles of fluorescence spectroscopy, 3rd Edition. Anal Bioanal Chem 390, 1223-1224.

Alekshun, M.N., Levy, S.B., 2006. Commensals upon us. Biochem Pharmacol 71, 893-900.

Althaus, E.W., Outten, C.E., Olson, K.E., Cao, H., O'Halloran, T.V., 1999. The ferric uptake regulation (Fur) repressor is a zinc metalloprotein. Biochemistry 38, 6559-6569.

Annamalai, R., Jin, B., Cao, Z., Newton, S.M., Klebba, P.E., 2004. Recognition of ferric catecholates by FepA. J Bacteriol 186, 3578-3589.

Aznar, A., Chen, N.W., Rigault, M., Riache, N., Joseph, D., Desmaele, D., Mouille, G., Boutet, S., Soubigou-Taconnat, L., Renou, J.P., Thomine, S., Expert, D., Dellagi, A., 2014. Scavenging iron: a novel mechanism of plant immunity activation by microbial siderophores. Plant Physiol 164, 2167-2183.

Bassford, P.J., Jr., Bradbeer, C., Kadner, R.J., Schnaitman, C.A., 1976. Transport of vitamin B12 in tonB mutants of Escherichia coli. J Bacteriol 128, 242-247.

Benson, S.A., Bremer, E., Silhavy, T.J., 1984. Intragenic regions required for LamB export. Proc Natl Acad Sci U S A 81, 3830-3834.

Bouveret, E., Derouiche, R., Rigal, A., Lloubes, R., Lazdunski, C., Benedetti, H., 1995. Peptidoglycan-associated lipoprotein-TolB interaction. A possible key to explaining the formation of contact sites between the inner and outer membranes of Escherichia coli. J Biol Chem 270, 11071-11077.

**Bradbeer, C., 1993. The proton motive force drives the outer membrane transport of cobalamin in Escherichia coli. J Bacteriol 175, 3146-3150.**

**Bradbeer, C., Kenley, J.S., Di Masi, D.R., Leighton, M., 1978. Transport of vitamin B12 in Escherichia coli. Corrinoid specificities of the periplasmic B12-binding protein and of energy-dependent B12 transport. J Biol Chem 253, 1347-1352.**

**Braun, M., Killmann, H., Braun, V., 1999. The beta-barrel domain of FhuADelta5-160 is sufficient for TonB-dependent FhuA activities of Escherichia coli. Mol Microbiol 33, 1037-1049.**

**Braun, V., 2003. Iron uptake by Escherichia coli. Frontiers in Biosciences 8, s1409-1421.**

**Braun, V., 2006. Energy transfer between biological membranes. ACS Chem Biol. 1, 352-354.**

**Braun, V., Endriss, F., 2007. Energy-coupled outer membrane transport proteins and regulatory proteins. Biometals. 20, 219-231. Epub 2007 Mar 2017.**

**Braun, V., Gaisser, S., Herrmann, C., Kampfenkel, K., Killmann, H., Traub, I., 1996. Energy-coupled transport across the outer membrane of Escherichia coli: ExbB binds ExbD and TonB in vitro, and leucine 132 in the periplasmic region and aspartate 25 in the transmembrane region are important for ExbD activity. J Bacteriol 178, 2836-2845.**

**Braun, V., Hantke, K., Koster, W., 1998. Bacterial iron transport: mechanisms, genetics, and regulation. Met Ions Biol Syst 35, 67-145.**

**Bullen, J.J., Rogers, H.J., Spalding, P.B., Ward, C.G., 2005. Iron and infection: the heart of the matter. FEMS Immunol Med Microbiol 43, 325-330.**

**Cadieux, N., Bradbeer, C., Kadner, R.J., 2000. Sequence changes in the Ton box region of BtuB affect Its transport activities and interaction with TonB protein. J Bacteriol 182, 5954-5961.**

Cadieux, N., Phan, P.G., Cafiso, D.S., Kadner, R.J., 2003. Differential substrate-induced signaling through the TonB-dependent transporter BtuB. Proc Natl Acad Sci U S A. 100, 10688-10693.

Callaway, T.R., Edrington, T.S., Anderson, R.C., Harvey, R.B., Genovese, K.J., Kennedy, C.N., Venn, D.W., Nisbet, D.J., 2008. Probiotics, prebiotics and competitive exclusion for prophylaxis against bacterial disease. Anim Health Res Rev 9, 217-225.

Cao, Z., Klebba, P.E., 2002. Mechanisms of colicin binding and transport through outer membrane porins. Biochimie 84, 399-412.

Cao, Z., Warfel, P., Newton, S.M., Klebba, P.E., 2003. Spectroscopic observations of ferric enterobactin transport. J Biol Chem 278, 1022-1028.

Carrano, C.J., Raymond, K.N., 1978. Coordination chemistry of microbial iron transport compounds: rhodotorulic acid and iron uptake in Rhodotorula pilimanae. J Bacteriol 136, 69-74.

Chakraborty, R., Lemke, E.A., Cao, Z., Klebba, P.E., van der Helm, D., 2003. Identification and mutational studies of conserved amino acids in the outer membrane receptor protein, FepA, which affect transport but not binding of ferric-enterobactin in Escherichia coli. Biometals 16, 507-518.

Chang, C., Mooser, A., Pluckthun, A., Wlodawer, A., 2001. Crystal structure of the dimeric C-terminal domain of TonB reveals a novel fold. J Biol Chem 276, 27535-27540.

Clements, J.D., Cardenas, L., 1990. Vaccines against enterotoxigenic bacterial pathogens based on hybrid Salmonella that express heterologous antigens. Res Microbiol 141, 981-993.

Cowan, S.W., Garavito, R.M., Jansonius, J.N., Jenkins, J.A., Karlsson, R., Konig, N., Pai, E.F., Pauptit, R.A., Rizkallah, P.J., Rosenbusch, J.P., et al., 1995. The structure of OmpF porin in a tetragonal crystal form. Structure 3, 1041-1050.

Dauros-Singorenko, P., Swift, S., 2014. The transition from iron starvation to iron sufficiency as an important step in the progression of infection. Sci Prog 97, 371-382.

de Pedro, M.A., Grunfelder, C.G., Schwarz, H., 2004. Restricted Mobility of Cell Surface Proteins in the Polar Regions of Escherichia coli. J Bacteriol 186, 2594-2602.

Dutton, R.J., Boyd, D., Berkmen, M., Beckwith, J., 2008. Bacterial species exhibit diversity in their mechanisms and capacity for protein disulfide bond formation. Proc Natl Acad Sci U S A 105, 11933-11938.

Endriss, F., Braun, M., Killmann, H., Braun, V., 2003. Mutant analysis of the Escherichia coli FhuA protein reveals sites of FhuA activity. J Bacteriol. 185, 4683-4692.

Escolar, L., Perez-Martin, J., de Lorenzo, V., 1998. Binding of the fur (ferric uptake regulator) repressor of Escherichia coli to arrays of the GATAAT sequence. J Mol Biol 283, 537-547.

Evans, J.S., Levine, B.A., Trayer, I.P., Dorman, C.J., Higgins, C.F., 1986. Sequence-imposed structural constraints in the TonB protein of E. coli. FEBS Lett 208, 211-216.

Faundez, G., Figueroa, G., Troncoso, M., Cabello, F.C., 1988. Characterization of enteroinvasive Escherichia coli strains isolated from children with diarrhea in Chile. J Clin Microbiol 26, 928-932.

Ferguson, A.D., Chakraborty, R., Smith, B.S., Esser, L., van der Helm, D., Deisenhofer, J., 2002a. Structural basis of gating by the outer membrane transporter FecA. Science 295, 1715-1719.

Ferguson, A.D., Chakraborty, R., Smith, B.S., Esser, L., van der Helm, D., Deisenhofer, J., 2002b. Structural basis of gating by the outer membrane transporter FecA. Science 295, 1715-1719.

Ferguson, A.D., Deisenhofer, J., 2002. TonB-dependent receptors-structural perspectives. Biochim Biophys Acta 1565, 318-332.

Fillat, M.F., 2014. The FUR (ferric uptake regulator) superfamily: diversity and versatility of key transcriptional regulators. Arch Biochem Biophys 546, 41-52.

Fischbach, M.A., Lin, H., Zhou, L., Yu, Y., Abergel, R.J., Liu, D.R., Raymond, K.N., Wanner, B.L., Strong, R.K., Walsh, C.T., Aderem,

A., Smith, K.D., 2006. The pathogen-associated iroA gene cluster mediates bacterial evasion of lipocalin 2. Proc Natl Acad Sci U S A 103, 16502-16507.

Freed, D.M., Lukasik, S.M., Sikora, A., Mokdad, A., Cafiso, D.S., 2013. Monomeric TonB and the Ton box are required for the formation of a high-affinity transporter-TonB complex. Biochemistry 52, 2638-2648.

Garcia-Herrero, A., Peacock, R.S., Howard, S.P., Vogel, H.J., 2007. The solution structure of the periplasmic domain of the TonB system ExbD protein reveals an unexpected structural homology with siderophore-binding proteins. Mol Microbiol 66, 872-889.

Gresock, M.G., Savenkova, M.I., Larsen, R.A., Ollis, A.A., Postle, K., 2011. Death of the TonB Shuttle Hypothesis. Front Microbiol 2, 206.

Guh, A.Y., McDonald, L.C., Sinkowitz-Cochran, R., 2013. Assessment of public health perspectives on responding to an emerging pathogen: carbapenem-resistant Enterobacteriaceae. J Public Health Manag Pract 19, E27-32.

Guterman, S.K., Dann, L., 1973. Excretion of enterochelin by exbA and exbB mutants of Escherichia coli. J Bacteriol 114, 1225-1230.

Heming, N., Montravers, P., Lasocki, S., 2011. Iron deficiency in critically ill patients: highlighting the role of hepcidin. Crit Care 15, 210.

Hentze, M.W., Muckenthaler, M.U., Galy, B., Camaschella, C., 2010. Two to tango: regulation of Mammalian iron metabolism. Cell 142, 24-38.

Higgs, P.I., Larsen, R.A., Postle, K., 2002a. Quantification of known components of the Escherichia coli TonB energy transduction system: TonB, ExbB, ExbD and FepA. Mol Microbiol 44, 271-281.

Higgs, P.I., Letain, T.E., Merriam, K.K., Burke, N.S., Park, H., Kang, C., Postle, K., 2002b. TonB interacts with nonreceptor proteins in the outer membrane of Escherichia coli. J Bacteriol. 184, 1640-1648.

Higgs, P.I., Myers, P.S., Postle, K., 1998. Interactions in the TonB-dependent energy transduction complex: ExbB and ExbD form homomultimers. J Bacteriol 180, 6031-6038.

Jaskula, J.C., Letain, T.E., Roof, S.K., Skare, J.T., Postle, K., 1994. Role of the TonB amino terminus in energy transduction between membranes. J Bacteriol 176, 2326-2338.

Johnson, E.E., Wessling-Resnick, M., 2012. Iron metabolism and the innate immune response to infection. Microbes Infect 14, 207-216.

Jordan, L.D., Zhou, Y., Smallwood, C.R., Lill, Y., Ritchie, K., Yip, W.T., Newton, S.M., Klebba, P.E., 2013. Energy-dependent motion of TonB in the Gram-negative bacterial inner membrane. Proc Natl Acad Sci U S A 110, 11553-11558.

Juers, D.H., Matthews, B.W., Huber, R.E., 2012. LacZ beta-galactosidase: structure and function of an enzyme of historical and molecular biological importance. Protein Sci 21, 1792-1807.

Kampfenkel, K., Braun, V., 1993. Membrane topologies of the TolQ and TolR proteins of Escherichia coli: inactivation of TolQ by a missense mutation in the proposed first transmembrane segment. J Bacteriol 175, 4485-4491.

Kaserer, W.A., Jiang, X., Xiao, Q., Scott, D.C., Bauler, M., Copeland, D., Newton, S.M., Klebba, P.E., 2008. Insight from TonB hybrid proteins into the mechanism of iron transport through the outer membrane. J Bacteriol. 190, 4001-4016. Epub 2008 Apr 4004.

Khursigara, C.M., De Crescenzo, G., Pawelek, P.D., Coulton, J.W., 2004. Enhanced binding of TonB to a ligand-loaded outer membrane receptor: role of the oligomeric state of TonB in formation of a functional FhuA.TonB complex. J Biol Chem. 279, 7405-7412. Epub 2003 Dec 7410.

Klebba, P.E., McIntosh, M.A., Neilands, J.B., 1982. Kinetics of biosynthesis of iron-regulated membrane proteins in Escherichia coli. J Bacteriol 149, 880-888.

Kneen, M., Farinas, J., Li, Y., Verkman, A.S., 1998. Green fluorescent protein as a noninvasive intracellular pH indicator. Biophys J 74, 1591-1599.

Koch, A.L., 1998. Orientation of the peptidoglycan chains in the sacculus of Escherichia coli. Res Microbiol 149, 689-701.

Koedding, J., Howard, P., Kaufmann, L., Polzer, P., Lustig, A., Welte, W., 2004. Dimerization of TonB is not essential for its binding to the outer membrane siderophore receptor FhuA of Escherichia coli. J Biol Chem. 279, 9978-9986. Epub 2003 Dec 9978.

Krewulak, K.D., Vogel, H.J., 2011. TonB or not TonB: is that the question? Biochem Cell Biol 89, 87-97.

Lambris, J.D., Ricklin, D., Geisbrecht, B.V., 2008. Complement evasion by human pathogens. Nat Rev Microbiol 6, 132-142.

Larrie-Bagha, S.M., Rasooli, I., Mousavi-Gargari, S.L., Rasooli, Z., Nazarian, S., 2013. Passive immunization by recombinant ferric enterobactin protein (FepA) from Escherichia coli O157. Iran J Microbiol. 5, 113-119.

Larsen, R.A., Thomas, M.G., Wood, G.E., Postle, K., 1994. Partial suppression of an Escherichia coli TonB transmembrane domain mutation (delta V17) by a missense mutation in ExbB. Mol Microbiol 13, 627-640.

Liu, Z., Reba, S., Chen, W.D., Porwal, S.K., Boom, W.H., Petersen, R.B., Rojas, R., Viswanathan, R., Devireddy, L., 2014. Regulation of mammalian siderophore 2,5-DHBA in the innate immune response to infection. J Exp Med 211, 1197-1213.

Ma, L., Kaserer, W., Annamalai, R., Scott, D.C., Jin, B., Jiang, X., Xiao, Q., Maymani, H., Massis, L.M., Ferreira, L.C., Newton, S.M., Klebba, P.E., 2007. Evidence of ball-and-chain transport of ferric enterobactin through FepA. J Biol Chem 282, 397-406.

Madar, M., Bencurova, E., Mlynarcik, P., Almeida, A.M., Soares, R., Bhide, K., Pulzova, L., Kovac, A., Coelho, A.V., Bhide, M., 2015. Exploitation of complement regulatory proteins by Borrelia and Francisella. Mol Biosyst 11, 1684-1695.

**Martin, J., Hudson, J., Hornung, T., Frasch, W.D., 2015. Fo-driven Rotation in the ATP Synthase Direction against the Force of F1 ATPase in the FoF1 ATP Synthase. J Biol Chem 290, 10717-10728.**

**Matthews, B.W., 2005. The structure of E. coli beta-galactosidase. C R Biol 328, 549-556.**

**Miethke, M., Marahiel, M.A., 2007. Siderophore-based iron acquisition and pathogen control. Microbiol Mol Biol Rev 71, 413-451.**

**Nairz, M., Schroll, A., Sonnweber, T., Weiss, G., 2010. The struggle for iron - a metal at the host-pathogen interface. Cell Microbiol 12, 1691-1702.**

**Nenninger, A., Mastroianni, G., Robson, A., Lenn, T., Xue, Q., Leake, M.C., Mullineaux, C.W., 2014. Independent mobility of proteins and lipids in the plasma membrane of Escherichia coli. Mol Microbiol. 92, 1142-1153. doi: 1110.1111/mmi.12619. Epub 12014 Apr 12630.**

**Newton, S.M., Igo, J.D., Scott, D.C., Klebba, P.E., 1999. Effect of loop deletions on the binding and transport of ferric enterobactin by FepA. Mol Microbiol 32, 1153-1165.**

**Nikaido, H., Rosenberg, E.Y., 1981. Effect on solute size on diffusion rates through the transmembrane pores of the outer membrane of Escherichia coli. J Gen Physiol 77, 121-135.**

**Noinaj, N., Guillier, M., Barnard, T.J., Buchanan, S.K., 2010. TonB-dependent transporters: regulation, structure, and function. Annu Rev Microbiol 64, 43-60.**

**Okumura, C.Y., Nizet, V., 2014. Subterfuge and sabotage: evasion of host innate defenses by invasive gram-positive bacterial pathogens. Annu Rev Microbiol 68, 439-458.**

**Ollis, A.A., Manning, M., Held, K.G., Postle, K., 2009. Cytoplasmic membrane protonmotive force energizes periplasmic interactions between ExbD and TonB. Mol Microbiol. 73, 466-481. Epub 2009 Jul 2016.**

**Pawelek, P.D., Croteau, N., Ng-Thow-Hing, C., Khursigara, C.M., Moiseeva, N., Allaire, M., Coulton, J.W., 2006. Structure of TonB in complex with FhuA, E. coli outer membrane receptor. Science. 312, 1399-1402.**

**Payne, M.A., Igo, J.D., Cao, Z., Foster, S.B., Newton, S.M., Klebba, P.E., 1997. Biphasic binding kinetics between FepA and its ligands. J Biol Chem 272, 21950-21955.**

**Peacock, R.S., Andrushchenko, V.V., Demcoe, A.R., Gehmlich, M., Lu, L.S., Herrero, A.G., Vogel, H.J., 2006. Characterization of TonB interactions with the FepA cork domain and FecA N-terminal signaling domain. Biometals. 19, 127-142.**

**Pi, H., Jones, S.A., Mercer, L.E., Meador, J.P., Caughron, J.E., Jordan, L., Newton, S.M., Conway, T., Klebba, P.E., 2012. Role of catecholate siderophores in gram-negative bacterial colonization of the mouse gut. PLoS One 7, e50020.**

**Postle, K., 1993. TonB protein and energy transduction between membranes. J Bioenerg Biomembr 25, 591-601.**

**Rabsch, W., Ma, L., Wiley, G., Najar, F.Z., Kaserer, W., Schuerch, D.W., Klebba, J.E., Roe, B.A., Laverde Gomez, J.A., Schallmey, M., Newton, S.M., Klebba, P.E., 2007. FepA- and TonB-dependent bacteriophage H8: receptor binding and genomic sequence. J Bacteriol 189, 5658-5674.**

**Raymond, K.N., Dertz, E.A., Kim, S.S., 2003. Enterobactin: an archetype for microbial iron transport. Proc Natl Acad Sci U S A 100, 3584-3588.**

**Roujeinikova, A., 2008. Crystal structure of the cell wall anchor domain of MotB, a stator component of the bacterial flagellar motor: implications for peptidoglycan recognition. Proc Natl Acad Sci U S A 105, 10348-10353.**

**Sauter, A., Howard, S.P., Braun, V., 2003. In vivo evidence for TonB dimerization. J Bacteriol. 185, 5747-5754.**

**Schaible, U.E., Kaufmann, S.H., 2004. Iron and microbial infection. Nat Rev Microbiol 2, 946-953.**

**Schmidt, M.A., 2010. LEEways: tales of EPEC, ATEC and EHEC. Cell Microbiol 12, 1544-1552.**

**Scott, D.C., Cao, Z., Qi, Z., Bauler, M., Igo, J.D., Newton, S.M., Klebba, P.E., 2001. Exchangeability of N termini in the ligand-gated porins of Escherichia coli. J Biol Chem 276, 13025-13033.**

**Scott, D.C., Newton, S.M., Klebba, P.E., 2002. Surface loop motion in FepA. J Bacteriol 184, 4906-4911.**

**Seo, S.W., Kim, D., Latif, H., O'Brien, E.J., Szubin, R., Palsson, B.O., 2014. Deciphering Fur transcriptional regulatory network highlights its complex role beyond iron metabolism in Escherichia coli. Nat Commun 5, 4910.**

**Shimomura, O., 2009. Discovery of green fluorescent protein (GFP) (Nobel Lecture). Angew Chem Int Ed Engl 48, 5590-5602.**

**Silhavy, T.J., Kahne, D., Walker, S., 2010. The bacterial cell envelope. Cold Spring Harb Perspect Biol 2, a000414.**

**Skare, J.T., Postle, K., 1991. Evidence for a TonB-dependent energy transduction complex in Escherichia coli. Mol Microbiol 5, 2883-2890.**

**Smallwood, C.R., Jordan, L., Trinh, V., Schuerch, D.W., Gala, A., Hanson, M., Shipelskiy, Y., Majumdar, A., Newton, S.M., Klebba, P.E., 2014. Concerted loop motion triggers induced fit of FepA to ferric enterobactin. J Gen Physiol 144, 71-80.**

**Smallwood, C.R., Marco, A.G., Xiao, Q., Trinh, V., Newton, S.M., Klebba, P.E., 2009. Fluoresceination of FepA during colicin B killing: effects of temperature, toxin and TonB. Mol Microbiol 72, 1171-1180.**

**Smit, J., Kamio, Y., Nikaido, H., 1975. Outer membrane of Salmonella typhimurium: chemical analysis and freeze- fracture studies with lipopolysaccharide mutants. J Bacteriol 124, 942-958.**

**Stevanovic, M., Lehmann, C., Schleiff, E., 2013. The response of the TonB-dependent transport network in Anabaena sp. PCC 7120 to cell density and metal availability. Biometals 26, 549-560.**

**Stintzi, A., Barnes, C., Xu, J., Raymond, K.N., 2000. Microbial iron transport via a siderophore shuttle: a membrane ion transport paradigm. Proc Natl Acad Sci U S A 97, 10691-10696.**

**Stojiljkovic, I., Baumler, A.J., Hantke, K., 1994. Fur regulon in gram-negative bacteria. Identification and characterization of new iron-regulated Escherichia coli genes by a fur titration assay [published erratum appears in J Mol Biol 1994 Jul 15;240(3):271]. J Mol Biol 236, 531-545.**

**Thulasiraman, P., Newton, S.M., Xu, J., Raymond, K.N., Mai, C., Hall, A., Montague, M.A., Klebba, P.E., 1998. Selectivity of ferric enterobactin binding and cooperativity of transport in gram-negative bacteria. J Bacteriol 180, 6689-6696.**

**Troxell, B., Hassan, H.M., 2013. Transcriptional regulation by Ferric Uptake Regulator (Fur) in pathogenic bacteria. Front Cell Infect Microbiol 3, 59.**

**Tsien, R.Y., 1998. The green fluorescent protein. Annu Rev Biochem 67, 509-544.**

**Udho, E., Jakes, K.S., Finkelstein, A., 2012. TonB-dependent transporter FhuA in planar lipid bilayers: partial exit of its plug from the barrel. Biochemistry 51, 6753-6759.**

**Vollmer, W., Blanot, D., de Pedro, M.A., 2008. Peptidoglycan structure and architecture. FEMS Microbiol Rev. 32, 149-167. Epub 2008 Jan 2008.**

**Xiao, Q., Jiang, X., Moore, K.J., Shao, Y., Pi, H., Dubail, I., Charbit, A., Newton, S.M., Klebba, P.E., 2011. Sortase independent and dependent systems for acquisition of haem and haemoglobin in Listeria monocytogenes. Mol Microbiol 80, 1581-1597.**

**Zeng, C., Chen, Q., Zhang, K., Chen, Q., Song, S., Fang, X., 2015. Hepatic hepcidin protects against polymicrobial sepsis in mice by regulating host iron status. Anesthesiology 122, 374-386.**

**Zhai, Y.F., Heijne, W., Saier, M.H., Jr., 2003. Molecular modeling of the bacterial outer membrane receptor energizer, ExbBD/TonB, based on homology with the flagellar motor, MotAB. Biochim Biophys Acta. 1614, 201-210.**